UNIVERSITY OF CAPE TOWN
IYUNIVESITHI YASEKAPA • UNIVERSITEIT VAN KAAPSTAD

Combustion Characteristics of Synthetic Gasoline in Modern Charge Boosted GDI Engines

Author:
T. Rockstroh

Thesis presented for the degree
Doctor of Philosophy

Sasol Advanced Fuels Laboratory
Department of Mechanical Engineering
University of Cape Town
June 10, 2015

Abstract

Sasols synthetically derived gasoline blending components have traditionally been combined predominantly according to process economics to formulate commercial fuel blends that meet in-house fit-for-purpose requirements and the legislated fuel specifications in South Africa. In this study the potential for optimisation of a fuel blend using full boiling range synthetic blending components to enhance its performance in a modern charge boosted gasoline direct injection engine was investigated.

An evaluation of detailed analytical fuel chemistry data was conducted followed by laminar flame speed experiments in a constant-volume combustion bomb apparatus in order to characterise the combustion behaviour of the blending components according to their characteristic chemical properties. A matrix of test fuels was established by splash blending the synthetic components with a commercial synthetic reference fuel. The performance of the fuels was subsequently evaluated using a modern, charge boosted, single cylinder GDI research engine. While the engine operation was verified to be in the negative-K region using model fuel components, anomalies in defining the K-value using the synthetic blends were discovered.

A fuel blending model was composed to allow prediction of linear and non-linear fuel properties of user defined synthetic blend ratios. By integrating an engine performance test fuel scoring system, the model could be used to define optimal fuel blends through selection of a desired performance criterion while constraining the optimisation process to adhere to the national legislated gasoline specifications. Four final fuel blends were optimised according to best power output, gravimetric specific fuel consumption, volumetric specific fuel consumption and specific legislated emissions. A fifth blend was optimised for highest power output with no regard for fuel property specifications other than Reid vapour pressure.

The performance of the optimised blends was evaluated on the test engine and the results indicated the potential to positively affect the performance characteristics of a synthetic fuel blend for use in a modern spark ignition engine. This study demonstrates a methodology for optimisation of a synthetic fuel to user-selected performance criteria and it is believed that this work represents a novel and valuable contribution to this field.

Acknowledgements

I wish to acknowledge and thank the following people for their contributions and support of this project:

- I would like to express my sincere gratitude to my academic supervisors, Professor Andy Yates and Dr. Gareth Floweday for their astute technical guidance and encouragement throughout the course of this project. Our discussions covering technical matters and other global happenings were always most enjoyable and rewarding.
- Thank you to Mr. Marlan Perumal for always providing an answer to any coding related questions and for going out of his way to help me out when I was in dire straits while attempting to compile this document.
- The workshop of the Department of Mechanical Engineering at the University of Cape Town, in particular Mr. Glen Newins and Mr. Hubert Tomlinson who delivered imperative assistance during the fabrication of the test cell equipment.
- Thank you to Mr. Mark Wattrus for providing valuable assistance in setting up the engine control unit.
- My gratitude is expressed to Mr. Dylan Smit and Mr. Victor Burger, for allowing me to use the laminar flame speed rig to conduct my tests as well as assisting with the experimental work and data interrogation. Thank you to Mr. Paul Schaberg for presenting the work at the SAE conference on my behalf.
- Dr. Faiza Khan, Dr. Rina van der Westhuizen and Dr. Riaan Bekker for conducting the complex chemical analysis of the fuel streams and data interpretation necessary for this study.
- Thank you to Mr. Gerhard Lourens, for all his help in and around the test cell. It is much appreciated.

- My fellow students at the Sasol Advanced Fuels Laboratory who have been a continuous source of stimulating technical discourse and general great times throughout this research.

- I am grateful for my family, as their continuous love and support has kept me going throughout this research journey.

- Lastly, this research would not have been possible without the required financial assistance. I would like to thank Mr. Paul Morgan, Senior Manager of New Energy and Mr. Nico Esterhuizen, Manager of Product and Application Development at Sasol for supporting me in this endeavor.

Table of Contents

List of Tables

List of Figures

Glossary of terms and abbreviations

A/D converter: A device that converts an analog signal (voltage) to a digital signal.
A/F ratio: The mass ratio of air to fuel present in the combustion chamber.
After-Bottom-Dead-Centre (ABDC): The crankshaft position when the piston has passed the BDC mark.
AI10: The duration of crankshaft rotation required to burn 10% of the air-fuel mixture.
AI50: The duration of crankshaft rotation required to burn 50% of the air-fuel mixture.
AI90-AI10: The crankshaft duration between the mass fraction of 10% burned until 90% burned.
Alkane: Organic molecule consisting of carbon and hydrogen connected by single bonds.
Alkene: A class of hydrocarbon consisting only of carbon and hydrogen containing at least one carbon-to-carbon double bond.
α-olefin: Olefin with a double bond at the primary position.
APMAX: The crankshaft position when the maximum cylinder pressure is measured.
Aromatic: A class of hydrocarbon with alternating double and single bonds between carbon atoms that form a ring structure.
Aggregate Server Access Protocol (ASAP): High-availability transfer mechanism that provides data transfer over IP networks.
ASTM International: An organisation that develops international standards.
After-Top-Dead-Centre (ATDC): The crankshaft position indicating the position when the piston has passed the TDC mark.
AVL: Austrian company distributing powertrain research tools.
Before-Bottom-Dead-Centre (BBDC): The crankshaft position indicating the position of the piston before the BDC mark.
Bottom-Dead-Centre (BDC): The point of engine crankshaft rotation when the piston is furthest from the cylinder head and the combustion chamber volume is at its maximum value.
Brake Mean Effective Pressure (BMEP): A comparative measure of engine torque output given by the engine crankshaft measured cycle work divided by the displaced cylinder volume.
Before-Top-Dead-Centre (BTDC): The crankshaft position indicating the position

of the piston before the TDC mark.

Crank Angle (CA): The crankshaft angle position.

Computer-aided design (CAD): Computer assisted design software.

Commercial Automotive Gasoline (CAG): Commercially available fuel for spark ignition engines.

Crude Commercial Automotive Gasoline (CCAG): Commercially available crude oil derived fuel for spark ignition engines.

Carbon dioxide (CO2): Naturally occuring chemical compound consisting of two oxygen atoms that are covalently double bonded to a carbon atom.

Compression Ratio (CR): The volume ratio of the combustion chamber given by the volume at BDC divided by the volume at TDC.

Computational Fluid Dynamics (CFD): The study of fluid mechanics using numerical methods and algorithms to analyse fluid flow problems.

Co-operative Fuels Research (CFR) engine: The engine required and used for the determination of Research and Motor Octane Numbers, RON and MON respectively.

Coefficient Of Variation (COV): A standardised measure of variability defined as the ratio of standard deviation to the mean expressed as a percentage.

Coordinating Research Council (CRC): A non-profit organisation that is supported by the petroleum and automotive industry.

Coal To Liquid (CTL): An automotive fuel derived from coal.

Cycloalkanes: A subclass of alkanes that have one or more rings of carbon atoms in the chemical structure.

Distributed Component Object Model (DCOM): A Microsoft technology that allows communication of software over a common distributed network.

Detailed Hydrocarbon Analysis (DHA): A gas chromatography technique used to define hydrocarbon classes in a fuel.

E20: A mixture of 20% Ethanol and 80% synthetic commercial gasoline.

E50: A mixture of 50% Ethanol and 50% synthetic commercial gasoline.

Engine Control Unit (ECU): Electronic device to control a series of actuators required to operate an internal combustion engine.

Exhaust Gas Temperature (EGT): Exhaust gas temperature measured in the exhaust manifold.

Equivalence ratio (ϕ): The ratio of a given fuel-air ratio to a stoichiometric fuel-air ratio. $\phi = 1$ is stoichiometric, $\phi < 1$ is lean and $\phi > 1$ is a rich mixture.

Exhaust Gas Recirculation (EGR): The method of external re-introduction of exhaust gas products into the inducted fuel-air mixture for combustion and/or emissions control.

F/A The mass ratio fuel to air present in the combustion chamber.

Fluid Catalytic Cracking (FCC): A chemical conversion process used in refineries to

convert heavy distillates into products such as gasoline.

Fluorescent Indicator Adsorption (FIA): Standard method according to ASTM1319 to determine the hydrocarbon types in a full boiling range fuel.

Flame Ionisation Detector (FID): A scientific instrument that used to measure the organic species in a gas stream.

Gas Chromatography-Mass Spectrometry (GC-MS): An analytical method used to identify different subclasses in fuel test sample by combining gas liquid chromatography and mass spectrometry.

Two-dimensional gas chromatography (GCxGC): An analytical method derived from GC-MS whereby two chromatography runs are implemented to differentiate the components more effectively.

Gasoline Direct Injection (GDI): A variant of a fuel injection method used to inject fuel directly into the cylinder.

Greenhouse gas (GHG): A gaseous mixture in the atmosphere that has the ability to absorb infrared radiation thereby confining the heat in the atmosphere.

Generalised Reduced Gradient (GRG): An algorithm in Microsoft Excel 2010 used for optimising non-linear problems.

Higher Heating Value (HHV): A measure of the gross heat energy released under standard ASTM D4809 conditions.

Heat of vaporization (ΔH_{vap}): The amount of heat that needs to be absorbed to vaporize a liquid at a constant temperature.

Homogeneous Charge Compression Ignition (HCCI): An engine technology where a nominally homogeneous air-fuel mixture is ignited by compression alone without the need of any additional ignition system.

High Performance Liquid Chromatography (HPLC): An analytical method used to identify different subclasses in fuel test sample.

High Temperature Fischer-Tropsch (HTFT): Proprietary technology of Sasol used to produce syncrude from syngas.

Hydrocarbon (HC) emissions: Engine exhaust emissions consisting usually of partially oxidised species of hydrocarbon radicals and molecules.

ifile A file format defined by the AVL company used for data storage in their combustion analysis tools.

Internal Gas Recirculation (IGR): Internal recirculation of exhaust gas in a internal combustion engine.

Indicated Mean Effective Pressure (IMEP): A comparative measure of indicated work output per unit swept volume.

Internal Combustion Engine (ICE): A thermodynamic heat engine that releases heat via a chemical combustion process inside the combustion chamber of the engine device.

Indicated Specific Carbonmonoxide (ISCO): Carbon monoxide emissions calcu-

lated on the basis of the indicated power output of the engine.
Indicated Specific Fuel Consumption (ISFC): Specific fuel consumption calculated on the basis of indicated power output.
Indicated Specific Hydrocarbon (ISHC): Hydrocarbon emissions calculated on the basis of the indicated power output of the engine.
Indicated Specific Nitrous Oxide (ISNOx): Nitrous oxide emissions calculated on the basis of the indicated power output of the engine.
Knock Limited Spark Advance (KLSA): The maximum spark advance before knocking combustion starts occurring.
(lambda or λ): The ratio of a given A/F ratio to a stoichiometric A/F ratio. $\lambda = 1$ is stoichiometric, $\lambda < 1$ is rich and $\lambda > 1$ is a lean mixture.
Laminar Flame Speed (LFS): The speed at which an un-stretched laminar flame propagates through a quiescent mixture.
Lower Heating Value (LHV): A measure of the net heat energy released under standard ASTM D4809 conditions.
Low Speed Pre-Ignition (LSPI): The undesired ignition of the air/fuel mixture in a gasoline engine before the spark is released.
Low Temperature Fischer-Tropsch (LTFT): Proprietary technology of Sasol used to produce syncrude from syngas.
Mass Fraction Burned (MFB): A measure of the fraction of charge burned in the cylinder at a specific crank angle position.
Maximum Brake Torque (MBT): The maximum brake torque produced by a spark ignition engine at optimal spark advance with wide open throttle.
Mega-knock: A severe form of engine knock, also known as super-knock, which has been found to occasionally occur in highly charge boosted SI-engines. **Motor Octane Number (MON)**: A standard test method (ASTM D 2700) for ascertaining the octane rating of a fuel. This method requires running the fuel at 900rpm in a CFR engine with a heated inlet air temperature.
Methyl tert-butyl ether (MTBE): An oxygenate used as a gasoline additive to enhance the octane number. **Naphthene**: Another term for a cycloalkane.
New European Driving Cycle (NEDC): A standard driving cycle used to assess the fuel consumption and emission levels of a passenger car.
Nitrous oxide (NOx): The regulated emission combination of NO and NO2 formed during combustion at high temperatures.
Nuclear magnetic resonance (NMR): An analytical method used to destinguish classes and sub-classes in a chemical compound such as gasoline.
Olefin: Another term for an alkene.
Original Equipment Manufacturers (OEMs): Manufacturer of vehicles and engines.
Oxygenate: A fuel additive that contains oxygen as part of its chemical structure.

Paraffins: Another term for an alkane.
Port Fuel Injected (PFI): A variant of a fuel injection method used to inject fuel into the intake manifold of the cylinder.
PMAX: The maximum cylinder pressure measured.
Primary Reference Fuels (PRFs): Iso-octane and n-heptane are the two fuels used to define the octane rating of a test fuel in the Research and Motor Octane test methods (ASTM D2699 and ASTMD2700 respectively). Iso-octane is defined as having an octane number of 100, while n-heptane is defined as having an octane number of zero. The octane rating of a PRF blend is determined by linear interpolation of the respective volumetric concentrations.
Reformed Exhaust Gas Recirculation (REGR): Recirculated exhaust gas that is passed over a reforming catalyst before being reintroduced into the combustion chamber.
Research Octane Number (RON): A standard test method (ASTM D 2699) for ascertaining the octane number of a fuel. By running the fuel in a CFR engine at standard knock intensity at 600 rpm, the test fuels are bracketed using PRF blends.
Reid Vapor Pressure (RVP): A standard method used to measure the volatility of a gasoline fuel according to ASTM D323.
rpm: Engine speed in crank angle revolutions per minute.
Spark Advance (SA): The crankshaft position in relation to TDC on the compression stroke at which point the spark is released.
South African National Standard (SANS): National standard by the South African Bureau of Standards.
SBA20: A mixture of 20% synthetic blend A and 80% synthetic commercial gasoline.
SBA50: A mixture of 50% synthetic blend A and 50% synthetic commercial gasoline.
SBB20: A mixture of 20% synthetic blend B and 80% synthetic commercial gasoline.
SBB50: A mixture of 50% synthetic blend B and 50% synthetic commercial gasoline.
SBC20: A mixture of 20% synthetic blend C and 80% synthetic commercial gasoline.
SBC50: A mixture of 50% synthetic blend C and 50% synthetic commercial gasoline.
SBD20: A mixture of 20% synthetic blend D and 80% synthetic commercial gasoline.
SBD50: A mixture of 50% synthetic blend D and 50% synthetic commercial gasoline.
SBE20: A mixture of 20% synthetic blend E and 80% synthetic commercial gasoline.
SBE50: A mixture of 50% synthetic blend E and 50% synthetic commercial gasoline.
SBF20: A mixture of 20% synthetic blend F and 80% synthetic commercial gasoline.
SBF50: A mixture of 50% synthetic blend F and 50% synthetic commercial gasoline.
SB-IMEP: Synthetic gasoline blend optimised for peak IMEP.
SB-ISFCM: Synthetic gasoline blend optimised for peak ISFC on a gravimetric basis.
SB-ISFCV: Synthetic gasoline blend optimised for peak ISFC on a volumetric basis.
SB-PP: Synthetic gasoline blend optimised for peak power output. The optimisation process for this blend did not consider fuel specification other than RVP.

SCAG: Synthetic commercial automotive gasoline.
Specific Energy Gravimetric (SE-G): Specific energy calculated on a gravimetric basis.
Specific Energy Volumetric (SE-V): Specific energy calculated on a volumetric basis.
Specific Fuel Consumption (SFC): A measure of the fuel efficiency with regard to the power output.
Supercritical fluid chromatography (SFC): An analytical method used to separate and quantify chemical components in a substance.
Spark-ignition (SI) engine: An ICE that ignites the fuel-air mixture with the aid of an electric spark plug. SI engines usually run on gasoline like fuels and combustion is controlled by the timing of the spark discharge.
Spark-ignition engine knock: An abnormal and potentially damaging combustion phenomenon where the unburned mixture within the cylinder is compressed by the piston and advancing flame front to the point of auto-ignition before it is consumed by flame propagation.
T20: A mixture of 20% TAME and 80% synthetic commercial gasoline.
T50: A mixture of 50% TAME and 50% synthetic commercial gasoline.
tert-Amyl methyl ether (TAME): An ether that can be used as a fuel oxygenate.
Top-Dead-Centre (TDC): The point of engine crankshaft rotation when the piston is closest to the cylinder head and the combustion chamber volume is at its minimum value.
Toluene Standardization Fuel (TSF): A fuel blend consisting of toluene and n-heptane or iso-octane.
Ultraviolet-visible spectroscopy (UV/VIS): An analytical method used to analyse components separated by SFC.
Variable Turbine Geometry (VTG): Exhaust gas turbocharger with variable guide vanes on the turbine that are used to control boost pressure.

Chapter 1

Introduction

This chapter introduces the reader to the thesis and illustrates the relevance of the conducted research. An outline of the thesis document structure is provided.

1.1 Background

A growing public awareness of the environmental implications of vehicle green house gas (GHG) emissions as well as increasingly stringent legislations over the last decade, have forced vehicle original equipment manufacturers (OEMs) to develop more efficient power-trains. In order to meet vehicle fleet CO_2 emissions as well as customer demand for lower fuel consumption while at the same time offering improved vehicle performance, OEMs have turned to electrification of the power-train as well as various other technologies to efficiently extract more performance out of internal combustion engines. For the spark ignition (SI) engine there has been a trend towards the implementation of direct fuel injection in combination with charge air boosting together with a reduction in engine capacity.

Fuel manufacture and engine technology have always been interrelated. Today an overall well-to-wheel life cycle analysis is prudent in the assessment of the GHG emissions and energy use of the vehicle transport sector. Long before environmental regulations, this relationship was evident in the steady increase of the octane rating of fuels witnessed from 1920 until 1955 thereby leading to significant improvement in engine efficiency and performance [1]. From 1947 till 1996 the coordinating research council (CRC) in the USA performed regular surveys to assess the octane requirement of the vehicle fleet to allow fuel manufacturers to refine their products accordingly [2]. With the advent of knock sensors and closed loop control on vehicles these annual investigations were adjourned. Moreover it has recently been shown that the motor octane number (MON) test, which

was originally intended to represent carburetted engines has an almost counter-intuitive influence in modern high performance engines inasmuch that gasolines with a given research octane number (RON) and a higher octane sensitivity (i.e lower MON) exhibit an enhanced knock resistance [3, 4]. Fuel components with higher laminar flame speed have been shown to provide performance benefits in spark ignition engines [5] and the latent heat of vaporization can have a profound effect on knock reduction and cylinder filling, especially in gasoline direct injection (GDI) engines [6]. These fuel related issues will be comprehensively discussed in this thesis.

Modern highly boosted spark ignition engines have been shown to exhibit abnormal combustion, which is currently being investigated by fuel [7, 8] and engine manufacturers [9, 10] alike. Current and future emission legislations ultimately need to be met by the OEMs who burn the fuels in their engines. It therefore places some technical demand on the fuel to enable clean combustion. This has cost implications for the fuel producers to adjust their refining processes as was evident in the phasing out of octane enhancing heavy metals [11].

The South African automotive fuels market is unique in terms of the vehicle parc it caters for and the technology used for locally produced transportation fuels. Vehicle technologies range from older pre-emissions legislation, to modern latest generation engine technology. While most of the fuel is produced in conventional crude oil refineries, about a third of the country's fuel is produced in Sasol's coal to liquid (CTL) high temperature Fischer-Tropsch (HTFT) plant. The HTFT plant was instigated following the 1973 "oil crisis" as a means to provide energy security for South Africa [11]. Coal is gasified to provide syngas (mixture of carbon monoxide (CO) and hydrogen (H_2)) which is then processed to syncrude using Sasol's proprietary Fischer-Tropsch technology. The olefin rich syncrude is further refined to formulate gasoline, among other fuels and chemical products. Most of this fuel is distributed to the inland area which houses the majority of the vehicle population at about 1500 m above sea level. The only other high-altitude locations in the world with such a notable vehicle density are Colorado and Mexico [12]. Historically Sasol conducted fit-for-purpose studies in order to identify the fuel requirements of the diverse vehicle population [13], while currently various CTL refinery streams are combined to meet the South African fuel specification (SANS1598-2006) in the most economical way while maintaining fit-for-purpose attributes.

1.2 Project motivation

In this thesis the reference to engine performance encompasses the maximum available work output at a given engine speed, gravimetric specific fuel consumption (as an indi-

cation of thermodynamic efficiency), volumetric specific fuel consumption and legislated exhaust emissions. The direct effect of fuel composition on engine power and efficiency during normal combustion in SI-engines is generally considered to be relatively small [1]. However, fuel composition can affect non-combustion related properties of a fuel, such as volatility and heat of vaporisation, which in turn can directly influence the performance of a gasoline engine. Researchers of racing fuels have shown that the power output of an engine is affected by the fuel's specific energy content, stoichiometric air to fuel ratio, molar products to reactants ratio, latent heat of vaporisation as well as its resistance to knock [14,15]. Additionally it has been accepted that a high burn rate improves the thermodynamic efficiency and reduces the knock propensity [5,16]. Apart from the turbulence intensity and mass flow in the cylinder, the burn rate is influenced by the characteristic laminar flame speed of the air-fuel mixture [17].

The performance characteristics of fuel components need to be considered in the context of prevailing fuel legislations which affect the fuel composition through restrictions on components such as benzene, sulphur and additives [18]. Aromatic components generally have a high density which positively influences the volumetric fuel consumption as it also inclines to correlate with the energy content of the fuel. However, due to its negative impact on deposit formation and regulated emissions the aromatic content in gasoline has been restricted to 50% for a category 1 fuel such as in South Africa, according to the Worldwide Fuel Charter [18]. Due to their reactive nature, olefins have been shown to contribute to ozone formation, predominantly through evaporative emissions rather than regulated engine exhaust emissions. In recent times, on-board vapour recovery systems on vehicles and at filling stations have minimized this problem [18]. However, olefins have also been linked to deposit formation in the intake system of an engine [19].

With the advent of knock control technology a significant improvement in engine efficiency has been achieved, as it allowed engine designers to optimise the compression ratio and ignition timing for part load conditions, which form the predominant part of the New European Driving Cycle (NEDC) driving cycle, while tolerating non-optimal knock limited operation at full load. This fuel related restriction has ironically also provided the opportunity for fuel composition to affect the maximum power performance and efficiency of an engine. GDI technology has been shown to create further scope due to its effect on mixture temperature and homogeneity [20], while charge boosted GDI further accentuated the effects of fuel compositional variations on the knock resistance outside the envelope of the octane rating method [4].

It is likely that the potential for varying the fuel composition in a synthetic refinery is much greater than in a conventional crude oil refinery although this has never been published in the context of its possible effects on engine performance. From the above points it follows that a modern, charge-boosted GDI engine would represent the best

candidate for investigating the possible performance variations that could be viable within the allowable blending envelope of a synthetic fuel refinery and thereby provide scope for optimisation. While it is recognised that the occurrence of abnormal combustion such as low speed pre-ignition (LSPI) often resulting in mega-knock or super-knock is of great importance when considering the fuel requirements of future highly charge-boosted GDI engines, this project pertains to fuel performance affects on current production engines. However, due the importance of LSPI a literature review has been included in order to be vigilant of any associated fuel property concerns.

The effect of a fuel's laminar flame speed has previously been studied in the context of performance in port fuel injected spark ignition engines [5]. It was acknowledged by the authors that the study should be conducted using more modern technology, but an investigation using a charge-boosted GDI engine has not been published thus far. Similarly the laminar flame speeds of blending components in a synthetic fuel refinery recently published by the author [21] represents an unexplored area for influencing engine performance.

1.3 Hypothesis foundation

It was hypothesised that the chemical composition of HTFT gasoline would be different from crude derived gasoline and that the HTFT blending components would exhibit a widely differentiated span in their individual properties. These distinct chemical properties of the fuels were presumed to have a distinguishable influence on their laminar flame speed characteristics. Furthermore, it was assumed that the chemical attributes would result in a measurable influence on engine performance which would correlate with fundamental fuel property measures such as flame speed, charge air cooling and octane number.

Finally it was envisaged that it would be possible to establish an effective fuel blend optimisation model, using engine test data of the fuel blending components, to produce a final product tailored to offer customers improved performance and fuel economy in a modern gasoline engine, while adhering to the prevailing fuel specifications.

1.4 Project scope

In order to test the above postulates, the project was formulated with the following process steps:

- A literature study was conducted to obtain information about the refining process of HTFT syncrude into gasoline products as well as the chemical characteristics of synthetic gasoline. Furthermore the recent changes in engine technology and fuel formulation issues that have been shown to impact engine operation were reviewed.
- Samples of eight synthetic gasoline blending components, a synthetic commercial automotive gasoline (SCAG) as well as two crude derived commercial automotive gasolines (CCAG) were obtained. A detailed property and chemical composition analysis was conducted on the fuel samples and the results were studied in detail.
- The laminar flame speed of the commercial automotive gasolines (CAG) as well as the synthetic blending components were characterized using an in-house flame speed rig. Using the detailed chemical analysis data, a correlation analysis was conducted to relate the flame speeds to chemical composition with comparison to relevant literature.
- Using SCAG as a base fuel, each of the synthetic components were binary-blended in pre-defined ratios. The SCAG was used as the reference fuel for comparison.
- The experimental process was carried out on a single cylinder research engine representative of current modern charge boosted GDI engines. Full load spark advance sweeps were conducted to evaluate the performance and specific fuel consumption attributes of the fuels in terms of knock limited spark advance (KLSA) and burn rate. Furthermore, the EGR tolerance of the fuels was investigated under full load conditions, due to its increased use by engine designers to reduce knock tendency and exhaust gas temperatures.
- Due to the engine's limited peak firing cylinder pressure of 100 bar, the opportunity for this study to include abnormal combustion leading to mega-knock occurrence was limited and was not the focus of this research. However, combustion events were continually monitored and relevant control system parameters were in place to prevent possible engine destruction.
- From the insights gained from the engine tests, laminar flame speed tests and chemical analysis work, a multidimensional bounded blend recipe solving model was established to define optimised synthetic gasoline blends based on peak performance and specific fuel consumption.
- The optimised fuel blends were evaluated on the test bench in terms of the defined performance criteria.
- Finally the insights gained from the overall investigation were harvested and recommendations for further research were made.

1.5 Thesis document overview

The thesis document begins with an introduction to the background that led to the initiation of this study. This is followed by the project motivation, hypotheses and definition of the project scope.

Chapter two introduces the reader to the experimental apparatuses and modelling tools that were utilised for this study.

The third chapter provides a relevant literature review on current synthetic gasoline and discusses the refinery blending components that were used for this research. Detail about the chemical characterization of the synthetic commercial automotive gasoline (CAG) fuel and blending components is given and the test fuels are established.

With reference to a recently published study by the author and co-workers, chapter four provides further details about the investigation into the laminar flame speed behaviour of synthetic gasoline components.

In order to gain insight on the recent developments in charge boosted GDI engine technology, a literature review is conducted in chapter five. A detailed description of the test method used for the combustion analysis investigation is given and the performance results are presented and discussed.

Chapter six describes the methods used to define optimised synthetic fuel blends. The optimization criteria is discussed and performance results are shown. A burn rate analysis is presented with reference to effects from the unique synthetic components' characteristics. The results are discussed with the aid of a GT-Power model of the single cylinder engine.

The results and discussions of chapters three to six are related to the overall thesis hypothesis and scope and concluded in chapter seven.

Chapter eight provides relevant recommendations for future work.

Chapter 2

Experimental apparatus and modelling tools

This chapter provides an overview of the experimental apparatuses used for this study. Relevant equipment, designed or customised by the author for this research, are explained in greater detail.

2.1 Laminar flame speed combustion bomb

The laminar flame speed rig was initially developed by Yates and co-workers [22] for the analysis of jet fuel components. Modifications to improve the valve actuator control and spark ignition system have resulted in a new bomb being designed and manufactured for a current post-graduate project. This rig was subsequently used to characterize the laminar flame speed behaviour of synthetic gasoline components as reported by Rockstroh et. al. [21]. With the aid of the schematic in figure 2.1, the experimental apparatus will be briefly explained.

The combustion chamber of the laminar flame speed rig is a spherical vessel of 100 mm diameter manufactured from stainless steel. It is equipped with band heaters to maintain air temperature up to 200 $^{\circ}C$ to within an accuracy of 0.5 $^{\circ}C$. Fuel was supplied to the combustion chamber by means of a modified automotive GDI solenoid injector. To avoid the risk of condensation in the bomb, due to a potential cold spot near the injector, a heating/cooling circuit was used to maintain the injector at a specified temperature. The appropriate control temperature was defined by creating a lean A/F mixture and then checking the ability to ignite it after a delay period. With an injector tip temperature of 90 $^{\circ}C$, a waiting period of up to an hour did not adversely affect the ignition of the mixture. The injected fuel quantity of each fuel was calibrated by defining the fuel mass

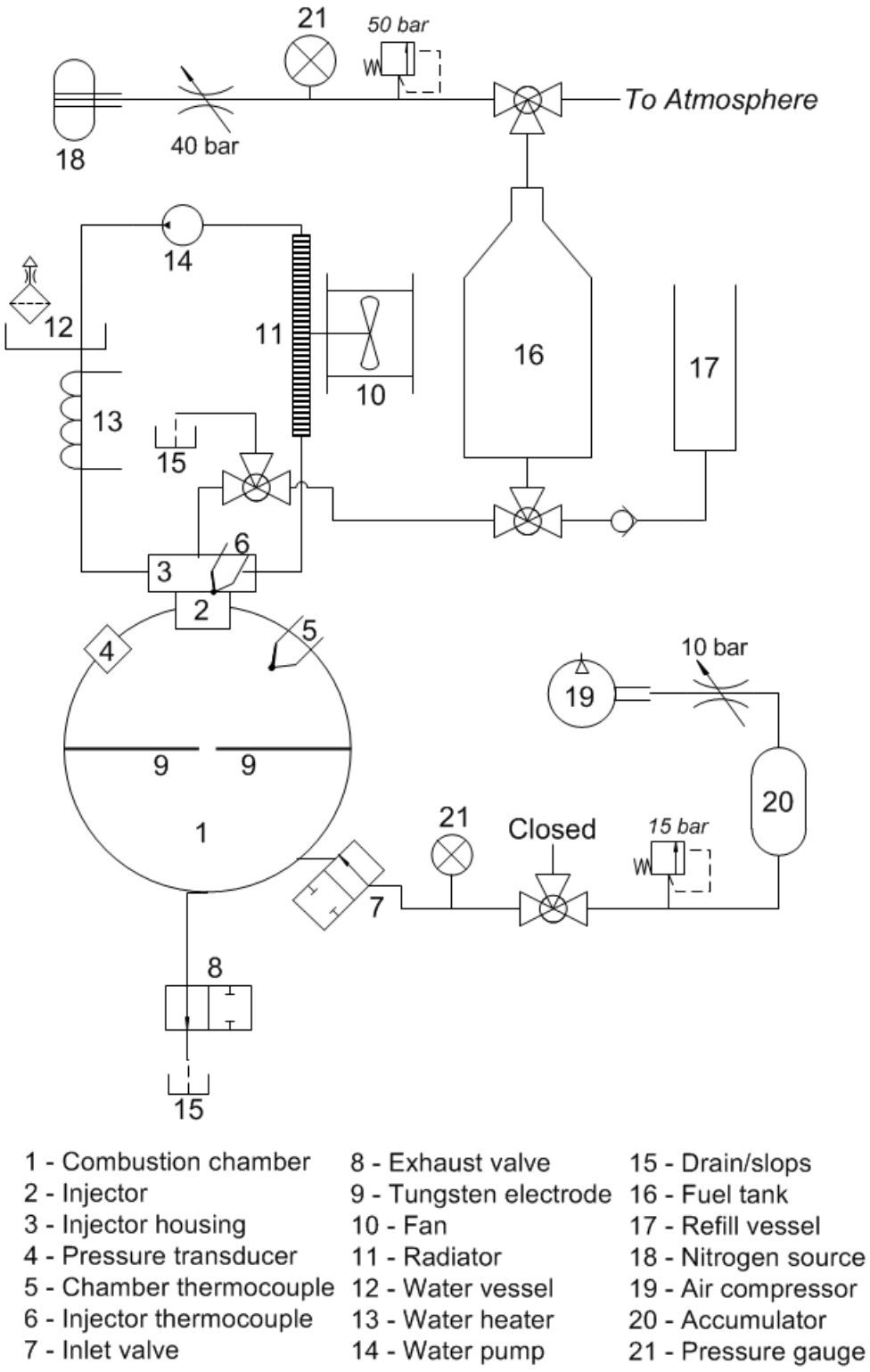

Figure 2.1: *Schematic of laminar flame speed rig*

at numerous injection durations. Fuel pressure was accurately maintained by supplying nitrogen to a pressurised container above the fuel.

Ignition was provided by two electrodes extending into the centre of the combustion chamber. An uncooled GH14D AVL piezo-electric pressure transducer was used to measure the chamber pressure and a strain gauge based pressure transducer, separate from the filling air supply line, supplied the absolute pressure reading.

Compressed air supply at 10 bar to the rig was used to purge and vent the combustion chamber via solenoid inlet and exhaust valves. Using a National Instruments CompactRIO control and monitoring system, the entire rig and data capturing process was automated. During the commissioning phase, the test sequences, event times as well as the required waiting periods were defined in order to enable adequate removal of burnt products and preparation of a homogeneous air-fuel mixture.

A summary of the method implemented to derive the laminar flame speed from the combustion pressure trace is provided in Appendix A.

2.2 Engine set-up

The planning of the test cell layout, design of various test cell ancillaries as well as the commissioning of the single cylinder engine was conducted by the author at the start of this research project.

2.2.1 Test engine

A new single cylinder AVL 5403 engine with a pent roof gasoline direct injection (GDI) cylinder head was obtained for this study. The spray guided injector as well as the spark plug were centrally mounted and an access port was provided to allow installation of a piezoelectric pressure transducer. The valves were operated by direct-attack of two overhead camshafts. Base specifications of the engine are provided in table 2.1

A cooled exhaust gas recirculation system was installed on the engine as shown in the schematic in figure 2.2. In order to limit inaccuracies in EGR flow rate due to pulsation, a 100 L vessel was installed ahead of the exhaust back pressure valve. The EGR flow was regulated by an EGR valve sourced from a VW 1.6L FSI engine while an EGR cooler from a Mercedes Benz C220 CDI engine was modified to suit this application.

Basic engine data	
Number of cylinders	1
Cylinder bore	$86mm$
Stroke	$86mm$
Swept Volume	$499.6cm^3$
Combustion chamber	4-valve pent roof GDI
Compression ratio	10:1
Fuel system	GDI piezo spray guided injector (BMW)
Ignition system	NGK spark plug, pencil coil (VW)
Rated speed	6000 rpm
Maximum speed	7000 rpm
Maximum cylinder pressure	100 bar
Balancing shafts	$1^{st}order$
Valve Timing	
Inlet valve open	34°BTDC
Inlet valve close	54°ABDC
Exhaust valve open	74°BBDC
Exhaust valve close	14°ATDC
Inlet valve peak lift	110°ATDC
Exhaust valve peak lift	110°BTDC
Camshaft duration	268°crank angle

Table 2.1: *Specifications of single cylinder research engine*

2.2.2 Test cell equipment

The engine was mounted on a fully instrumented test bed to an asynchronous dynamometer as shown in figure 2.3. Operational control, algorithm programming and data capturing of all relevant test parameters was provided by the software package STARS from Horiba.

An external conditioning unit for the engine oil and coolant was developed and manufactured by the author. This unit enabled accurate control of the supply pressure and temperature for both the engine oil and coolant.

Emissions were monitored by a Horiba Mexa 7200D gas analyser. Standard regulated emissions such as hydrocarbons (HC), carbon monoxide (CO) and oxides of nitrogen (NO_x) as well as carbon dioxide (CO_2) and oxygen (O_2) content were recorded.

In order to accurately control the supply air boost pressure and temperature, a charge air boosting system, consisting of an external compressor, water/air intercooler and an electric air heater was designed and installed in the test facility.

The engine was supplied with fuel from an external high pressure fuel pump unit rated to 200 bar. Fuel temperature was regulated and consumption was measured by an AVL

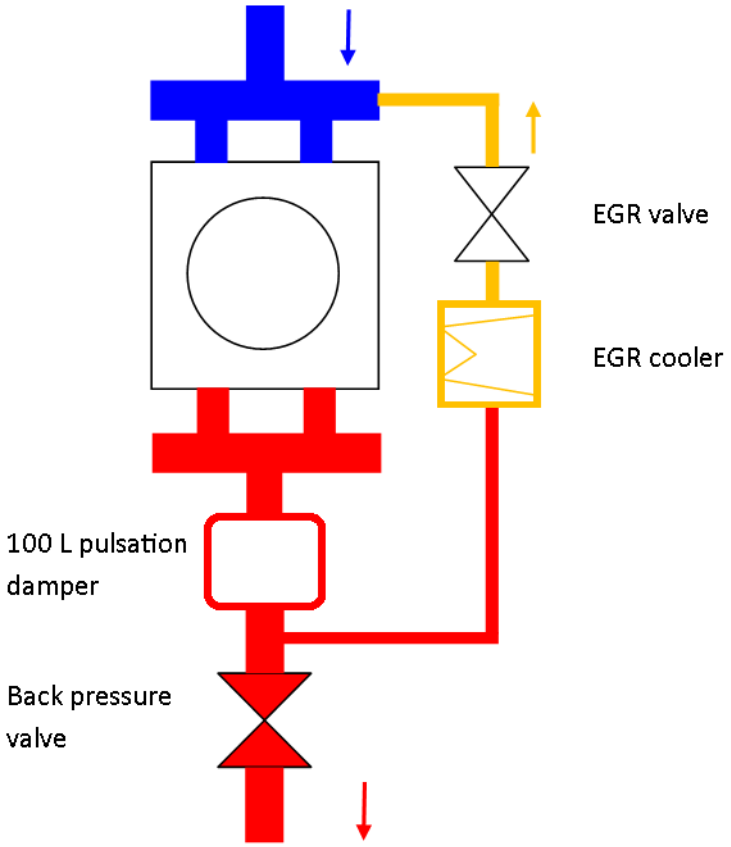

Figure 2.2: *Schematic of cooled EGR loop*

735/753 fuel mass balance and conditioning unit.

2.2.3 Engine control system

The engine control unit (ECU) was built on the foundation of a National Instruments CompactRio system, making use of Drivven modules to control the various actuators and read sensor feedback signals. Labview, a graphical programming language, was used to build the engine control program and graphical user interface as seen in figure 2.4. Proportional integral differential control loop feedback was implemented for the pressure systems, exhaust gas recirculation as well as lambda control. Provision was made to allow for the storage of operation point dependent calibration maps of key engine control parameters. The aggregate server access protocol (ASAP) was used to interface with the STARS test cell control software in order to allow capturing of relevant ECU data as well as activation of safety shut down sequences.

In order to protect the engine from excessive peak cylinder pressures, an interface with the indicating equipment was provided to enable a safety shut down by cutting the fuel injector signal.

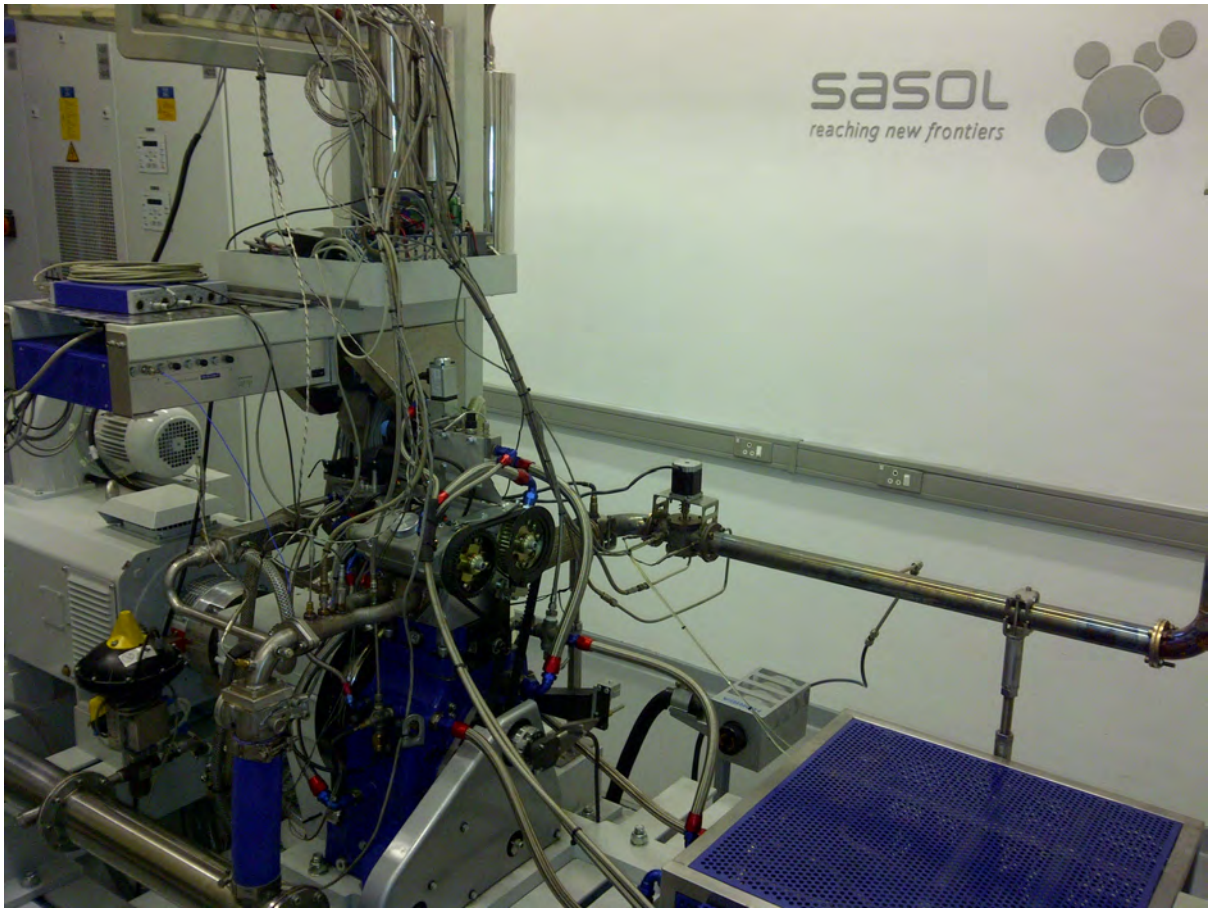

Figure 2.3: *Instrumented engine test bench*

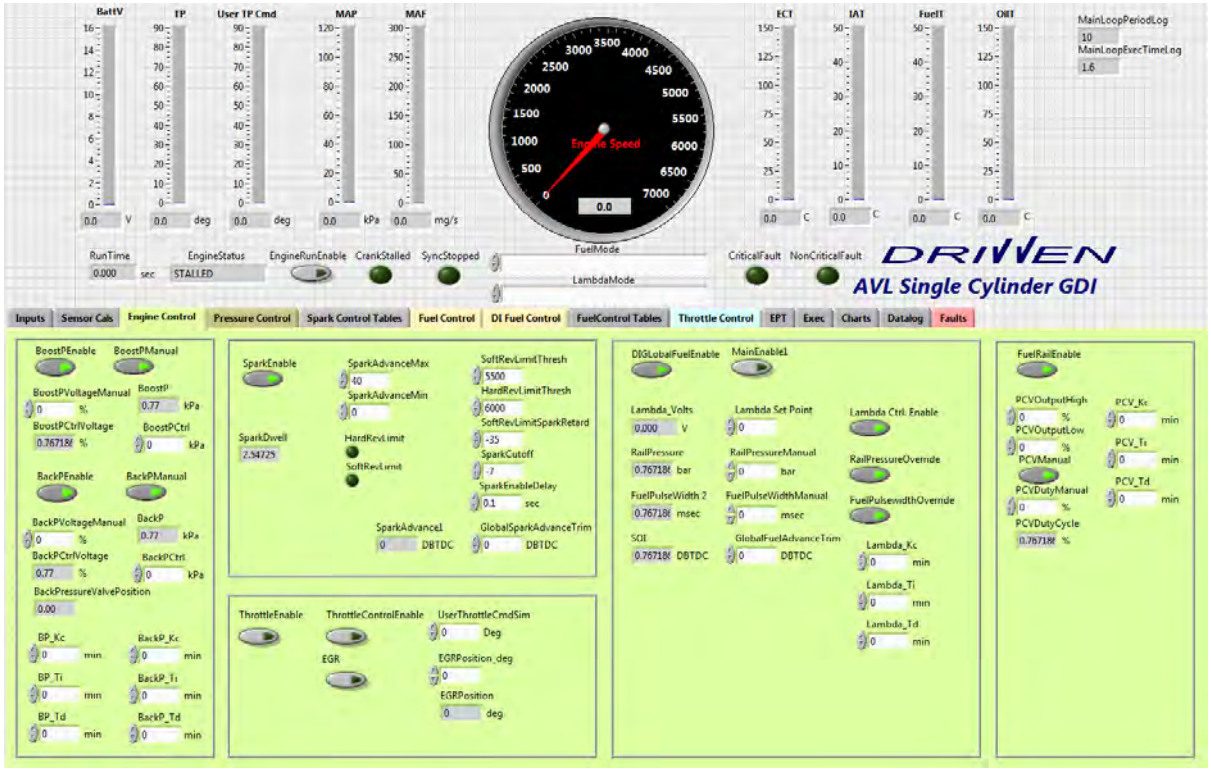

Figure 2.4: *Graphical user interface of engine control unit*

2.2.4 Indicating equipment

An AVL GU22C piezo-electric uncooled pressure transducer was installed in the cylinder head and Kistler 4075 A10 piezo resistive transducers were installed on the inlet and exhaust manifold respectively. The exhaust transducer was protected from excessive heat load using a water cooled adapter. The pressure signals were amplified using an AVL MicroIfem charge amplifier and recorded using the AVL indicating tool Indismart together with the combustion analysis software AVL IndiCom 2.4. At regular intervals the calibration of the measurement chain (pressure transducer-charge amplifier-A/D-converter) was checked using a dead weight tester.

Thermodynamic data, such as indicated mean effective pressure (IMEP) and mass fraction burned (MFB) were calculated at a resolution of 1 °crank angle, while knock detection measurements were calculated at 0.1 °crank angle resolution in Indicom. A distributed component object model (DCOM) protocol was used to transfer the average data to the STARS software. Due to the low data transfer rate, detailed analysis of the combustion data necessitated the interrogation of the Indicom data recorded in AVL's ifile format.

2.3 Modelling tools

2.3.1 Heat release analysis

The open source combustion analysis software (catool) was used to import the combustion (AVL ifile) data into Matlab to allow post processing. For detailed burn rate and heat loss analysis calculations the commercial software TIGER was used [23].

The burn rate (Qb) was calculated using the first law of thermodynamics, the ideal gas law and the energy balance. Other than calculating the change in internal energy (U) and volume (V) with respect to crank angle, the wall heat losses (Q_w) as well as the energy loss due to leakage (H_L) was taken into account.

$$\frac{dQb}{d\theta} = \frac{dU}{d\theta} - \frac{dQ_w}{d\theta} + p\frac{dV}{d\theta} - \frac{dH_L}{d\theta} \tag{2.1}$$

For the energy balance, the fuel mass flow rate and exhaust products were considered. Further detailed discussion on the heat release method used for the thermodynamic analysis of the engine combustion data is provided in chapter 6.

2.3.2 GT-Power modelling tool

An elementary model of the single cylinder engine was generated using GT-Power by Gamma Technologies as is shown in figure 2.5. More details about engine modelling with this software is provided in [24].

The single cylinder engine manufacturer provided geometry data of the single cylinder engine, some of which is shown in table 2.1. The piston bowl geometry as well as the surface area of the piston and cylinder head were taken from a CAD model of the top end of the engine. The required valve lift profiles and camshaft timing angles were also provided by the engine manufacturer. Measurements of the intake and exhaust manifold were taken and entered in the model while the surface finish was estimated using the equivalent roughness values from the drop down menus in GT-Power. Charge air boosting was provided by merely raising the ambient pressure of the initial state conditions. The initial cylinder head, piston and cylinder temperatures were estimated using the default values provided in GT-Power and the recommended WoschniGT heat transfer model was chosen. The default cylinder flow sub-model with the standard parameters was used, while combustion was simulated using the predictive spark-ignition turbulent flame ('EngCylCombSITurb') model available in GT-Power. While the default parameters were chosen where possible, further details about the rate of vaporisation assumptions for the model fuels will be provided in chapter 6 where the model was implemented.

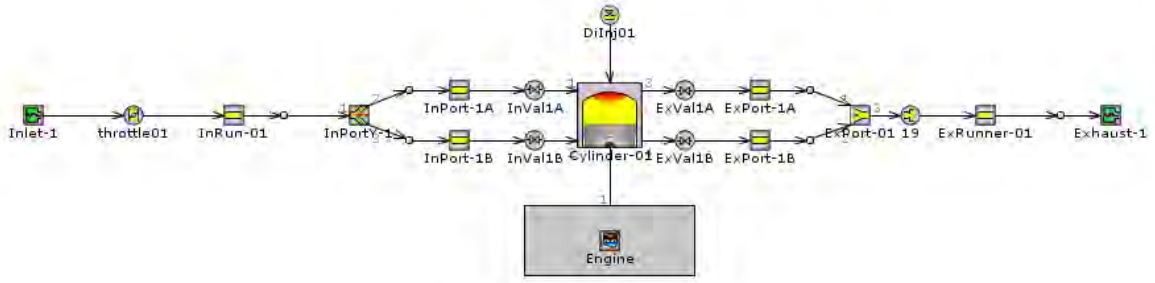

Figure 2.5: *GT-Power model of AVL single cylinder GDI engine*

Chapter 3

Synthetic gasoline and blending components

This chapter provides a brief overview on the development of modern synthetic gasoline. The chemical analysis of the refinery blending components is discussed and the test fuel blends are defined.

3.1 Literature review on synthetic gasoline

Historical key development aspects of the Fischer-Tropsch refining process have been described rigorously by de Klerk [11, 25]. Detailed discussion on the intricacies of the refining processes is beyond the scope of this thesis. An overview to highlight the relevant differences between conventional crude oil and syncrude derived gasoline will be provided here with emphasis on HTFT gasoline used for the investigations presented in this thesis.

3.1.1 Fischer-Tropsch overview

According to de Klerk [11], the overall process can be described with the aid of a simplified flowchart on indirect liquefaction shown in figure 3.1. Three key procedures are required to convert the feedstock into a final product, with Fischer-Tropsch being the most common synthesis process used on an industrial scale. Although the process lends itself to a variety of feedstocks, large scale commercial production of synthetic fuel is currently only done using coal to liquid (CTL) and gas to liquid (GTL) Fischer-Tropsch refinery processes [11].

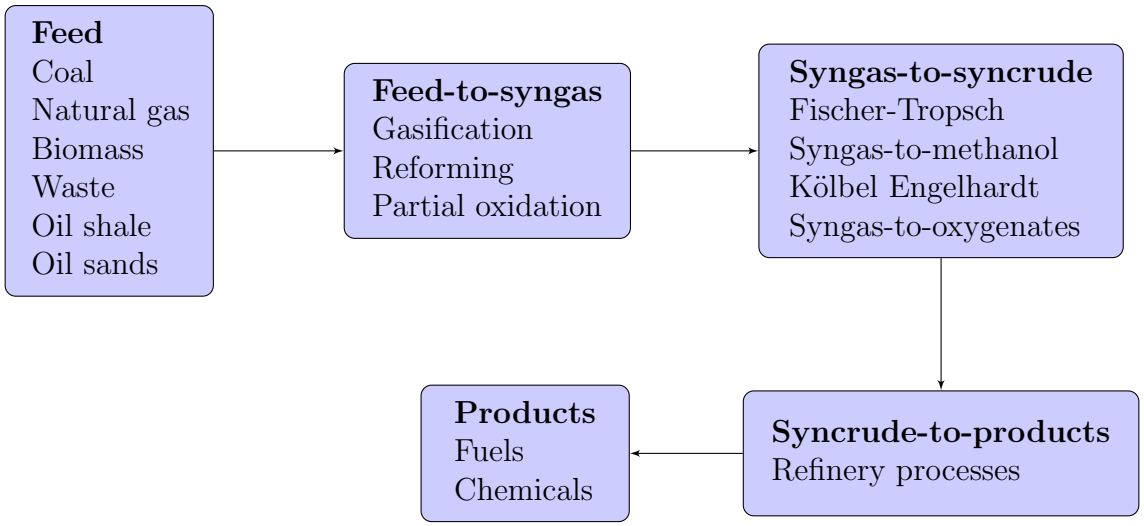

Figure 3.1: *Simplified definition of indirect liquefaction process for feed-to-liquids conversion. Adapted from [11]*

3.1.2 Syncrude vs crude oil

The conversion of syngas to syncrude can be done using what is known as high temperature Fischer-Tropsch (HTFT) or low temperature Fischer-Tropsch (LTFT) synthesis processes [11]. The composition of the resulting syncrude is different as shown in table 3.1 in comparison to a crude oil derivative.

Compound class	**HTFT[a]**	**LTFT[b]**	**Crude oil[c]**
Alkanes (paraffins)	$> 10\%$	Major product	Major product
Cyclo-alkanes (naphthenes)	$< 1\%$	$< 1\%$	Major product
Alkenes (olefins)	Major product	$> 10\%$	None
Aromatics	$5 - 10\%$	$< 1\%$	Major product
Oxygenates	$5 - 15\%$	$5 - 15\%$	$< 1\% O(heavy)$
Sulphur compounds	None	None	$0.1 - 5\% S$
Nitrogen compounds	None	None	$< 1\% N$
Organometallics	Carboxylates	Carboxylates	Phorphyrines
Water	Major by-product	Major by-product	0-2%

[a]Sasol Advanced Synthol (Secunda)
[b]Sasol Slurry Phase Distillate (SSDP) process (Ras Laffan and Sasolburg)
[c]Different crude oil types can vary significantly in composition

Table 3.1: *Comparison between composition of syncrude and conventional crude oil. Adapted from [11, 26]*

3.1.2.1 Crude oil

Conventional crude oil mainly consists of alkanes, cycloalkanes and aromatic hydrocarbon compound classes [11]. Alkenes are not found at all or in very small quantities [11], while dienes and alkynes generally do not appear in crude oil [27]. However, during the refining process of crude oil, such unsaturated aliphatic compounds are produced. Alkanes are commonly referred to as paraffins, cycloalkanes are also known as naphthenes and alkenes are frequently named olefins. These terms will be used interchangeable throughout this thesis. According to de Klerk [11], syncrude is similar to conventional crude in that it has a high linear hydrocarbon content which requires refining to improve the quality of the straight run products. Cycloalkanes in crude oil most often have five or six membered rings that appear as monocyclic and multicyclic compounds, while multicyclic compounds with four and five membered rings are occasionally found. On average the aromatic content of straight run naphtha is 10%, but varies depending on the crude oil used, while mono-, di-, and polynuclear aromatics can generally also be found in appreciable concentrations.

Sulphur content in most crude oils falls in the range of $0.05 - 6.0\%$ of mass, while generally $0.1 - 5\%$ mass can be expected [27]. Another undesirable heteroatom are nitrogen compounds which are most frequently found in crude oil fractions with a boiling point above 250 °C. Depending on the crude oil, the content can be as high as 2% mass but is generally lower than 0.5% mass [27]. The oxygenate concentration in crude oil range is quite low from 0.05% to 1.5% and mainly consists of furans, phenols, esters and carboxylic acids [27]. Only the organic acids can be of concern due to corrosion when it comes to crude refining.

Nickel and vanadium are the major metal impurities in crude oil with iron and other metals such as mercury and arsenic being present at a lower quantities [11]. Depending on the crude oil, the amount of metal may range from 1 to 1000 $\mu g.g^{-1}$. High metal content can lead to deposit formation on refining catalysts which reduces their life span.

3.1.2.2 HTFT and LTFT syncrude

Considerable energy is expended in crude refineries on the removal of heteroatoms such as sulphur and nitrogen while syncrude is intrinsically almost free from these species [11, 26, 28]. In addition the low polynuclear aromatic content further suggests that synthetic fuel could play a significant part in the continuous quest for cleaner fuels [29].

The significant oxygenate content in syncrude includes very useful components such as lubricity improving long chain carboxylic acids and high octane ethanol [26]. A major difference is the significant olefin content in syncrude [26, 29], which according to de

Klerk [26] provides refiners of syncrude with the ability to define synthetic products, whereas this capability is only available in crude refineries after olefin production in units such as fluid catalytic crackers (FCC).

The very high olefin as well as some aromatic content in HTFT syncrude, results in a higher octane for the straight run product than either LTFT syncrude or different cuts of Arabian crude oil as shown in table 3.2. The high linear paraffin as well as low aromatic content of LTFT syncrude do not result in a high RON, therefore making that product more suitable for Diesel production as is evident from the high cetane value of hydrogenated LTFT straight distillate [11, 26]. It was therefore argued that HTFT syncrude possesses intrinsically superior properties for the production of gasoline than crude oil.

According to de Klerk [26], the HTFT straight run product can be improved without difficulty by double bond isomerisation using a low temperature catalytic reaction. It was argued that the linear α-olefins in HTFT syncrude have a significantly lower octane number than the equivalent linear internal olefins, implying that there is significant potential for octane improvement. While 1-hexene has a low research octane number (RON) of 76.4 and motor octane number (MON) of 63.4, trans-2-hexene improves to RON of 92.7 and MON of 80.8. Further potential was expressed by the ability of double bond isomerisation at higher temperatures whereby octane improvement coincides with the removal of undesired oxygenates [26].

It is however apparent from table 3.2 that the HTFT straight run naphtha still needs significant refining in order to meet current gasoline fuel specifications. Refining processes such as oligomerization, hydrocracking, aromatization and hydrogenation have emerged over time to allow production of appropriate fuel components [29].

Property	**HTFT[a]**	**LTFT[b]**	**Arabian light crude**	
Boiling range (°C)	$20-105$	$20-100$	$20-80$	$80-180$
Fraction of total (%)	30	10	5	15
RON	68	43	61	24
Density[c] (kg m^{-3})	680	680	660	750
Olefins (%)	2	2	2	2
Aromatics (%)	2	0	2	14

[a]Synthol stabilised light oil
[b]SSDP cold condensate with oxygenates removed
[c]ASTM D4052 - 11

Table 3.2: *Comparison of the straight run naphtha properties of syncrude and crude oil. Adapted from [26]*

.

3.1.3 HTFT gasoline products

The Sasol HTFT refinery in Secunda produces a variety of product streams (value chains) consisting of different hydrocarbon components. After chemicals have been separated from these value chains, the resulting fuel streams are then blended in the proportions required to meet the relevant fuel specifications. The properties of the final fuel is influenced by the quantity and chemical characteristics of the fuel streams used [11,29]. When tetraethyl lead was used to improve octane up until December 2005 in South Africa, the refinery processes consisted mainly of distillation, hydrogenation and oligomerization of the olefins [29]. Kamara et. al. [29] further state that other than a small quantity of butane, HTFT components below C5 cannot be used in the final fuel blend and are therefore processed using alkylation, aromatization and oligomerization. The highly olefinic HTFT products lend themselves to carbon number distribution shifting by means of oligomerization [30–32], to produce heavier, reasonably branched olefins with high octane number thereby making them optimal blending components [29]. In order to address fuel stability, which is mostly dependent on mono- and diolefin concentration, hydrogenation of some olefinic components to paraffins may be necessary although this may cause a reduction in the octane value [29].

The key considerations for the refining process of straight run naphtha to gasoline are paraffin quality, octane number as well as the benzene concentration, while adhering to the restrictions placed on aromatic, olefin and oxygenate compound classes [26]. According to Kamara et. al. [29] the relatively low octane value of HTFT syncrude can be altered due to the high olefin content without much difficulty, by using processes such as skeletal isomerization with the option of etherification [33, 34]. Further octane improvement can be obtained by addressing the low degree of branching through use of skeletal isomerization of the paraffins [35, 36] as well as increasing the aromatic content through selective aromatization or reforming [37–39]. The α-olefins in syncrude are generally extracted for the production of chemicals, however double-bond isomerization is also an effective means to improve octane [29]. The octane number of Sasol's synthetic gasoline can further be improved effectively through the addition of ethers and ethanol from the HTFT process [11, 29].

3.2 Synthetic gasoline and blending components

3.2.1 Commercial automotive gasoline

A typical batch of synthetic 95 RON CAG fuel from Sasol's HTFT refinery in Secunda was used as the reference fuel for the investigations presented in this research project.

Additionally a typical crude derived South African 95 RON CAG as well as a 93 RON CAG fuel were analysed. The 93 RON fuel was included for this investigation since it is freely available in South Africa at altitudes above 1200 m. A standard analysis of the CAG fuels is presented in table 3.3.

Commercial fuel	95 RON SCAG	95 RON CCAG	93 RON CCAG	Specification SANS 342:2006
RON[a]	95.5	95.1	93.2	min. 93/95
MON[a]	85.7	85.2	83.6	min. 83/85
Density (kg/m^3)[b]	736.3	746.8	739.0	730 – 785
RVP (kPa)[c]	64	59	58	45 – 75
Paraffins (% Vol)[d]	40	33	54	NS[h]
Olefins (% Vol)[d]	20	23	14	NS
Aromatics (% Vol)[d]	37.9	44.5	31.7	max. 50
Benzene (% Vol)[e]	2	2.1	2.3	max. 5
Boiling range (°C)[f]	30.4 – 190.2	31.1 – 194.2	32.5 – 207.7	max. 65 - max. 215
Net heating value (MJ/kg)[g]	41.8	42.3	42.5	NS

[a] ASTM D2699-13b/ASTM D2700-14
[b] ASTM D4052 - 11
[c] ASTM D323-08(2014)
[d] ASTM D1319-14
[e] ASTM D3606 - 10
[f] ASTM D86-12
[g] ASTM D4809
[h] NS = not specified

Table 3.3: *Standard fuel specification analysis and heating value of 95 RON SCAG and 95/93 RON CCAG*

Since all fuels adhered to the fuel specifications, no major differences in the standard analysis were expected. It was however noted that the synthetic gasoline had a lower olefin content in comparison to the equivalent crude derived fuel. As synthetic gasoline is known to be inherently rich in olefin content due to the predominantly olefinic nature of HTFT syncrude, this discovery was surprising. However, syncrude can undergo significant refining with processes such as hydrogenation and skeletal isomerization to convert linear olefins into branched paraffins with improved octane [11, 29]. It was also found that the standard FIA method used for the detection of olefin, aromatic and paraffin content was subject to limitations and inaccuracies which are discussed in more detail in a following section. The net heating value is not regulated by specification but was found to be similar for all fuels.

3.2.2 Synthetic gasoline blending components

Eight synthetic gasoline blending components (SGBC), each exhibiting distinctly different properties, were chosen for the current investigation as shown in table 3.4. The blend

components are produced using Sasol's proprietary HTFT technology and have therefore been identified simply as SGBC A to F.

Blending component	SGBC A	SGBC B	SGBC C	SGBC D	SGBC E	SGBC F	Ethanol	TAME
RON[a]	84.1	97.6	93.2	76.8	98.4	92.5	109	112
MON[a]	82.2	82.4	84.1	70.5	86.1	78	90	98
Density (kg/m^3)[b]	731.1	722.5	779.0	802.1	812.5	646.9	789	744
RVP (kPa)[c]	40	42	52	25	29	115	20	19
Paraffins (% Vol)[d]	84	8	48	46	19	23	NA	NA
Olefins (% Vol)[d]	4	90	5	4	15	73	NA	NA
Aromatics (% Vol)[d]	12	1	47	50	66	4	NA	NA
Benzene (% Vol)[e]	4.4	1.5	2.7	20.7	14.2	0.0	NA	NA
Boiling range (°C)[f]	41.3 – 179.8	37.7 – 168.2	32.1 – 195.8	54.6 – 203.6	54 – 208	29.4 – 49.8	78	80.7 – 91.9
Net heating value (MJ/kg)[g]	43.0	43.4	41.9	41.7	41.1	43.5	27.0	36.4

[a] ASTM D2699-13b/ASTM D2700-14
[b] ASTM D4052 - 11
[c] ASTM D323-08(2014)
[d] ASTM D1319-14
[e] ASTM D3606 - 10
[f] ASTM D86-12
[g] ASTM D4809

Table 3.4: *Standard fuel specification analysis and heating value of HTFT synthetic gasoline blending components (SGBC)*

The synthetic blending components were found to differ significantly in terms of the standard analysis required for conformance with fuel specifications and it was found that no single fuel component would meet the current South African fuel legislation. Synthetic blending component A was predominantly paraffinic in nature with a minor aromatic and olefin content. Synthetic blending components B and F were identified to be predominantly olefinic in nature while synthetic blending components C, D and E had a high aromatic content suggesting that these blending components may have undergone catalytic reforming or aromatization for improved octane [11]. However, synthetic blending component D was found to have very poor octane rating although the benzene content, suggesting good octane, was very high. As expected a correlation between the aromatic content and density was patently noticeable which in turn also influenced the boiling range.

3.3 Detailed chemical characterization

The conventional fuel analysis, according to the ASTM D1319-14 standard method [40], only provides an indication of the classes of hydrocarbons in the fuel. However, it has been shown that the molecular structure of hydrocarbons can result in radically different properties which can have a profound effect on fundamental behaviour such as the laminar flame speed [41–43] or autoignition quality [17, 44, 45]. The two paraffinic reference fuels used to define the octane number of a fuel are a prime examples in this case. N-heptane is a straight chain paraffin with a very high propensity for autoignition while iso-octane, with its similar carbon number length but branched structure, has a very high resistance to autoignition. In order to be able to correlate engine performance results to fuel chemical component data, it was therefore necessary to define the sub-classes within hydrocarbons.

3.3.1 Comparison of methods

A comparison of the fuel component identification analytical methods that were evaluated for this investigation is presented below. Three standardised ASTM methods were evaluated for their suitability.

3.3.1.1 FIA

Fluorescent indicator adsorption (FIA), according to the ASTM D1319-14 method [40], is the industry standard approach to determine hydrocarbon types in full boiling range fuel products.

For this procedure the fuel sample is introduced into an activated silica gel and fluorescent dye containing glass adsorption column. After the fuel has been adsorbed onto the gel, alcohol is added that enables desorption of the sample down the column. Due to the different adsorption affinities of aromatics, olefin and saturates, they separate along with the dyes, which then allow identification and quantification according to zone length along the column using ultraviolet light.

According to the ASTM D1319-14 method description [40], the test method can be used to determine hydrocarbon types ranging from 5 to 99 volume % aromatics, 0.3 to 55 volume % olefins and 1 to 95 volume % saturates in petroleum fractions up to a boiling point of 315° C. The precision outside these ranges has not been determined. It further states that the suitability of the test method for products derived from alternative fossil fuels such as coal has not been determined.

During the perusal of the initial fuel analysis results it was found that the FIA method did not offer consistent results when comparing different fuel blends of the same synthetic gasoline blending components at various mixture strengths. This necessitated investigation of other analytical methods in order to obtain accurate and consistent fuel analysis data. In light of the apparent short fall in terms of accuracy, several alternative methods have been investigated in order to propose a suitable replacement [46].

3.3.1.2 Bromine number

The bromine test according to the ASTM D1159 standard method [47] can be used to quantify the bromine reactive components and thereby measure the quantity of unsaturated hydrocarbons in a sample. However this method makes the assumption that the sample contains no or a negligible amount of aromatics. Additionally the average molecular mass of the olefins present in the sample needs to be known or estimated, which can introduce significant uncertainty into the results [48].

3.3.1.3 DHA

According to the ASTM D6729 standard [49], this method is utilised to define the "PONA" components (Paraffins, Olefins, Naphthalenes and Aromatics). The detailed hydrocarbon analysis (DHA) is a gas chromatography (GC) technique that makes use of a premium quality capillary GC column which is indicated to result in high efficiency and reproducibility. For gas chromatography the fuel sample is separated into its chemical components in a specialised glass tube or column, containing a special adsorbent coating or packing material. As the gasified sample enters the column, the flow rate of the different components varies according to their physical and chemical properties, the geometry and temperature of the column, as well as their interplay with the stationary phase and carrier gas in the column. The resulting differences in retention times of the various components are measured by observing the properties of the gas exiting the column with a flame ionization detector (FID).

In the experience of the senior scientists at Sasol's analytical chemistry laboratory [48], this method is prone to co-elution of naphthenes above C8 and olefins above C7 with other component classes. This requires that care be taken when analysing samples with significant fractions of these components and compositional results require checking with other analytical methods. These findings are echoed by [46] in their investigation of DHA as a suitable replacement candidate for FIA.

Additionally, all of the methods described above do not allow characterisation of the sub-classes. A series of detailed analysis procedures were thus investigated by Sasol's

analytical chemistry laboratory, resulting in the use of three methods that are briefly described below with information from Sasol's senior scientists [48]. For a more thorough description of these methods, the reader is referred to Appendix B.

3.3.1.4 SFC

Supercritical fluid chromatography (SFC) is a particular implementation of high-performance liquid chromatography (HPLC). For this method the sample is combined with a solvent and then pumped through a specialised glass column charged with a solid adsorbent material. Through light interaction with the specialised adsorbent material, it causes the various components in the sample to transverse the column at a pace specific to their physical and chemical properties. As the different components result in differing retention times in the column, it allows for separation and quantification. CO_2 in its supercritical state is used as the solvent in SFC which implies that the complete chromatographic path needs to be controlled at a high pressure and low temperature. The analysis at column exit can be done using ultraviolet-visible spectroscopy (UV/VIS), mass spectrometry or flame ionisation detector (FID).

3.3.1.5 NMR

Nuclear magnetic resonance spectroscopy (NMR) makes use of a magnetic field to induce electromagnetic radiation emissions from the nuclei of the various molecules in a fuel sample. This radiation emission correlates with the resonant frequencies of the various nuclei structures contained in the sample and identification as well as quantification of its composition can therefore be deduced from an analysis of these emissions.

According to Sasol's senior scientists [48], NMR could be used to differentiate between olefin classes in gasoline samples. The accuracy of the method was shown by comparing the calculated results with a known test sample and is described in further detail in Appendix B.

3.3.1.6 GCxGC

Two-dimensional gas chromatography (GCxGC) is derived from gas chromatography-mass spectrometry (GC-MS) whereby two chromatography runs are implemented to more effectively differentiate the components in a sample before feeding them into a mass spectrometer to identify and quantify them based on mass-to-charge ratio and quantity of gas-phase ions present. For hydrocarbon analysis, the two separations are traditionally done first by volatility (using a non-polar carrier) and then by polarity (using a polar carrier).

However, it has been demonstrated that the reverse order extends the separation space and thus provides improved resolution for the characterization of Fischer Tropsch fuels as well as the characterisation of the aromatic fraction in petroleum middle-distillates [50].

Since the GCxGC separation space is a two-dimensional plane rather than a straight line separation space as in 1D-GC, it results in indisputable chemical compound identification as well as group classification [48].

3.3.2 Summary of analysis process

For the complex fuel samples used in this investigation it was necessary to make use of a combination of the techniques described in the previous section. The sequence of methods used for the analysis can be summarised as follows:

- GCxGC used to define iso-paraffins, linear paraffins and aromatics. It was also used to define olefins or naphthenes in cases where only one of these classes was present.
- SFC used to separate the paraffins, olefins and aromatics
- NMR used to determine the olefinic sub-classes
- cyclic paraffins were calculated from the difference between the GCxGC sum of linear- and iso-paraffins and the total paraffin content defined by SFC

3.3.3 Summary of analysis results

A summary of the final analysis results are presented in table 3.5. The 93 RON CCAG was found to contain 4.8% oxygenates, while the 95 RON SCAG has a oxygenate content of 14.7% consisting mainly of ethers. These are listed in the table as 'other' components. It should be noted that different methods were used to define the components and their subclasses and therefore the total content does in some cases not equate to exactly 100%, due to small inaccuracies in the methods.

The synthetic blending components exhibit significant differences in their respective classes and subclasses. Synthetic blending component B and F are both characterized with a high content of olefins, but consisting of very different subclasses.

When comparing the results from the FIA method in table 3.4, with the detailed analysis in table 3.5, some discrepancies were found which can be expected since the FIA method is a simplified approach. However the olefin content for both the synthetic CAG as well as the crude derived fuel was found to be roughly double using the FIA method, which

is quite significant. For ease of reference a table combining all of the fuel properties is provided in Appendix C.

Sample	SGBC A	SGBC B	SGBC C	SGBC D	SGBC E	SGBC F	95 RON SCAG	95 RON CCAG	93 RON CCAG
Linear paraffins	12.5	0.3	21.2	19	11	21.2	18.6	26.8	31.6
Iso-paraffins	61.4	0	19.6	11.6	3.3	8.1	17.7	13	15.6
Cyclic paraffins	5.1	6.2	0	9.2	0	0	7.4	5.1	0
Total paraffins	79	6.5	40.8	39.8	14.3	29.3	43.7	44.9	47.2
α-olefins	0	0	0	0	2.1	21.7	0	0	0
Internal olefins	0	4.8	0	0	1.2	43.6	2.1	0.1	1.9
Branched olefins	0	28	0	0	2.8	5.5	3	0.3	3.5
Other olefins	0	60.4	0	0	9.3	0	5.8	11.6	9.5
Total olefins	0	93.2	0	0	15.4	70.8	10.9	12	14.9
Aromatics	19	0.3	60.5	57.7	70.7	0	28.9	43.17	37.1
Other	0	0	0	0.2	0	0	14.7	0	4.8
Total	98	100	101.4	97.7	100.8	100	98.1	100	103.9

Table 3.5: *Final analysis results showing the percentage mass fraction of chemical classes and subclasses in the HTFT synthetic gasoline blending components (SGBC) and the commercial gasolines*

3.4 Summary and discussion

An investigation into the refining process of synthetic gasoline indicated considerable differences in terms of chemical composition from crude derived gasoline. Primarily this can be traced back to the significant compositional dissimilarities between syncrude and conventional crude oil. HTFT syncrude consists mostly of alkenes with a low alkane and aromatic content. Straight run naphtha from HTFT syncrude has an inherently higher octane rating than the product from conventional crude oil. The high alkene content enables significant refining potential to manufacture a product that meets the relevant fuel specifications [11].

A standard fuel analysis of synthetic 95 RON CAG was compared to crude derived 95 RON and 93 RON CAG. Surprisingly the olefin content of the inherently olefin rich HTFT fuel was found to be lower than the comparable crude derived fuel but this was deemed to be a result of extensive refining of the olefin components. Eight synthetic gasoline

blend components were also analysed using the standard method and the results revealed that four of the components with high paraffin or aromatic content exhibited a low olefin concentration.

Since the characteristic behaviour of a hydrocarbon class depends on its structure, it was important to define the major subclasses. Special emphasis was placed on olefins, due to the nature of syncrude, as well as paraffins since fuel manufacturers are required to include them as they are the only compound not constrained by fuel specifications. A detailed chemical analysis was conducted on the CAG fuels and the synthetic gasoline blending components. Detailed chemical speciation of full boiling range fuels is inherently complex and an analysis process involving several techniques was defined by Sasol's chemical analyses laboratory to obtain acceptable results.

As discussed in the previous section some discrepancies were found between the results from the standard FIA analysis and the detailed chemical method. This warrants further investigation into the techniques applied for the purpose of legislative fuel specification purposes as already instigated by the European Committee of Standardisation in 2003 [46].

The detailed fuel analysis suggests that, apart from the oxygenate content, 95 RON synthetic and crude derived gasoline are quite different in terms of chemical classes as well as subclasses. The synthetic blending components exhibit significant differences in chemical structure which should have an appreciable effect on their flame speed and ultimately on the burn rate in a spark ignition engine.

Chapter 4

Laminar flame speed characterization

This chapter provides details about the laminar flame speed measurements during the first part of the experimental investigation.

As shown in Chapter 3, synthetic gasoline may be equivalent to crude-derived gasoline in terms of fuel specification, while exhibiting distinct differences in chemical composition. Due to the significance in the fuel molecular structure effect on the flame speed of a fuel, a laminar flame speed characterization was conducted as presented by Rockstroh et. al. [21]. The test procedure, results and a more thorough discussion with regards to the detailed fuel analysis will be presented here.

4.1 Literature review on laminar flame speed

4.1.1 Laminar flame speed investigation

A significant amount of information on the laminar flame speed characteristics of the primary reference fuel components as well as blends thereof exists [42, 51–57]. Due to the complex nature of full boiling range gasoline, consisting of hundreds of hydrocarbon species, primary reference fuels (PRF) are frequently used to portray the octane properties of gasoline. While it has been assumed that the PRF characteristics can be extended to other combustion phenomena, investigations revealed that only an approximate agreement exists between the laminar flame speed of PRF and full boiling range CAG fuels [58, 59]. Jerzembeck et. al. compared the flame speed of a PRF87 blend to a commercial gasoline fuel and found that while the correlation was good for lean mixtures, there was a significant discrepancy at stoichiometric and rich conditions [60].

Similarly, Stanglmaier et al. stated that the laminar flame speed of gasoline was found to be significantly higher than iso-octane, especially at elevated temperatures and pressure [16]. Johnston and Farrell conducted a detailed study on the laminar flame speed characteristics of aromatic fuel components [43]. Pitz et. al. suggested that surrogate gasoline blends should include n-heptane, iso-octane and toluene in order to be representative of a full boiling range fuel [61]. Toluene was chosen because it is the most common aromatic in gasoline and although not as widely investigated as n-heptane or iso-octane, a few reports on its laminar flame velocity exist [41, 43, 62–65]. Very few reports on the flame velocity of gasoline exist and the variety of mixtures in commercial gasolines makes it complicated to state a typical laminar flame speed. The laminar flame speed of real gasoline is generally compared to those of specified surrogate blends in order to examine its accuracy [56, 58, 60].

Since the 1950's a considerable amount of experimental data for fuels in the range of C1 - C8 has been reported on, notably Gibbs and Calcote's contribution on the effect of molecular structure on the burning velocity [66]. However, significant disparities between measured burning velocities were often observed. This has subsequently been explained to be related to varying flame stretch rates due to flame curvature and aerodynamic strain that resulted in significant scatter in the data. Research in the past two decades has led to the quantification of the effects of stretch and to define test methods that allow stretch-free burn velocity measurements such as counter flow axisymmetric burners and constant volume combustion chambers [67, 68]. Only a limited amount of fuel data is available from these techniques. Although it is difficult to quantify the absolute flame speed of fuel components using the data from the older methods, they have served to provide general agreement with regards to the relative fuel structural effect on flame velocity. More recent evaluations of the fuel structural effect on laminar flame speed includes that of Davis and Law using a counterflow twin flame configuration [42]. Farrell et. al. used a constant volume combustion bomb to define the fuel effects for alkanes, alkenes, alkynes, aromatics and oxygenates under the same experimental conditions [41]. Their data confirmed the general consensus of alkynes having a faster flame speed than the corresponding alkenes which in turn are faster than alkanes with the same carbon connectivity. A comprehensive assessment of the flame speed of aromatic components showed a wide variation spectrum, which was stated to be sensitive to the site and degree of alkyl substitution [41, 43].

4.1.2 Laminar flame speed measurement procedure

A thorough review on a variety of experimental techniques to determine laminar flame speed was provided by Rallis and Garforth [69]. The counter flow twin-flame appara-

tus and the closed combustion bomb were highlighted as the most suitable methods. Although optical Schlieren techniques are often used, it has been recognized that it is possible to calculate the flame speed from the combustion bomb pressure alone [52,70,71]. After careful assessment of the calculation methods, Lewis and von Elbe remarked that the pressure based analysis technique had the most potential for high experimental precision [72]. Due to the ability of modern instrumentation and data acquisition tools it allows for a high volume of very precise measurements of global bomb parameters. Even though the benefits of a combined pressure and Schlieren method were recognized, the constant volume bomb apparatus developed by Yates and co-workers [22] was regarded as suitable for this part of the investigation.

4.1.3 Blending effect on laminar flame speed

The burning velocity of a fuel is dependent on its kinetic, thermal as well as transport properties and components such as hydrogen have been shown to enhance its reactivity [73, 74]. Blending in a component with higher adiabatic flame temperature, which is related to the heat of combustion, can result in a different mixture reactivity even if the underlying reaction mechanism remains the same [75]. The diffusivity of a blend component such as hydrogen can lead to changes of the mixture concentration in the flame structure [75]. The complexity of discerning between thermal and chemical effects for fuel blends, as a result of the thermokinetic coupling, makes the definition of a blending rule challenging. It has been shown that linear approaches based on the volume concentrations are not reliable [63, 76]. Spalding suggested a mixing law that equates the square of the flame speed of the blend to the sum of squares of the flame speeds of the individual components weighted by their mass concentrations [77]. For binary fuel blends, Bradley et. al. used the volumetric heat release rate to define their mixing rule [78] while another approach was the use of the adiabatic flame temperature [63]. Sileghem et. al. compared a variety of simple mixing rules for simulation programs to allow accurate prediction of laminar flame speed [79]. For their investigation of gasoline-ethanol blends, they found that the thermal property, due to the difference in heating value, dominated the flame velocity and three mixing rules were found to give very accurate results. The methods were based on the energy fraction of the components, the adiabatic flame temperature and Le Chatelier's principle of flame theory. For the analysis of gasoline and ternary blends of iso-octane, n-heptane and toluene, Sileghem et. al. chose the energy fraction mixing rule, although the difference between the results was reported to be small [59].

4.2 Experimental procedure

4.2.1 Test method

For each fuel, measurements were performed at five different air-fuel ratios. At each air-fuel ratio, six repeat pressure traces were recorded, each containing about 90 data points. Two starting temperatures were required for the analysis method and these were chosen as 100 and 150 °C. The fuel pressure was maintained at 40 bar throughout the test. The following test procedure was followed for each test fuel:

- Calibration of injector by measuring the fuel mass at various injection durations
- Heating up of combustion bomb to 100 °C and allow to stabilise for one hour
- Conduct a leak check by charging the vessel with air at 10 bar and monitor the pressure drop when inlet valve closes
- Conduct tests spanning from lean to rich air-fuel ratio (ϕ 0.7 - 1.3)
- Heating up of combustion bomb to 150 °C and allow to stabilise for one hour
- Conduct a leak check by charging the vessel with air at 10 bar and monitor the pressure drop when inlet valve closes
- Conduct tests spanning from lean to rich air-fuel ratio (ϕ 0.7 - 1.3)

4.2.2 Assessment of analysis procedure and apparatus

Before embarking on the laminar flame speed analysis of the test fuels, known reference fuels were used to check the experimental procedure and apparatus. In table 4.1 the experimental flame speed for stoichiometric mixtures of three fuels at standard reference conditions 25 °C and 1 bar pressure is displayed along with corresponding literature data. The peak flame speed of n-heptane and iso-octane was found to be slightly lower than reported in literature.

Fuel	Experimental flame velocity (m/s)	Literature values (m/s) [80–82]
n-heptane	0.378	$0.385 - 0.395$
iso-octane	0.337	$0.345 - 0.350$
Ethanol	0.407	$0.400 - 0.470$

Table 4.1: *Laminar flame velocities of the reference fuels, (computed for ϕ= 1 at 25 °C and 1 bar pressure)*

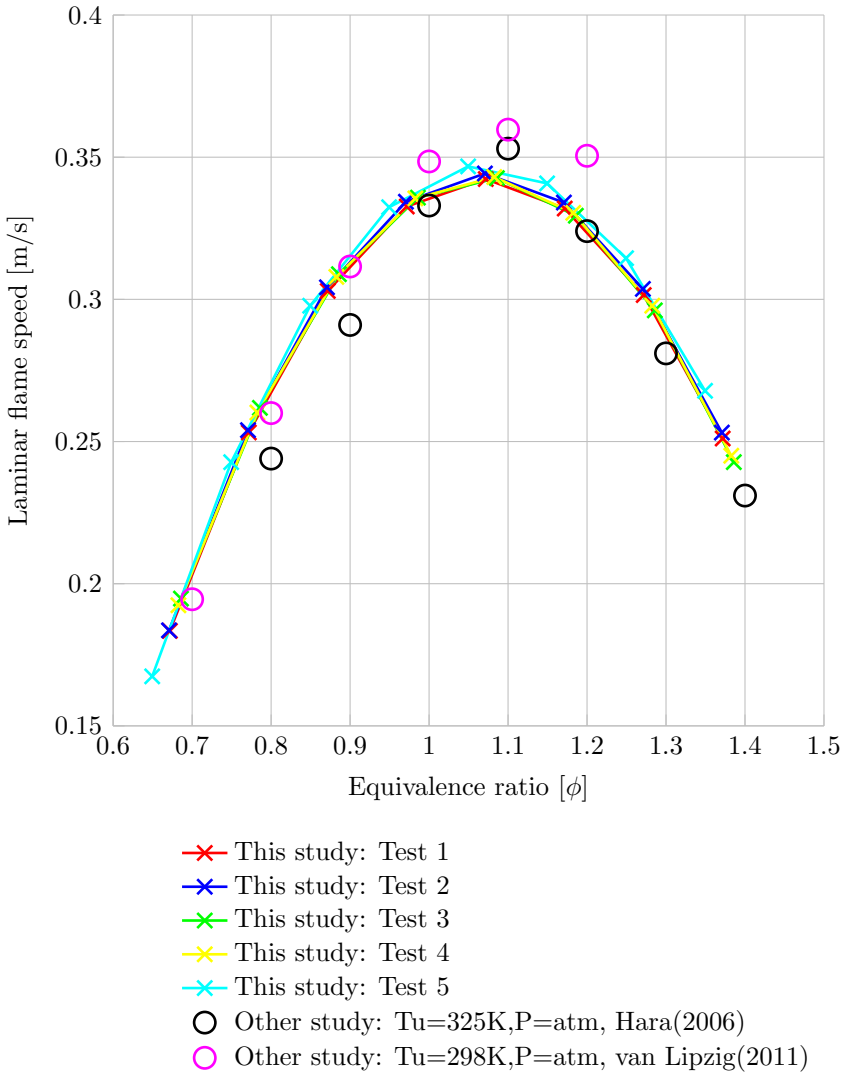

Figure 4.1: *Repeated laminar flame speed measurements, Iso-octane (at standard conditions 25* deg*C and 1 bar pressure) compared to literature [53, 81]*

To obtain an assessment of the repeatability of the test rig, several tests using iso-octane were done on different days. The laminar flame speed at various air-fuel ratios shown in figure 4.1, indicates minimal variation in results and compares favourably with corresponding data from literature [53, 59].

4.2.3 Analysis of test fuels

For the laminar flame speed analysis the test fuels could be broadly divided into three fuel types as shown in table 4.2. Fuel analysis data is provided in table C.1 and table C.2 Appendix C.

With the exception of the oxygenate blend components and synthetic blending component F, the fuel blends as well as CAG fuels are all predominantly pure hydrocarbons

Pump fuels	Synthetic blend components	Oxygenate blend components
95 RON CCAG	SGBC A, SGBC D	TAME
93 RON CCAG	SGBC B, SGBC E	Ethanol
95 RON SCAG	SGBC C, SGBC F	

Table 4.2: *Fuel types investigated*

with similar average carbon number lengths. Yates et. al. found that fuels with such similarity could be grouped together using common values for the pressure and temperature parameters [22]. Following preliminary data analysis, it too was found that only the peak laminar flame velocity and Markstein length descriptor needed to be fuel-specific, thereby reducing the number of degrees of freedom and improving the robustness of the regression analysis. The oxygenate blend components as well as synthetic blending component F, due to its lower carbon number length, were treated separately.

4.3 Results and discussion

4.3.1 Laminar Flame Speed Comparison

Figure 4.2 shows a comparison of the peak laminar flame speed measurements of the eleven test fuels at the reference condition of 25° C and atmospheric pressure condition. If one corrects for the different temperature conditions, the 93 and 95 RON CCAG fuels exhibited a similar peak flame velocity to the experimental results by Zhao et. al. [58].

The 95 RON SCAG fuel was found to have an appreciably higher flame velocity than the equivalent crude derived fuel. It was also noted that all the synthetic blends A to F burned faster than the 95 RON CCAG fuel. Furthermore, the synthetic fuel blends exhibited a distinct variation in peak laminar flame speed, which seems to suggest that the laminar flame speed behaviour of a synthetic CAG fuel could potentially be influenced. Ethanol was used as a reference fuel and the flame speed was found to compare favourably with findings by other researchers [53, 82].

The laminar flame speeds across the entire air-fuel ratio range is presented in figure 4.3. For most of the test fuels, the peak flame velocity was measured at an air-fuel ratio slightly rich of stoichiometric at about ϕ= 1.1. This agrees with comparable data presented in literature [58, 60, 83].

The peak flame velocity of TAME, ethanol and synthetic blending component F was measured at slightly richer air-fuel ratios than the other fuels. Some literature sources have shown ethanol to exhibit its peak laminar flame speed at air-fuel ratios just rich of

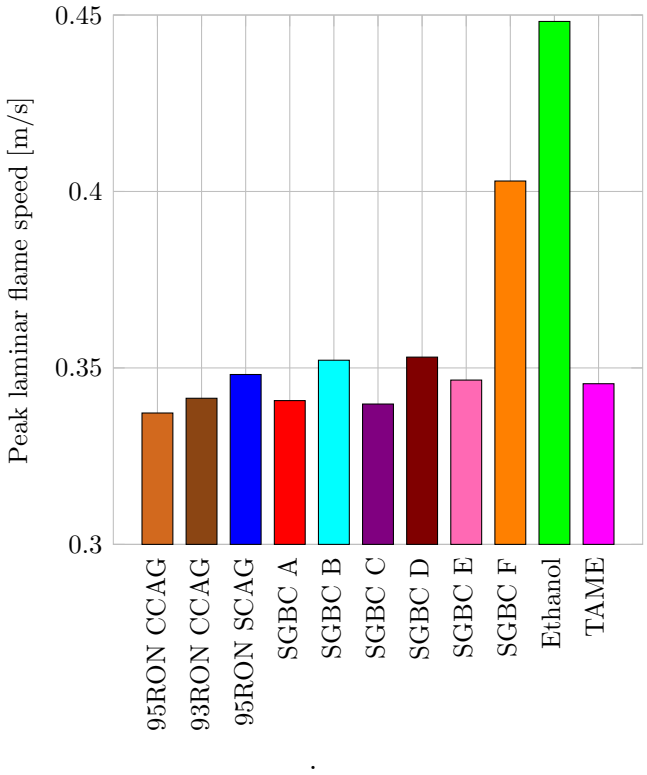

Figure 4.2: *Peak laminar flame speed of all test fuels (at standard conditions 25° C and 1 bar pressure). Adapted from [21]*

stoichiometric, while Beeckman et al. also presented data indicating ϕ= 1.2 to be where maximum flame velocity occurred [84]. Blending component F was a predominantly olefinic hydrocarbon blend with a low molecular weight. The flame speed measurements of C5 alkenes by Farrell et al., similarly indicate peak flame speed to occur at ϕ= 1.2 [41]. Due to the lack of test result data for TAME in literature, a comparison with a more well documented ether was made in order to rate the flame speed of the oxygenates used in this analysis. Methyl tert-butyl ether (MTBE) is similar in heating value as well as molecular weight to TAME and was distinguished with a significantly lower burn velocity than ethanol [41].

4.3.2 Correlation Analysis of Peak LFS Results

From theoretical considerations, it is evident that the laminar flame speed is dependent on a number of fuel related properties, most importantly the adiabatic flame temperature, transport properties as well as the molecular structure [74]. In order to analyse the fuel specific properties and their relationship with the peak laminar flame velocities, Rockstroh et al. [21] made use of a correlation analysis as shown in figure 4.4. The fuel data was analysed and defined as discussed in Chapter 3 and is summarised in table C.2 presented in Appendix C.

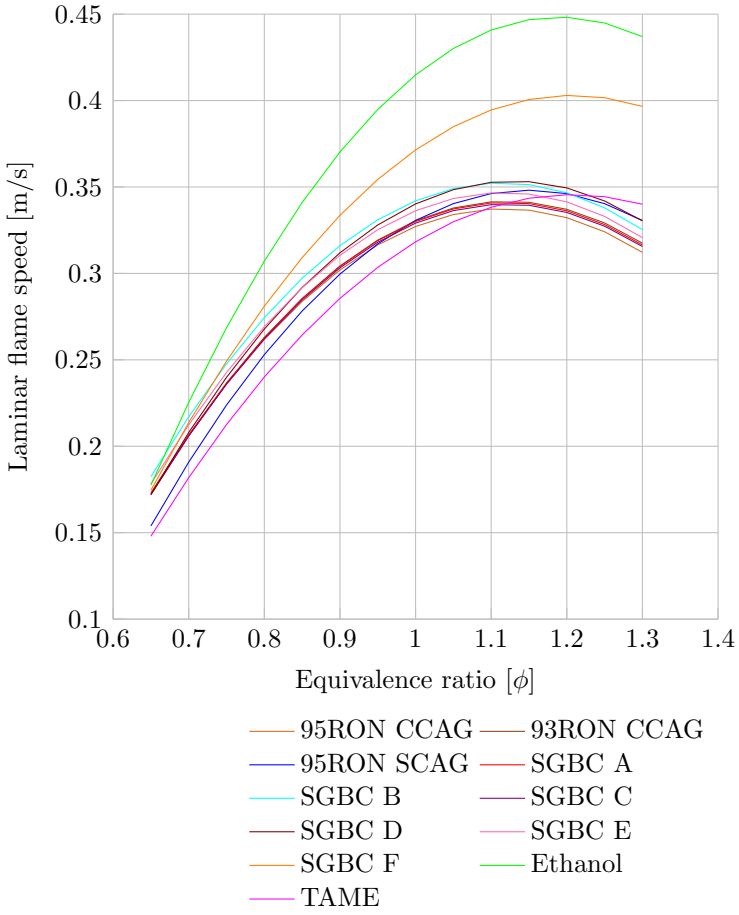

Figure 4.3: *Laminar flame speed variation with equivalence ratio (ϕ) of all test fuels (at standard conditions 25° C and 1 bar pressure)*

	Max LFS	RON	MON	Heating Value	Atomic C/H ratio	Density	n-Paraffins	Iso-Paraffins	Cyclic Paraffins	Olefins	Benzene	Other Aromatics	Naphthalenes	Oxygenate	Molecular Mass
Max LFS	1.00														
RON	0.12	1.00													
MON	-0.57	0.68	1.00												
Heating Value	0.48	0.08	-0.23	1.00											
Atomic C/H ratio	-0.34	-0.13	0.02	-0.88	1.00										
Density	-0.72	-0.27	0.19	-0.88	0.87	1.00									
n-Paraffins	0.04	-0.10	-0.07	-0.14	0.01	-0.08	1.00								
Iso-Paraffins	-0.30	-0.49	0.07	0.19	-0.34	-0.08	0.06	1.00							
Cyclic Paraffins	-0.09	-0.83	-0.72	-0.10	0.26	0.35	-0.12	0.03	1.00						
Olefins	0.62	0.49	-0.14	0.68	-0.52	-0.67	-0.46	-0.49	-0.20	1.00					
Benzene	-0.15	-0.66	-0.50	-0.58	0.73	0.69	-0.15	-0.08	0.75	-0.42	1.00				
Other Aromatics	-0.60	0.07	0.42	-0.88	0.78	0.79	0.37	-0.12	-0.10	-0.74	0.28	1.00			
Naphthalenes	-0.51	0.23	0.49	-0.84	0.71	0.70	0.29	-0.20	-0.22	-0.60	0.13	0.97	1.00		
Oxygenate	-0.06	0.18	0.28	-0.25	-0.20	-0.01	0.02	0.03	-0.25	-0.06	-0.18	0.04	0.14	1.00	
Molecular Mass	-0.83	-0.57	0.07	-0.44	0.35	0.74	-0.16	0.34	0.56	-0.59	0.49	0.39	0.28	0.08	1.00

< -0.7 -- > 0.7 significant correlation | > |0.5| -- > |0.7| less significant correlation | < |0.5| insignificant correlation

.

Figure 4.4: *Correlation analysis of peak laminar flame speed results. Adapted from [21]*

The oxygenates, TAME and ethanol, were omitted for this part of the investigation as they were found to desensitise the results of the correlation analysis due to being pure components. In the left most column of the matrix shown in figure 4.4, the fuel properties that were considered for the analysis are displayed. For each column the correlation coefficients indicating the significance to the respective properties was calculated. If coefficients were greater than 0.7 or less than -0.7 they were deemed to be of significant correlation, while absolute coefficients between 0.5 and 0.7 denoted a less significant correlation. Insignificant correlation was shown by coefficients between 0.5 and -0.5.

4.3.2.1 Adiabatic flame temperature

The heating value of a fuel can directly effect its adiabatic flame temperature and a correlation with the peak laminar flame speed could subsequently be assumed [74]. However, the small differences in heating value between the fuels resulted in a correlation coefficient of 0.48 which indicated that in this instance there was no significant correlation with the laminar flame speed.

The correlation showed that aromatic and naphthalene content had a negative correlation with the gravimetric heating value of the fuel. On the contrary, a high olefin content resulted in a higher heat of combustion. However, only minor portions of naphthalene were found in the fuel blends. A high hydrogen to carbon ratio was shown to coincide with an increased heat of combustion of a fuel, as to be expected.

4.3.2.2 Transport properties

The transport properties are primarily influenced by the molecular mass which implies that there is a direct correlation between the laminar flame speed of a fuel and its molecular mass [74]. As the fuel components generally had a similar molecular weight, the inclusion of synthetic blend component F was responsible for the strong correlation between flame speed and molecular mass. Blending component F had a low molecular weight and high flame speed, but was included in order to support the evaluation of the chemical structure effect on the flame velocity.

Density and molecular mass were related with positive correlation coefficients. Aromatics are generally known to have a strong effect on the density of a fuel. It was therefore not surprising to find a positive correlation between density, benzene and other aromatics. The negative correlation coefficients between aromatics and laminar flame speed as well as between olefin and density explain the overall negative correlation between density and the laminar flame velocity.

4.3.2.3 Molecular structure

A correlation with peak laminar flame speed was found between olefin and aromatic content. The analysis suggested that olefins had a positive influence on the flame velocity with the opposite being the case for aromatic components. Benzene was separated from the total aromatic content as it is known to be characterised with relatively high flame speed.

In order to provide a comprehensive assessment of the chemical structure effect on the laminar flame speed, detailed speciation of the fuel blends was required. In addition, care was required in designing a fuel matrix whose chemical components were designed to minimize statistical aliasing, similar to efforts by Davis and Law as well as Farrell et. al. [41,42]. The technical challenges involved in analysing full boiling range higher carbon number fuels and the limited fuel matrix available meant that the correlation analysis [21] was mostly restricted to chemical classes. Some subclasses were subsequently defined as discussed in the fuel analysis section in Chapter 3. The differentiation of subclasses for the olefin components of the test fuels is shown in table 4.3.

Fuel	**Peak LFS**	**α-olefins**	**Internal olefins**	**Branched olefins**	**Other olefins**	**Total olefins**
95 RON CCAG	0.337		0.1	0.3	11.6	12
93 RON CCAG	0.341		1.9	3.5	9.5	14.9
95 RON SCAG	0.348		2.1	3	5.8	10.9
SGBC A	0.341					
SGBC B	0.352		4.8	28	60.4	93.2
SGBC C	0.340					
SGBC D	0.353					
SGBC E	0.347	2.1	1.2	2.8	9.3	15.4
SGBC F	0.403	21.7	43.6	5.5		70.8

Table 4.3: *Subclasses of olefin components*

Synthetic blend components B and F were predominantly olefinic hydrocarbons and both were characterized with a comparatively high laminar flame speed. Synthetic blend component D did not contain any olefins but was very rich in benzene, which has been shown to have a high flame speed, about 20% higher than toluene [41–43]. Synthetic blend component F had the highest laminar flame speed by some margin which was partly related to its lower molecular mass as well as its high α-olefin content. Farrell et. al. [41] investigated various C5 alkenes and found that terminal double bonds consistently resulted in a higher flame speed than comparable internal bonds. Furthermore they found that although burning velocity of alkenes is sensitive to chain branching it is largely unaffected by the chain length for C3 and larger fuel molecules. The comparatively lower flame

speed of synthetic blend component B could therefore largely be ascribed to it consisting mainly of branched olefins.

4.4 Summary and discussion

The laminar flame speed behaviour of the CAG fuels as well as the synthetic blending components was characterized. It was found that the commercial gasolines exhibited a similar flame speed performance with the synthetic fuel being the highest amongst the them. Appreciable variation was detected among the synthetic blending components suggesting potential to optimise the laminar flame speed behaviour of a synthetic CAG fuel. Blending components with a high olefin content indicated an improved flame speed in contrast to those with predominant aromatic or paraffin concentration. Ethanol was found to have a very high flame speed as supported by literature findings [53], while TAME was found to display a comparatively low flame speed which should have interesting implications on the burn rate in an engine when choosing an oxygenate to improve the octane rating.

The findings from the assessment of the laminar flame speed behaviour suggested that the burn rate in a spark ignition engine would be affected by the various blending components, which could ultimately influence the engine performance. This lead to a detailed combustion analysis using a modern GDI engine as is discussed in Chapter 5.

Chapter 5

Charge boosted gasoline direct injection combustion analysis

This chapter discusses details regarding the engine combustion analysis conducted during the second part of the experimental investigation.

5.1 Literature review on charge boosted GDI combustion

Although commonly marketed as a modern technology, the idea of injecting fuel directly into the combustion chamber of a spark ignition (SI) engine was included in Nikolaus August Otto's patent describing the constant volume cycle which is representative of the ideal combustion process in this type of engine. A thorough historic review of the development of gasoline direct injection (GDI) engine technology is provided in textbooks dedicated to this subject matter by van Basshuysen [85] and Zhao [86].

5.1.1 GDI engine technology

Stratified-charge has been investigated since the 1920's as a means to combine the best features of the spark-ignition and compression ignition engine [17]. As recollected by Zhao, when the first generation of modern GDI engines was launched in early 2000, the emphasis of improved efficiency was squarely placed on the ability to run in stratified charge mode. Due to the need for complicated NO_x storage systems and the restricted fuel efficiency as a result of the limited operating range in this mode, automotive manufacturers soon switched to homogeneous charge mode while still maintaining the benefit

of higher compression ratios possible due to the enhanced charge cooling effect. In recent years some manufacturers re-introduced lean-burn combustion mode in the so called second generation gasoline direct injection engines, albeit still with a limited operating envelope restricted to part load conditions [86].

While the goal with gasoline direct injection engines ultimately has to be the use of a lean burn stratified combustion principle and in the process de-throttled operation of the spark ignition engine, charge boosted production engines currently operate in stoichiometric homogeneous mode [86]. In the light of ever tightening emission legislations, treatment of nitrous oxides (NO_x) for any stratified combustion method adds complexity and has associated cost implications [17,85,86]. A practical approach in avoiding throttling losses while making use of conventional three-way catalytic converters has established itself in the form of engine downsizing by making use of significant synergies found between direct injection and turbo-charging [87–89].

In engines with external mixture preparation, charge boosting resulted in knock limitations that generally required a significant reduction in compression ratio, spark retard, charge air temperature reduction and/or enrichment of air/fuel ratio [17]. In gasoline direct injection engines, the fuel evaporative effect removes the heat of vaporization from the air in the cylinder thereby depressing the mixture temperature (and cylinder wall temperature) and increasing the knock resistance. With the aid of variable valve phasing, over-scavenging can be used to remove all burnt gases without introducing un-burnt air-fuel mixture into the exhaust gas stream, because of the flexibility in timing the injection [86]. These characteristics allow higher compression ratios and operation at more optimised spark advance as well as requiring less enrichment for knock suppression in GDI engines.

Key to engine downsizing is the use of charge boosting, which is where GDI technology has been instrumental. Apart from the higher knock resistance, there have been marked improvements in driveability of turbocharged SI-engines [86]. With the aid of variable valve timing, so called "compressor map shifting" has been implemented to reduce the charge build up delay period while also allowing the reduction of pumping losses at part load condition [86, 90]. Twin-turbo charge boosting [91] as well as sequential charging by means of a supercharger in combination with turbocharging have been introduced in production engines. Alternative systems such as twin scroll technology have been shown to significantly improve low down torque characteristics [92] while variable turbine geometry (VTG), which is common in diesel engines, has been introduced in a high performance gasoline engine [93].

The loading in downsized gasoline engines is considerably higher than in naturally aspirated port fuel injected derivatives. Non-boosted high performance spark ignition engines

achieve maximum brake mean effective pressures (BMEP) of up to 15 bar, boosted engine increase this value to 20 bar while high-load downsized engines operate above 20 bar BMEP [94, 95]. That load level is set to increase with more aggressive downsizing strategies and several researchers have reported engine operation in the range of 25-35 bar BMEP [96–99]. At this point it may be worth noting that during the turbocharged Formula 1 era in the 1980's the BMEP level of the engines could exceed 55 bar [100]. Interestingly the authors [100] remarked that they experienced changing knocking conditions with different fuel components even though the RON was always maintained at 102. This seems to suggest that the engine may have been operating in a range that was not covered by the RON test method and/or that the toluene ratio in the fuel significantly affected the latent heat of vaporisation. Both of these fuel related phenomenon will be discussed in subsequent sections.

Despite the obvious benefits of GDI technology, charge boosted engines are still constrained by knocking combustion under full load conditions. Additionally, highly charge boosted GDI engines have been found to exhibit abnormal combustion leading to extremely high levels of knocking combustion termed mega-knock or super-knock. These issues will be discussed in more detail in the following section.

5.1.2 Knock and abnormal combustion

5.1.2.1 Spark knock

Sir Harry Ricardo was one of the first to investigate the occurrence of knock at the beginning of the 20th century and defined a process by which it occurs that is still relevant today [86,101]. Due to its impact on engine performance and efficiency, knock occurrence in SI-engines has been well researched and is described in reference textbooks [1, 17]. A more recent textbook by Zhao discusses this with specific regard to charge boosted GDI engines [86]. Spark knock can be defined as the undesired autoignition of a portion of the end gas ahead of the propagating flame [17].

When this autoignition occurs, a high amount of heat is released almost instantaneously resulting in pressure waves of significant magnitude travelling through the combustion chamber and in the process exciting the engine structure thereby creating the distinctive noise [17]. It has been shown that if autoignition occurs under favourable in-cylinder conditions the flame front can travel at 10-20 times the normal flame speed [102, 103]. If not detected and rectified the high local pressure and heat release rate can destroy an engine within a few combustion cycles.

Knock damage has been investigated in detail and found to occur either due to excessive local mechanical and thermal loading or as a result of global heat flux in the combustion

chamber [104,105]. Fitton and Nates determined that erosion damage depended strongly on geometry and temperature but found little correlation with the conventional knock severity indication of peak-to-peak pressure amplitudes which was in fact calculated to be significantly higher. However, the pressure at the onset of autoignition corresponded with the erosion damage measurements [106]. Nates further showed the significance of thermal stress on the surface damage caused by knock erosion [107].

It needs to be borne in mind that autoignition does not have to result in engine destruction due to knock, as can be seen by its use in homogeneous charge compression ignition (HCCI) engine. The knock occurrence measured during the RON/MON tests in the cooperative fuels research (CFR) engine, also does not result in destructive autoignition despite possible occurrences of auto-ignition of a large volume of end gas and has been shown to be significantly different to the occurrence in modern spark ignition engines [13]. However, the combustion chamber volume in modern four-valve engines is significantly smaller but the high heat release rates during knocking combustion generally result in serious engine damage [86].

The extremity of the autoignition is dependent on the local temperature gradient which can be influenced by exothermic centres that develop due to the hot combustion chamber surface or pockets of residual hot burned gas [108–110]. Five different types of flame propagation have been described [110]. According to Zhao [86] the three most important are, a high thermal gradient of 100 K/mm causing a deflagrating flame, a medium gradient of 12.5 K/mm resulting in developing detonation where as a low value of below 1.25 K/mm leads to a thermal explosion. Developing detonation has been linked to engine damaging knock occurrence [86]. Rothe et. al. investigated the knock onset locations and the knock intensities under full load conditions and concluded that if autoignition occurs in the exothermic centres, the knock severity and inflicted damage depends on the proportion of charge in the end gas [111]. They found that the ability to control autoignition was also made difficult by an increase in charge. It is therefore evident that a charge boosted spark ignition engine is automatically more prone to autoignition due to the increased thermal loading and the boost effect on the end gas pressure and temperature history. At full load in a charge boosted engine the increased charge mass also leads to higher knock severity than in a comparable naturally aspirated engine.

5.1.2.2 Knock prediction modelling

A simplified predictor of the ignition delay time was defined by Livengood-Wu in 1955 and is an integral equation which declares that autoignition in the end gas will occur if the equation reaches unity [112].

$$\int \frac{1}{\tau} dt = 1 \tag{5.1}$$

The autoignition delay time is represented by the parameter t at the instantaneous temperature and pressure of the mixture which is explained by the Arrhenius rate equation

$$\tau = Ap^{-n} exp\left[\frac{B}{T}\right] \tag{5.2}$$

A, n and B are fuel specific constants which vary for different fuels as well as different engines and engine conditions. If the combustion is completed before the equation reaches unity then autoignition does not take place. It is important to note that the simple Livengood-Wu single-stage model is not able to represent detail regarding the cool-flame phenomena which is pertinent to knock investigations. A rather elegant empirical auto ignition model makes use of two Arrhenius functions to also describe the cool flame temperature rise occurring in typical hydrocarbon fuels [113].

5.1.2.3 Spark knock prevention benefits of GDI

The use of gasoline direct injection has major benefits in reducing the knock tendency in spark ignition engines by introducing the fuel directly into the combustion chamber and thereby making use of the heat of vaporization in cooling the charge air more effectively than is possible with port fuel injection. Although gasoline has a relatively low heat of vaporization, this form of knock prevention is still effective and engine developers have made use of extra injections during the compression stroke to combat knock under high load conditions [114]. Alcohol fuels have been shown to have even better knock prevention due to their ability to cool the combustion chamber gases very effectively [6, 115].

Kasseris and Heywood in a two part paper investigated the charge cooling and chemistry effect of gasoline-ethanol blends on engine knock. They quantified the charge cooling effect by heating the inlet air temperature conditions of the direct injected (DI) engine to obtain the same borderline knock as for the port fuel injected (PFI). It was found that the charge cooling effect of gasoline was 14° C while it increased to 49° C for E85. The high intake air temperatures required for high ethanol blends were believed to have contributed to the high charge cooling effects by increasing the fuel evaporation rate. An effective octane number was calculated for the different fuel blends that excluded the charge cooling effect. It was found that the chemical antiknock benefit of ethanol did not improve the performance beyond a content of about 40%. Higher ethanol concentration was only beneficial in a direct injection engine, due to the charge cooling effect [116, 117].

In order to obtain the maximum benefit from the vaporization, air fuel mixing is of great importance. Early gasoline direct injection engines made use of wall and air guided mixing principles. The second generation of homogeneous GDI engines make use of central position spray guided systems, close to the spark plug, where the injector nozzle is aligned with the high velocity of air stream at the top of the inlet port. This system has been used primarily for stratified charge engines and has also been shown to be valuable in the development of downsized engines. Due to the high flow rate of the injector it results in a shorter injection duration thereby allowing more time for evaporation [94]. The injection pressure has been shown to be very important in terms of fuel vaporization and fuel pressures up to 200 bar are generally reported [91, 94, 118].

5.1.2.4 Beyond RON

The relevance of traditional ASTM octane test methods with modern spark ignition engines has been subject to numerous investigations [3, 4, 13, 119, 120]. Kalghatgi found that the antiknock quality of a practical, non-PRF fuel, was best defined by an octane index of the form: OI = RON - KS. The index is a linear function of RON and the fuel's sensitivity (RON-MON), with the K value being dependent on operating conditions and engine technology [119]. In an evaluation of various vehicles equipped with knock control it was further shown that the K value was negative in most cases, meaning that for a fuel of a given RON a lower MON would result in better performance due to higher anti-knock quality [3]. A careful analysis of the cylinder pressure and temperature profiles of knock limited spark advance data of a carburettor engine and more modern fuel injected engines was conducted by Yates and co-workers [4]. They similarly found that while the research and motor method perfectly straddled the knock limited operating range of the carburettor fed engine, the port fuel injected engines were solely defined by the research method. It was therefore postulated that charge boosted and intercooled engines would operate in a pressure and temperature domain "beyond RON". Various researchers have subsequently shown that modern charge boosted engines would benefit in terms of performance from fuels with a lower MON number [121–124].

Mittal and Heywood conducted experiments to define the knock limits of a port fuel injected single cylinder engine fitted with a pent roof, 4 valve cylinder head using a range of fuels that included paraffins, olefins, aromatics and alcohols [120,125]. The knock limited cylinder pressure was found to increase linearly with increasing sensitivity regardless of the fuel chemistry once again implying that for a fixed RON, a fuel with a higher sensitivity has a better anti-knock characteristic. The authors went on to define the K value experimentally for various operating conditions and found it to depend strongly on intake air temperature, engine speed and intake pressure with less association to the relative

air-fuel ratio. Importantly the K value did not seem dependent on compression ratio and spark plug location thereby leading the authors to suggest modified test conditions for the RON and MON test using the CFR engine. However, it was acknowledged that a stronger dependence of the K value on compression ratio was found by Kalghatgi [119, 126]. It was assumed that the discrepancy was caused due to the different methods used to determine the OI. Mittal and Heywood compared the knock limited spark advance of the test fuels to that of PRFs under the same operating conditions and thereby ascertained the OI [120]. Kalghatgi meanwhile determined the OI, for a variety of different fuels, by applying a multiple linear regression which allowed the KLSA to be expressed as a linear function of RON and MON [119].

At this point it is interesting to note that the olefin (Iso-octene) and the aromatic (Toluene) used in both studies to adjust the sensitivity of the fuel blends, exhibit a very similar laminar flame speed [41]. It would be interesting to evaluate the OI using olefin and aromatic components with different burn speeds.

5.1.2.5 Low Speed Pre-Ignition

The high specific loading of downsized engines have led to the observation of a new type of combustion phenomena, particularly at full load and low engine speed. Low speed pre-ignition (LSPI) results in much higher pressure rises than normal combustion and can easily pass into heavy knock, termed mega-knock or super-knock. Due to the likelihood of severe engine damage being caused, LSPI has been described as a limiting factor for further down-sizing [127].

Dahnz et. al. did a study on the reason for the manifestation of stochastic pre-ignition in highly supercharged spark ignition engines and concluded that the most likely cause is the release of lubricant droplets from the cylinder liner [128, 129]. Although it was stated that no auto ignition data for lubricating oil existed, it was assumed that the long-chain molecules of oils are associated with short auto-ignition times. Subsequent publications by other researchers have agreed with the hypothesis of LSPI being caused by the interaction of fuel and engine lubricant [130–134]. Investigations to understand the ignition propensity of engine lubricant base stocks have also been conducted which further substantiate the notion of their contribution to LSPI [135].

Kalghatgi and Bradley analysed the origin of pre-ignition at a solid surface and in the gas phase [8]. By comparing the pre-ignition rating of various fuels to their RON and MON it was confirmed that autoignition of the air-fuel mixture due to the hot combustion chamber walls, was unlikely. The gas-phase autoignition was suggested to be the dominant driver of pre-ignition but that the ignition delay data for the pressures and temperatures at which pre-ignition was observed, could not be ascribed to the main air-fuel

mixture. As suggested by Dahnz et. al. [128], oil droplets were believed to potentially be the ignition source, although the required ignition delay time and the critical initiating flame size required that the oil have a higher autoignition quality than n-heptane. It was further speculated that small particles and catalysis could augment the development of pre-ignition. It was surmised that by reducing the laminar burning velocity the probability of pre-ignition occurrence is reduced. Cooled exhaust gas recirculation is an effective way to reduce the flame speed of an air-fuel mixture and is often used in highly boosted spark ignition engines to reduce the spark knock tendency and reduction in exhaust gas temperatures.

5.1.3 Impact of GDI on pollutant emissions

Charge boosting systems offer both opportunities and challenges for the emissions characteristics of spark ignition engines. An exhaust gas turbocharger significantly increases the thermal inertia of the exhaust system which can have negative implications on the catalyst light-off and hence the ability to convert pollutants after cold start during emissions test cycles. In a homogeneous-charge-mode engine, GDI enables split injection during the engine warm up period whereby a non-homogeneous locally rich mixture is generated close to the spark plug. The improved combustion stability allows greater spark retard to increase catalyst heating while unburned hydrocarbons are reduced due to leaner mixture conditions [91, 118]. In order to reduce the wall wetting the fuel pressure and injection pulses can be varied which reduces the risk of oil dilution and soot formation. A double pulse strategy can be applied at mid load while a triple injection at full load significantly reduces the penetration of the fuel spray [91]. This way the fuel consumption penalty can be reduced while providing high exhaust gas temperature due to the delayed burn. In turn the emissions are reduced and faster catalyst light off is ensured thereby reducing the inertia inherent to turbocharged gasoline engines. After light off the conventional stoichiometric operation can resume.

GDI engines have been shown to exhibit high particle emissions [136], with the predominant part of the cumulative particle number during the NEDC cycle being emitted during the cold start [137]. It was further found that particle emissions were related to engine load suggesting that incomplete vaporisation of the fuel led to fuel droplets during the combustion process. The fuel volatility is of importance for mixture formation [138] and ultimately on emissions [139]. Fuel related combustion chamber deposits have been shown to be more likely in GDI engines [140], which can also have a negative impact on emissions by increasing both HC and CO emissions [141].

5.1.4 Benefits of EGR in GDI engines

The use of cooled exhaust gas recirculation (EGR) has been shown to be a very effective means of knock suppression in spark ignition engines [142–147]. While its emissions as well as fuel consumption benefits have been shown in naturally aspirated [148] and charge boosted PFI engines [143, 144], Alger and co-workers pointed out major synergies between EGR, direct injection and charge boosting [145]. By using cooled EGR they found that a CO_2 reduction of up to 20% was possible due to higher knock resistance while CO could be lowered by 95% at high speed and load conditions. This was due to a decrease in knock tendency and subsequent improvement in combustion phasing and reduction in exhaust gas temperature that eliminated the requirement for over-fueling. At low and part loads, uncooled EGR led to a fuel consumption improvement of up to 4%, by reducing the pumping losses and pre-heating the charge. In another study, the concept of excess fuel, excess air and EGR were compared with regards to knock suppression. It was found that EGR was the most effective alternative method which allowed more advanced phasing and more stable combustion over a wider operating range [149]. The same authors investigated the use of different EGR loop strategies and summarised that while pre-turbine to post-compressor was beneficial in terms of improved transient response due to lower dead volume and higher compressor efficiencies, it was not possible to achieve enough EGR flow rate for the required operating map [150]. Due to these challenges it was stated that pre-compressor EGR supply from post-turbine may be inevitable, which would have the benefit of reduced EGR cooling demands. Turner and co-workers reported on different EGR architectures on an optimised downsizing concept using an integrated exhaust manifold that is cooled directly using engine coolant. At high load this has the benefit that heat is removed directly between the combustion chamber and the turbine entry thereby requiring less fuel enrichment while at the same time requiring significantly less EGR for optimal fuel efficiency [151]. It was hence argued that a low pressure loop with significantly lower cooling requirement could be used to avoid the challenge of additional heat load on the engine cooling system as pointed out by other researchers using intermediate or high pressure loops [145, 149]. Taylor et. al. noted that a water cooled exhaust manifold also placed additional strain on the cooling system although it did improve the engine warm up time which gave an improvement in the cycle fuel consumption [142]. Although the pre-turbine enthalpy was reduced, it was argued that this could be overcome by appropriate turbocharger matching as well as valve train hardware and that it opened the door for the application of variable turbine geometry (VTG) turbocharger technology on gasoline engines. A further benefit of low-pressure EGR is the ability to use exhaust gas downstream of the catalytic converter whereby nitrous oxides, that have been shown to encourage autoignition [152, 153], could be removed [154]. A "hybrid" high pressure and low pressure loop EGR system was presented

by Roth and co-workers where by the total operating range of a gasoline engine could be covered to allow optimal efficiency and lowest emissions [147].

Bourhis et. al. investigated low pressure EGR and internal gas recirculation (IGR) to compare their effect on fuel consumption at moderate engine load. Although higher wall heat losses occur due to increased gas temperature at the start of combustion, low pressure EGR has a positive effect on indicated specific fuel consumption (ISFC) and mean effective pressure (IMEP) due to reduced peak combustion temperatures as well as improved combustion phasing once knock occurrence starts to come into effect. IGR increased the knock tendency due to elevated temperature at the end of compression while the delayed combustion phasing, although reducing the wall heat losses, further negatively impacted overall efficiency [155].

EGR reduces the combustion peak temperature thereby reducing the formation of NO_x. Reducing the combustion temperature also leads to lower wall-heat transfer and improves thermal efficiency [94, 145]. However, the downside of adding the burned exhaust (inert) gas to the combustion air, is the resultant lower burn rate and hence further deviation from the ideal constant-volume combustion [94]. EGR dilution levels are ultimately limited by cycle-to-cycle variability and misfire. The nature of this variability has been found to be largely deterministic, thereby opening the door for control strategies to allow operation near the boundaries of stability and extension of the dilution limit which would offer significant efficiency gains [156]. In order to increase the EGR tolerance and allow ignition of highly diluted air-fuel mixtures, dual coil ignition systems have been developed that generate an extended continuous spark [157, 158].

In order to improve the EGR tolerance at low speed, researchers have looked at increasing the tumble ratio of the intake ports in a single cylinder research engine with a low-pressure EGR route [159]. They found that high tumble increased the EGR tolerance, high load capability and improved thermal efficiency by advancing the knock limited combustion phasing, whereas extremely high tumble was found to increase the propensity to knock.

Alger and co-workers investigated the potential of adding pure hydrogen, known for its high laminar flame speed [160], up to a maximum of 1% by volume to increase the EGR tolerance in spark ignition engines [161]. It was found that at an EGR level that resulted in the coefficient of variation (COV) of IMEP to be $> 5\%$ only a small amount of hydrogen was required to obtain stable engine operation. Equally by fixing the addition of hydrogen to 1% the EGR level could be increased from 25% to over 50% for gasoline. A similar strategy to improve the EGR tolerance has been investigated through the use of reformed exhaust gas recirculation (REGR) which is the on-board generation of hydrogen rich gas using the waste exhaust gas heat [162]. Hydrocarbon fuel and exhaust gas are passed over a reforming catalyst, where an endothermic reaction, driven by the exhaust

heat, converts liquid fuel into reformate which is a hydrogen rich gas. This results in an increase of the overall fuel energy which is proportional to the waste heat from the exhaust. Experimental results using a single cylinder GDI engine to compare conventional EGR to REGR found that improved combustion stability existed with REGR and that it allowed a higher amount of recirculation as well as mixture dilution. By allowing more fuel to be reformed a higher amount of energy would be reused. NOx and HC emissions were improved in comparison to EGR while the particulate matter was similar.

5.1.5 Current trends for GDI technology

Taylor et al. have investigated discrepancies in fuel consumption measured during regulated cycles and real world driving conditions, but their results indicate that there is potential for downsized engine technology to further reduce fuel consumption in both regulated driving cycles and real world conditions [163].

The benchmark for future gasoline engine concepts was stated in 2007 to be 100 kW/litre and 200 Nm/litre which results in a brake mean effective pressure of 25 bar at 1500 rpm [164]. In 2013 an automotive manufacturer launched a compact vehicle with a high performance charge boosted four cylinder engine with 133 kW/litre and 226 Nm/litre resulting in a BMEP in excess of 28 bar [165]. Due to the engine being designed for a performance vehicle, the fuel efficiency is not representative of a classical downsized spark ignition engine.

Turner and co-workers reported on the development of a four cylinder engine, downsized by 60% over a 5.0 litre V8, but with the same torque characteristics of the large capacity naturally aspirated engine [96]. The project aimed to showcase the ability of downsizing to enable a 35% reduction in CO_2 exhaust emission measured over the New European Driving Cycle (NEDC).

Charge boosting assisted by an electrically driven compressor has been shown in a 3 cylinder engine with BMEP of up to 30 bar, with improved dynamic response [97]. Additionally the energy used for electric boosting could be recuperated using a 2-3 kW generator.

The benefit of pressure charging in combination with stratified operation has been shown as having the potential to significantly increase the operating range thereby improving fuel efficiency and exhaust emissions [94,166,167]. Spicher et. al. investigated the effects on combustion in stratified mode at the upper load limit by increasing fuel injection pressure to 1000 bar and found potential to extend the operating range as well as achieve remarkable improvements in mixture preparation and soot formation [168].

Researchers at the Southwest Research Institute developed a concept vehicle using, what they termed, a dedicated EGR engine based on a four cylinder 2.0 L GDI engine [169]. One of the cylinders is dedicated to the production of EGR which it supplies, at a nominal rate of 25%, to the remaining cylinders whose compression ratio has been increased to 11.7:1 to make use of the increased knock resistance. By running the dedicated cylinder at an equivalence ratio of 1.3 to 1.4, rich combustion reformat consisting of carbon monoxide and hydrogen was formed that improved the knock tolerance further while the hydrogen allowed the engine to operate at 25% EGR. The concept required the use of a supercharger in order to meet the BMEP target of 17 bar from 1500 to 5500 rpm while allowing a BSFC reduction of at least 10% over a comparable naturally aspirated GDI engined vehicle.

5.2 Thermodynamic analysis of GDI combustion

The efficiency advantages of the direct injection gasoline engine are best discussed by considering the ideal constant-volume process (Otto cycle) for this engine. In the Otto cycle, isentropic compression is followed by constant volume combustion at top dead centre which is then followed by isentropic expansion and heat rejection at constant volume. Assuming the working fluid to be ideal gas, the thermal efficiency can be described as follows [17]:

$$\eta_{f,i} = 1 - \frac{1}{r_c^{\gamma-1}} \tag{5.3}$$

In the absence of losses with the assumption of a closed process without fuel conversion, the efficiency is therefore only dependent on the compression ratio r_c of the engine and the isentropic exponent γ. A high compression ratio and large isentropic exponent, which is dependent on temperature and mixture composition, therefore result in the highest achievable efficiency.

By directly injecting fuel into the combustion chamber the sensible enthalpy is reduced due to the vaporisation of the fuel which causes evaporative cooling. This results in decreased temperature at the end of compression which in turn results in lower knock tendency than equivalent port fuel injected engines. The compression ratio can therefore be increased which results in improved thermal efficiency. With lean charge stratified combustion mode, the highest efficiency gain is due to lower pumping losses since this type of engine operates un-throttled. A lean air fuel mixture also increases the isentropic exponent towards the maximum value of pure air (γ= 1.4), which again improves the thermal efficiency. However, the lean burn combustion process has been shown to exhibit a distinctively early 50% mass fraction burn (MFB) point due to the rate of flame prop-

agation in a stratified charge. In the enriched mixture zone near the spark plug the burn rate accelerates quickly and then slows down when it reaches the lean region, thereby deviating from the ideal constant volume process which results in reduced efficiency [86]. By increasing the turbulence and appropriately directing the charge movement in the combustion chamber the slowing of the burn rate can be overcome.

Van Basshuysen describes the combustion process of direct injection in homogeneous mode to be similar to port fuel injected engines. From the spark plug an almost spherical flame front propagates through the combustion chamber and the flame surface tends to become convoluted by turbulence and in-cylinder charge motion [85]. If a perfectly homogeneous mixture exists, the combustion will take place without the occurrence of diffusion flame and can be defined by an ideal premixed flame. Despite similarities to port fuel injected engines, direct injection does not allow for perfect mixture homogenisation which results in cyclic variation of the mixture state and in turn effects the flame stability negatively [17, 85].

5.2.1 Indicated data analysis

As the friction losses of a single cylinder research engine are not representative of a multi cylinder derivative, it is customary to analyse and report on indicated performance parameters. However, the measured brake torque was recorded and used as a cross check for the indicated data analysis. The in-cylinder pressure parameters were recorded and analysed using the AVL Indismart equipment described in chapter 2. Some of the considerations crucial to enable accurate data signal processing are discussed below.

5.2.1.1 TDC determination

AVL Indicom allows the determination of top dead centre (TDC) by calculating the mean value from ten successive motored pressure cycles. A thermodynamic loss angle of 0.7 deg CA at 2000 rpm was used as a correction value [170].

5.2.1.2 Pressure reference method

A number of referencing methods were evaluated by Randolph to peg the relative pressure measured by the piezoelectric transducer to an absolute value. The two main methods identified were referencing a point within the engine cycle to a measured or estimated value and alternatively fitting the compression to a polytropic process [171]. It was noted that while referencing to the intake manifold pressure at bottom dead centre worked well for the part load conditions and the specific test engine without intake manifold

tuning, the dynamic pressure fluctuations inherent to production manifolds as well as elevated engine speeds would reduce the accuracy of this method. Brunt et al suggested that polytropic indexing is the most accurate way of pegging, other than for very lean mixtures where the polytropic index is not known [172].

A pressure correction by means of the polytropic process can be applied to each data point:

$$P_{actual} = P_{measured} + P_{correction} \tag{5.4}$$

where:

$$P_{correction} = \frac{P_2 - P_1}{(\frac{V_1}{V_2})^n - 1} \tag{5.5}$$

P_n is the pressure and V_n the volume in the compression region. A constant polytropic exponent of 1.32 was applied between 100 and 70 degrees BTDC [170–172].

Data pegging is important when trying to accurately define absolute values such as peak cylinder pressure, whereas the location of peak pressure, maximum pressure rise rate or indicated mean effective pressure recordings are not effected [173].

5.2.1.3 Thermal shock

Rai et. al. investigated the influence of thermal shock on piezoelectric transducers during cylinder pressure measurements which they found to be greatly affected by transducer type [174]. They found that thermal shock was most pronounced at low engine speed, high load, advanced ignition timing and low exhaust gas recirculation rate. According to the specification sheet of the AVL transducer used for the experiments presented in this thesis, the error due to thermal shock was given as smaller than 1% at 9 bar IMEP and 1500 rpm [175].

5.2.1.4 Indicated mean effective pressure

Indicated mean effective pressure is the indicated work output per unit swept volume. Stone defines it as [176]:

$$imep = \frac{W_i}{V_s} \tag{5.6}$$

where:

W_i is the indicated work in Newton metres and the V_s the swept volume in cubic meters

A computationally efficient and most commonly applied IMEP calculation is [177]:

$$imep = \frac{\Delta\theta}{V_s} \sum p.\frac{dV}{d\theta} \tag{5.7}$$

where:

θ is the change in crank angle position in degrees
V_s is the cylinder swept volume in cubic meters
p is the cylinder pressure in bar
$\frac{dV}{d\theta}$ is the change in volume with respect to crank angle position

AVL Indicom calculates the IMEP at one crank degree intervals over the entire combustion cycle.

The coefficient of variation in IMEP is used to define the combustion stability and is defined as [178]:

$$C_v = \frac{\sqrt{\sum^N (p_i - \bar{p_i})^2/(N-1)}}{\bar{p_i}} \tag{5.8}$$

where:

N is the sampled number of cycles

5.2.1.5 Mass fraction burned analysis

There are generally two approaches when doing a thermodynamic analyses of the cylinder pressure data, the burn rate analysis and the heat release analysis. The burn rate analysis is most often used to define the burn angles in gasoline engines and results in the mass fraction burned which is a normalised scale from 0 to 100%. Heat release analysis is calculated from the first law of thermodynamics and results in the total energy released in unit of Joule or the heat release per crank angle and is most frequently used for diesel engine combustion analysis [176, 179].

The mass fraction burned is, to this day, often calculated using the Rassweiler and Withrow method developed in 1938 [180] as it is both computationally efficient and quite accurate [181]. The standard algorithm in AVL Indicom makes use of the first law of thermodynamics [176] to calculate the heat release in real time:

$$Q_i = \frac{K}{\kappa - 1}[\kappa.p_i(V_{i+n} - V_{i-n}) + V_i.(p_{i+n} - p_{i-n})] \tag{5.9}$$

where:

n is the crank interval (1 ° CA)
κ is the polytropic coefficient
p is the cylinder pressure in bar
V is the cylinder volume in cubic meter
K is a constant of 100 for the unit conversion

Since the polytropic coefficient is dependent on temperature, Indicom makes use of two coefficients. For the compression process a coefficient of 1.35 is used and the expansion process uses 1.3 [170]. By reducing the coefficient for the expansion process it ensures that the heat release integral does not increase further after end of combustion.

5.2.1.6 Knock detection

The AVL knock algorithm calculates the knock integral and peak knock value from the cylinder pressure measurement signal which is first subjected to a high pass filter as well as rectification. A knock integral of 2 as well as a peak knock value of 2 bar was chosen and a dynamic mean value filter with a cut-off frequency of 40 kHz was applied to the pressure signal. The minimum knock peak threshold was defined as 0.3 bar. After each engine cycle these characteristics are compared to the previous cycle and a decision is made whether to classify it as a knock event. The knock events were summarised over 100 cycles after which a knock frequency was calculated. Once a knock frequency of 10% was measured, this was defined as the knock threshold.

5.3 Test method

The combustion analysis was conducted using the single cylinder engine test facility developed for this research project as discussed in Chapter 2. Two aspects of charge boosted direct injection gasoline combustion were found to be relevant with respect to the synthetic fuel blend properties defined in Chapter 3 and the laminar flame speed characterisation presented in Chapter 4.

5.3.1 Full load spark advance sweeps

As reported in the literature review, fuel components with higher laminar flame velocity can decrease the burn duration and by so doing approach the ideal constant volume combustion process which leads to higher thermal efficiency [5]. Modern engines have also been shown to operate in a temperature pressure regime that lies "beyond RON", which implies that the octane sensitivity can greatly influence the performance of these engines due to higher knock resistance allowing more advanced ignition timing [3,4]. The maximum allowable peak cylinder pressure of the research engine was limited to 100 bar, which restricted the boost to a gauge pressure of 0.5 bar. From chapter 3 it has become known that some of the synthetic blending components can potentially alter the sensitivity of a final fuel blend. To investigate the performance characteristics of the test fuels, full load spark advance sweeps were conducted with the operating parameters shown in table 5.1. Due to the improved torque at low engine speeds of modern charge boosted engines, 1500 rpm was chosen due to its relevance in evaluating knock resistance at low engine speed and high load. The engines characteristic maximum torque was found at 3500 rpm while peak power occurred at 5000 rpm.

Engine speed	**Air fuel ratio (λ)**	**Charge boost (bar)**	**Charge temperature (°C)**	**Coolant temperature (°C)**	**Oil temperature (°C)**
1500	0.9	0.5	30	90	100
3500	0.9	0.5	30	90	100
5000	0.9	0.5	30	90	100

Table 5.1: *Engine parameters for full load spark advance sweeps*

5.3.2 K-value determination

The K-value has been stated to be dependent on the engine as well as the operating condition and its determination requires the knock limited spark advance data of different fuels with varying levels of sensitivity that is independent of RON [119]. While the test fuel blends varied in sensitivity and RON number it was decided to include two primary reference fuels (PRF95 and PRF90) with zero sensitivity by definition and two toluene standardization fuels (TSF94.8 and TSF89.5) with significant sensitivity. The highest K-value is typically found at stoichiometric air-fuel ratio and reduces as the mixture becomes either rich or lean [119, 120]. All the spark advance sweeps were conducted at slightly rich conditions as indicated in table 5.1.

5.3.3 Full load EGR sweeps

Exhaust gas recirculation has been shown to be very effective in improving the knock resistance while also enabling a significant reduction in the exhaust gas temperature. It is therefore expected that future downsized engine concepts will make extensive use of this technology. As the exhaust gas drastically reduces the laminar flame speed of the air fuel mixture, fuel components with inherently higher flame speed have been shown to improve EGR tolerance resulting in lower cyclic variation and improved combustion stability [161]. In order to characterize the test fuels with respect to their EGR tolerance, full load EGR sweeps were conducted at 1500 rpm and 3500 rpm as shown in table 5.2. As discussed in chapter 2, the engine was equipped with a cooled EGR loop for this purpose.

Engine speed	**Air fuel ratio (λ)**	**Charge boost (bar)**	**Exh. back pressure (bar)**	**Charge temperature (°C)**	**Coolant temperature (°C)**	**Oil temperature (°C)**
1500	1	0.5	0.6	30	90	100
3500	1	0.5	0.6	30	90	100

Table 5.2: *Engine parameters for full load EGR sweeps*

At each EGR rate set point the spark advance was adjusted until maximum brake torque (MBT) was obtained or when the knock threshold was reached. Due to the limitation in allowable back pressure, the EGR rate was restricted to approximately 18% at 1500 rpm which did not allow to reach the EGR tolerance limit.

5.3.4 Engine test procedure

The engine tests were run in a S-X-X-S formation, where S represents the 95 RON SCAG fuel that was used as a reference and X represents the test fuels defined in chapter 3.

At the beginning of each day or after an extended break between tests the following start up procedure was followed:

- Switch on conditioning unit to pre-heat engine oil and coolant
- Activate start up procedure of Mexa emission measurement and perform calibration
- Perform fuel swap
- Switch on AVL fuel flow meter and fuel conditioning system and allow to stabilise
- Start engine and run for 30 minutes to ensure engine is warmed up

- Set test engine speed and allow to stabilize for 10 minutes before commencing with test

Upon completion of the first test runs a significant amount of scatter among the reference fuel tests was noted. Due to an appreciable variance in atmospheric pressure from one day to the next, a correction factor normalising to 990 kPa was applied. Since the charge air was passed through a dryer on the compressor before being controlled to 30° C in the charge air control unit, no temperature and humidity correction was required. However, the pressure correction did not alleviate the scatter sufficiently, necessitating further interrogation of the engine control parameters such as boost and fuel injection pressure and test bench measurements such as engine coolant temperature and HC emissions. A multiple linear regression model was set up in Microsoft Excel 2010 to try and relate small variations in engine control parameters and relevant test bench measurements to the IMEP fluctuations. No significant correlation was found. The engine test procedure was re-visited and the quandary was finally solved by adding dye to a test fuel which revealed that an extra 2 litres of fuel were required to adequately flush the fuel system. Subsequent testing confirmed that the undesired mixing of the fuels was the reason for the muddled results. Although the matter was eventually narrowed down to an unfortunate case of operator error, the detailed interrogation of the engine control and test cell set-up subsequently instilled a high degree of confidence in the recorded data.

5.3.5 Test fuel blends

The test fuel blends consisted of the 93 and 95 RON crude derived CAG, the 95 RON synthetic CAG and synthetic CAG spiked with the respective synthetic blending components as tabulated in 5.3. Some test blends with a 10% spiking ratio were evaluated initially, but the test results were found to be not clearly distinguishable. The 20% blends provided the expected distinction and the 50% ratio was chosen as the highest admixture due to the very low octane rating of some of the synthetic blending components.

A standard fuel analysis of the 20% and 50% blends is provided in Appendix C.

Test fuel description	Accronym
Crude derived 93 RON CAG	CCAG93
Crude derived 95 RON CAG	CCAG95
Synthetic derived 95 RON CAG	SCAG95
Synthetic 95 RON CAG + 20% SGBC A	SBA20
Synthetic 95 RON CAG + 20% SGBC B	SBB20
Synthetic 95 RON CAG + 20% SGBC C	SBC20
Synthetic 95 RON CAG + 20% SGBC D	SBD20
Synthetic 95 RON CAG + 20% SGBC E	SBE20
Synthetic 95 RON CAG + 20% SGBC F	SBF20
Synthetic 95 RON CAG + 20% Ethanol	E20
Synthetic 95 RON CAG + 20% TAME	T20
Synthetic 95 RON CAG + 50% SGBC A	SBA50
Synthetic 95 RON CAG + 50% SGBC B	SBA50
Synthetic 95 RON CAG + 50% SGBC C	SBA50
Synthetic 95 RON CAG + 50% SGBC D	SBA50
Synthetic 95 RON CAG + 50% SGBC E	SBA50
Synthetic 95 RON CAG + 50% SGBC F	SBA50
Synthetic 95 RON CAG + 50% Ethanol	E50
Synthetic 95 RON CAG + 50% TAME	T50
Primary reference fuel 95 RON	PRF95
Primary reference fuel 90 RON	PRF90
Toluene standardisation fuel 94.8 RON	TSF94.8
Toluene standardisation fuel 89.5 RON	TSF89.5

Table 5.3: *Test fuel blends used for engine combustion analysis*

5.4 Results and discussion

5.4.1 KLSA and the K-value

The knock limited spark timing was found for the test fuel blends defined in chapter 3 and tabulated in Appendix C. Due to the peak cylinder pressure limitation of 100 bar, it was not possible to establish the knock limit for a majority of the fuel blends at 5000 rpm under boosted conditions. The synthetic fuel blends with 50% ethanol and TAME content were similarly limited by the allowable peak combustion pressure rather than knock and were therefore excluded for this part of the investigation. In table 5.4 the octane properties of the fuels along with the knock limited spark advance (KLSA), peak combustion pressure (PMAX) and the 50% mass fraction burned (AI50) are shown. Although the commercial gasolines, synthetic blending components and oxygenate blends resulted in a fuel set where RON only had a weak correlation with MON ($R^2 = 0.52$), it was found that the resultant K-values were slightly positive as shown in figure 5.1. This was unexpected as the charge boosting and inlet air cooling would suggest that the engine should be operating well "beyond RON" with a negative K value [182]. In general it has been found that as engine speed increases so does the K value [119, 120, 126], however this has been shown to not always be the case [183]. The K value has been stated to be

dependent on engine design as well as on the operating conditions and in principle not be fuel property dependent [119, 182]. It has been shown to be strongly dependent on intake air temperature and pressure while being almost independent of spark plug location and compression ratio. Air fuel ratio was found to only affect the K value greatly under very rich or very lean mixture conditions [120].

Fuel	RON	MON	S	1500			3500		
				$KLSA$	$PMAX$	$AI50$	$KLSA$	$PMAX$	$AI50$
ModelFuels									
$PRF95$	95	95	0	1	56.11	24.33	3	57.06	27.81
$PRF90$	90	90	0	-1	51.64	27.20	1	51.27	31.42
$TSF94.8$	94.8	82.7	12.1	5	69.06	17.53	9	78.58	18.42
$TSF89.5$	89.5	77.9	11.6	2	60.40	21.81	6	67.66	22.85
CommercialFuels									
$SG95$	95.5	85.7	9.8	3.2	65.49	19.95	7	75.49	20.28
$CG93$	93.2	83.6	9.6	2	61.89	21.27	4	64.79	24.35
$CG95$	95.1	85.2	9.9	4	67.15	18.37	7	73.46	20.37
Isoparaf.Comp.									
$SBA20$	94.1	84.7	9.4	2	60.95	21.68	5	66.83	23.61
$SBA50$	91.2	85	6.2	0	56.73	24.58	2	58.49	28.11
Olef.Comp.									
$SBB20$	97.1	84.7	12.4	5	68.33	17.73	9	78.94	18.09
$SBB50$	97.7	84.8	12.9	5.4	70.47	17.30	8	77.49	19.40
$SBF20$	95.6	83.6	12	3	64.30	19.91	6	72.03	21.42
$SBF50$	94.4	82.2	12.2	1.2	63.14	21.34	5	71.43	22.30
Arom.Comp.									
$SBC20$	95.2	84.6	10.6	3.2	63.48	20.19	7	72.48	20.78
$SBC50$	95.2	85.4	9.8	3	63.79	20.36	6	69.25	22.71
$SBD20$	93.1	83.2	9.9	2	61.46	21.46	6	70.51	22.06
$SBD50$	89.4	80	9.4	0	58.06	24.11	2	60.03	27.59
$SBE20$	96.5	83.9	12.6	3.4	64.85	19.58	7	74.89	19.88
$SBE50$	96.3	83.6	12.7	5	70.15	17.10	8	77.72	18.89
Oxyg.comp									
$E20$	100.1	87.2	12.9	9	80.63	12.98	13	94.57	13.32
$T20$	98.5	87.2	11.3	6.2	73.11	16.06	10	85.00	16.51

Table 5.4: *Knock limited spark advance data at specified engine conditions for all test fuels*

In this study it was found that the choice of fuel did seem to influence the calculated K value. This can be depicted by comparing the correlation between octane index and the knock limited spark advance for the different fuels selected. For each of the fuel sets the interdependence between RON and MON was checked and R^2 found to be less than 0.1, implying no correlation.

In figure 5.2 the model fuel components and the three CAG fuels were used to calculate the octane index which resulted in a fairly good correlation for 1500 rpm while at 3500 rpm the fit was poorer. By adding the two oxygenate blends, the correlation at both engine speeds is improved as seen in figure 5.3. Replacing the oxygenate blends with synthetic blend component A, which is high in iso-paraffins and has significant aromatic content, results in less correlation as shown in figure 5.4. Similarly the predominantly

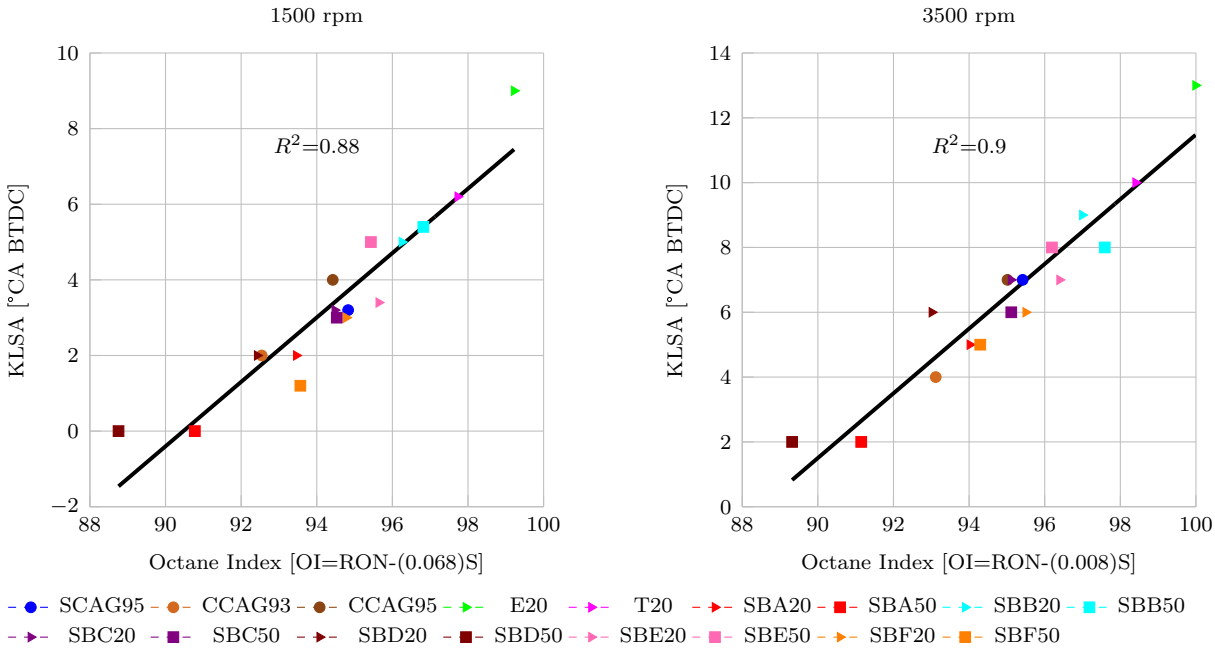

Figure 5.1: *KLSA vs Octane Index for commercial fuels and all synthetic gasoline test blends*

aromatic components C, D and E, shown in figure 5.5, result in a poorer correlation between OI and KLSA, and the olefinic component blends were found to have a very poor relationship as depicted in figure 5.6. In all cases the agreement was better at 1500 rpm than at 3500 rpm. Furthermore an appreciable variation in the K-value was found when using different fuel types. As mentioned in the literature review of this chapter, the K-value is generally defined using model fuel components. The respective olefin and aromatic surrogates, Iso-octene and Toluene, where found to exhibit a very similar laminar flame speed. The refinery fuel component blends used in this study on the other hand showed distinct dissimilarity in their characteristic flame speed.

By adding the model fuel components to the synthetic blends as well as commercial fuels, K was determined to be approximately -0.34 at 1500 rpm and -0.505 at 3500 rpm when calculating the octane index for the entire fuel set as shown in figure 5.7. The correlation coefficient for the entire fuel set was found to be 0.1, reiterating that the calculation method for the K-value seems to be extremely sensitive to any interrelationship between RON and MON as is evident from the comparative results depicted in figure 5.1.

Kalghatgi and co workers recently investigated the fuel effects on knock in a highly boosted direct injection spark ignition engine and conceded that defining the knock behaviour exclusively by the octane index is not ideal [183]. The effect of the fuel's burn rate is not taken into account and the effect of charge cooling is of particular importance in GDI engines. However, it was mentioned that the improved charge cooling would lead to a higher volumetric efficiency and therefore increased pressure that could counteract the

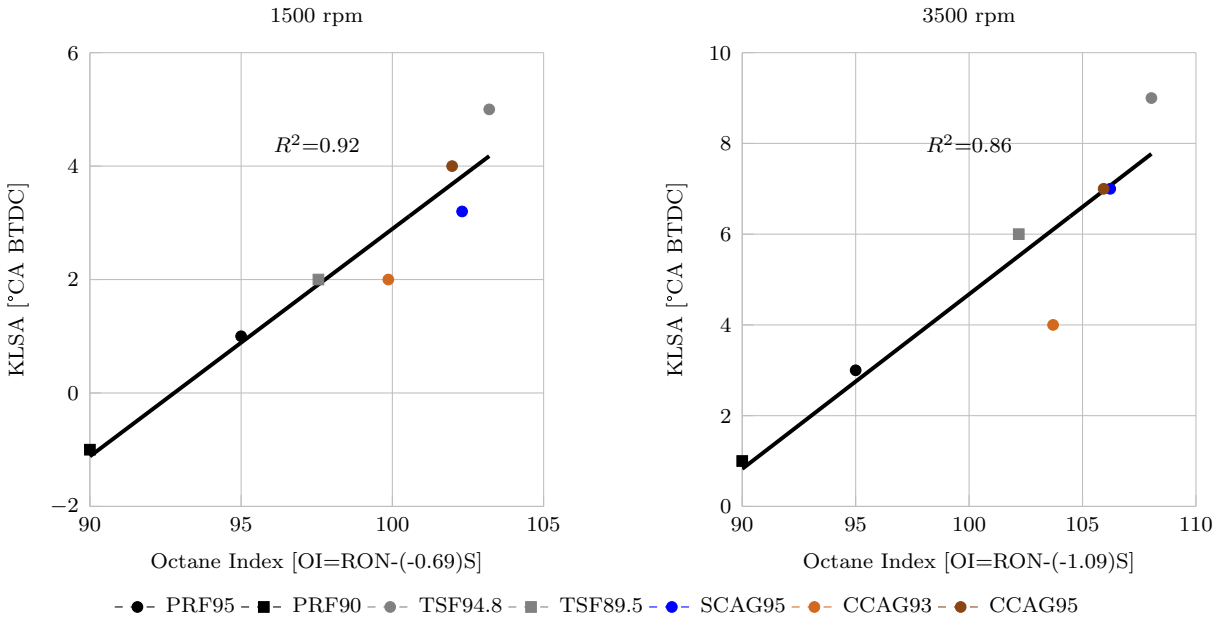

Figure 5.2: *KLSA vs Octane Index for commercial fuels and model fuel blends*

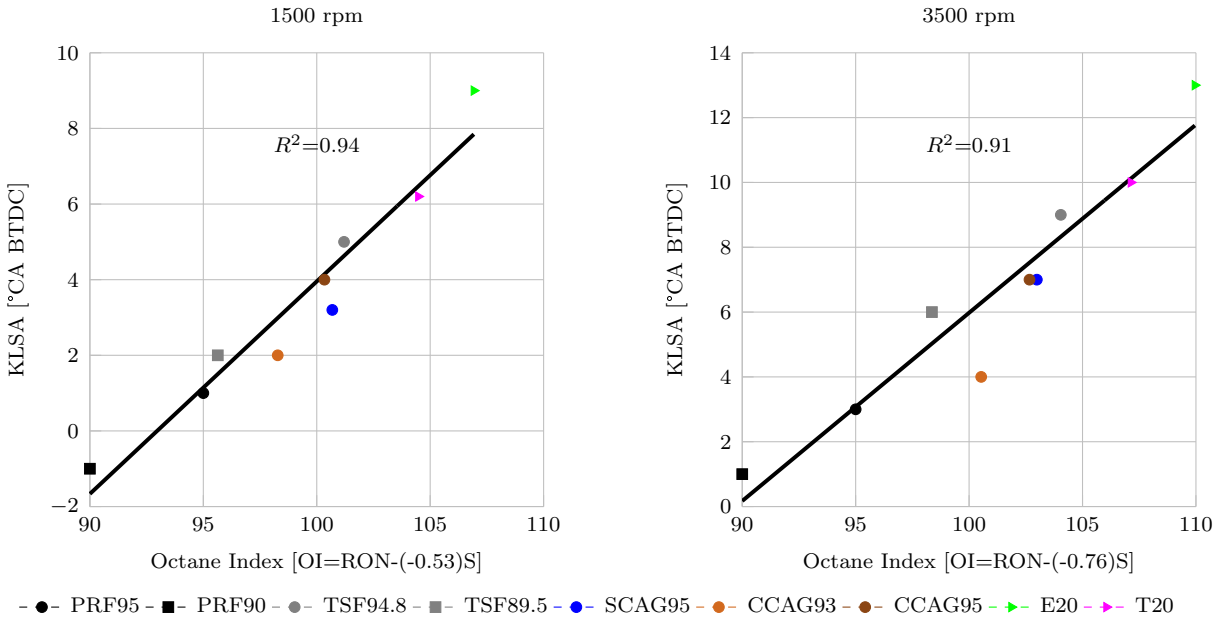

Figure 5.3: *KLSA vs Octane Index for model fuels, commercial fuels and synthetic oxygenate test blends*

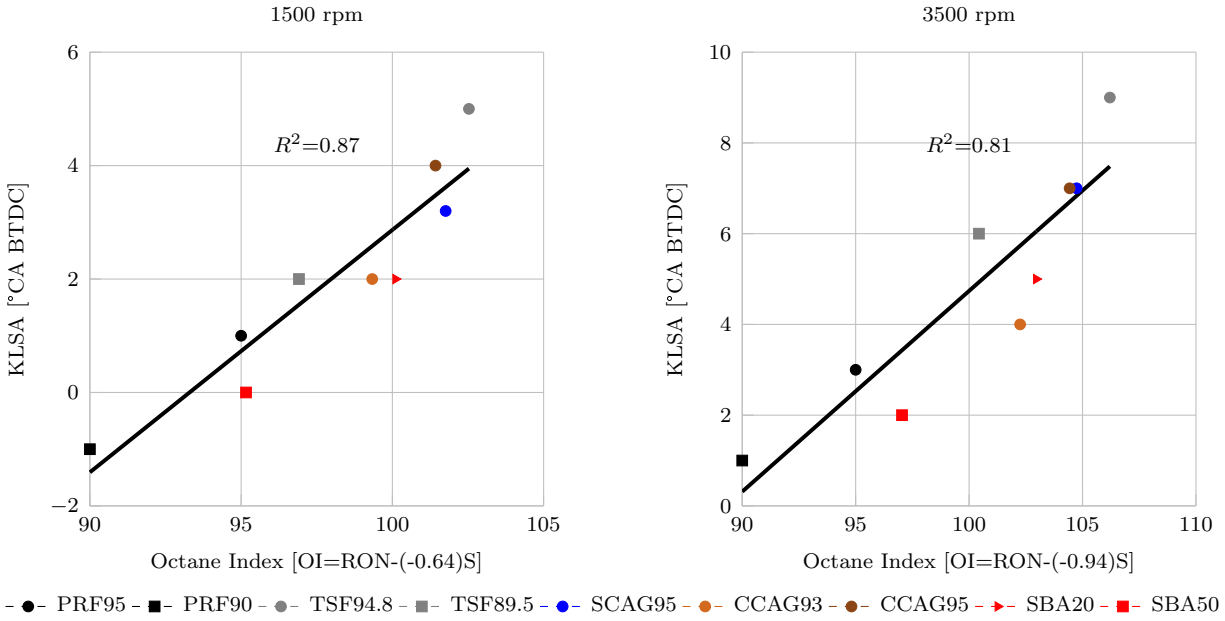

Figure 5.4: *KLSA vs Octane Index for model fuels, commercial fuels and synthetic iso-paraffin test blends*

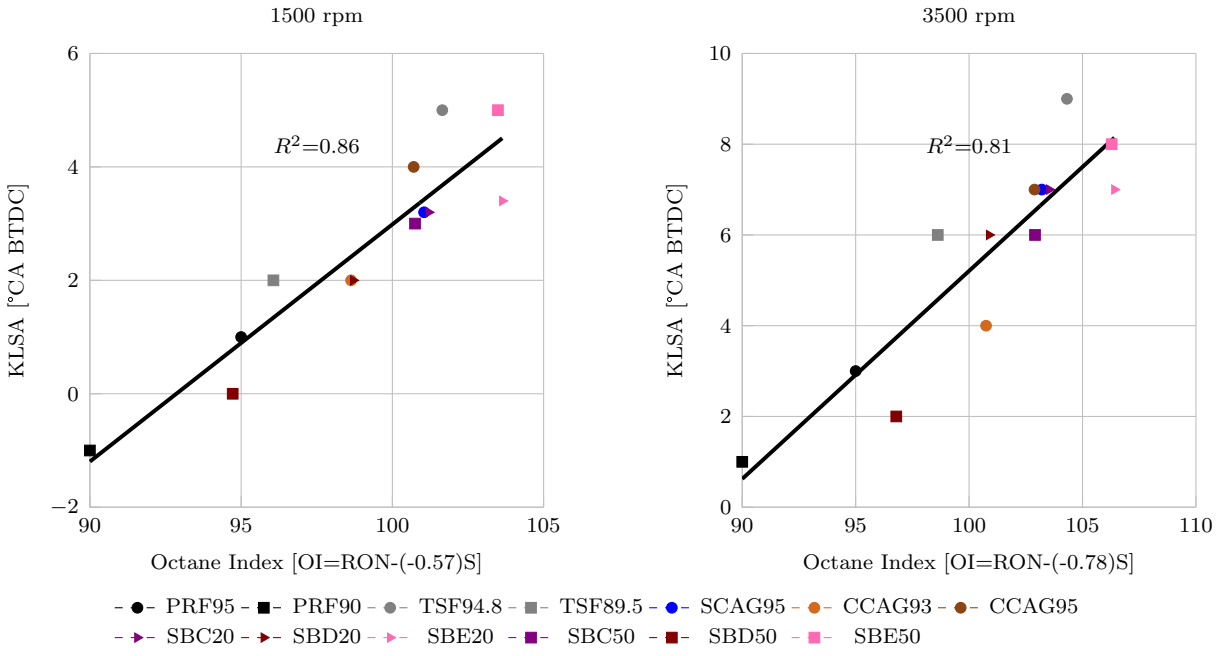

Figure 5.5: *KLSA vs Octane Index for model fuels, commercial fuels and synthetic aromatic test blends*

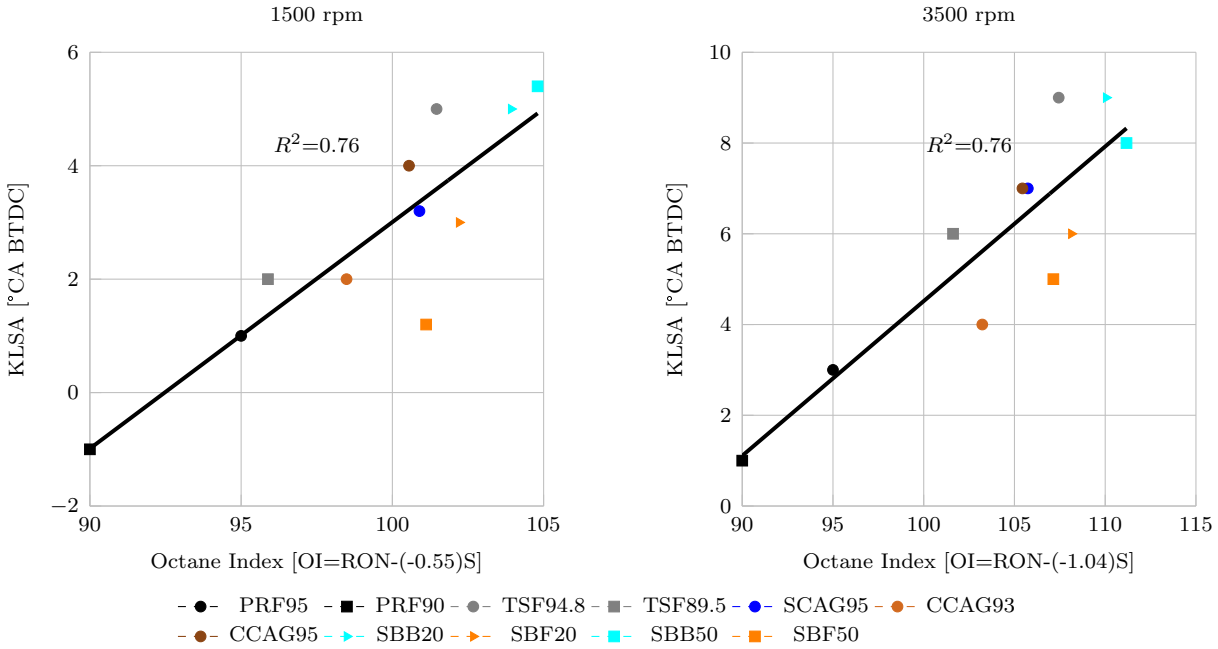

Figure 5.6: *KLSA vs Octane Index for model fuels, commercial fuels and synthetic olefin test blends*

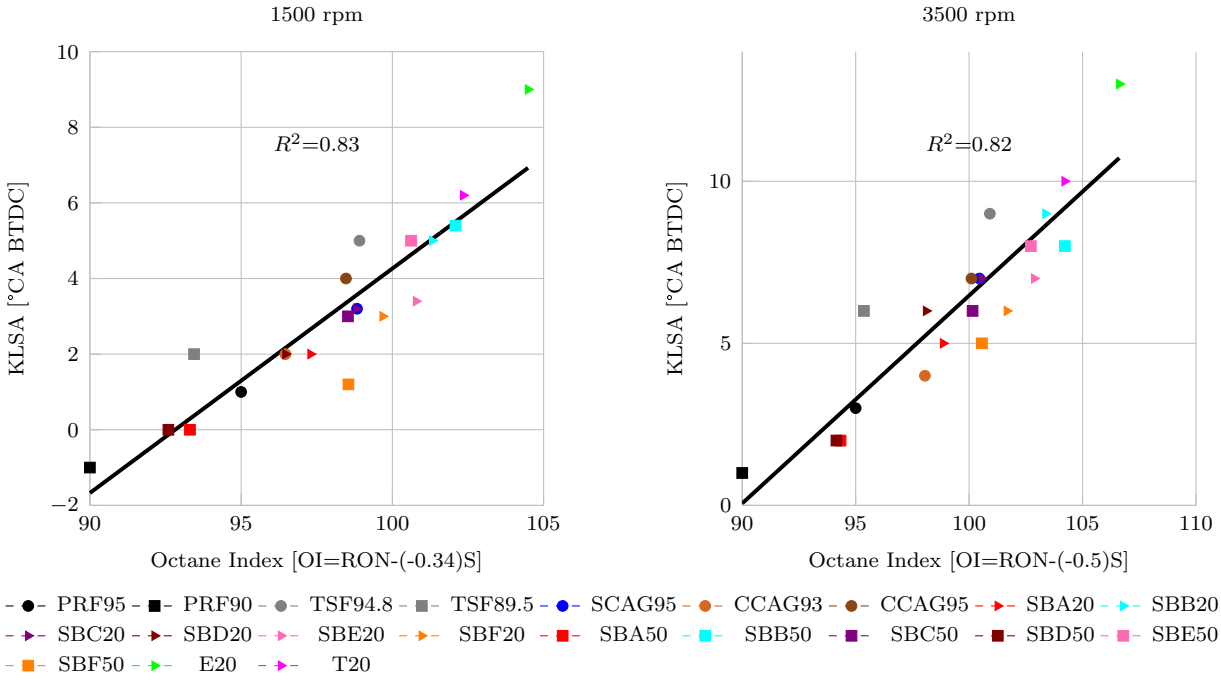

Figure 5.7: *KLSA vs Octane Index for all test fuels combined*

reduction in temperature. Although it was recognized that differences in burn rate and latent heat of vaporization exist, it was argued that differences in auto-ignition chemistry dominate the knock behaviour. While an almost ideal relationship between octane index and knock limited spark advance was found previously [119], this relationship was not found to be perfect in the analysis of the highly boosted engine data, although a similar trend was apparent [183]. This coincides with the findings of this investigation, wherein a higher sensitivity for a similar RON resulted in more allowable spark advance. This in turn led to a higher peak combustion pressure and more optimal combustion phasing as indicated by the 50% mass fraction burned. Interestingly the synthetic blending component F, which is highly olefinic, resulted in a lower KLSA than TSF94.8 which has a similar RON and sensitivity. However, the latent heat of vaporisation of TSF94.8 at 25° C and 1 bar was calculated to be 401 kJ/kg, which is significantly higher than that of SBF20 at 267.4 kJ/kg and SBF50 at 301.1 kJ/kg, thereby resulting in more charge cooling and subsequently higher knock resistance in the GDI engine.

5.4.2 Performance analysis

The phasing of the peak combustion pressure along with the indicated mean effective pressure can be used to examine the combustion efficiency of an engine while the combustion stability is most often defined by the coefficient of variation in IMEP and PMAX [17]. The early flame kernel growth period can be measured by the 0-10% mass fraction burned duration (AI10), while the 0-50% mass fraction burned (AI50) is an important indicator for the work output of an engine [61]. Combustion duration can be accessed by investigating the 10-90% MFB (AI90-AI10) period. In order to allow a comparison, the coefficient of variation of these parameters was also plotted on the same figures.

5.4.2.1 Crude derived gasoline

In figure 5.8 the peak cylinder pressure and its crank angle location (APMAX) as well as the indicated mean effective pressure are depicted at the three engine speeds. The blue markers represent the 95 RON SCAG fuel that was used as a bracket fuel throughout this experimental process while light brown represents the 93 RON CCAG fuel and the 95 RON CCAG is depicted in dark brown. The knock limited spark advance for the 93 RON fuel was found, depending on engine speed, to be 2 - 4 degrees lower than the 95 RON fuels, as to be expected. No significant difference was found between the fuels in terms of peak cylinder pressure, peak pressure phasing or the performance as denoted by IMEP under non knock limited conditions. By optimising the spark advance a reduction in cyclic variability, shown by COV, was achieved. Overall the engine performance was

found to be severely knock limited using 95 RON CAG fuel which is a result of charge boosting in combination with a fairly high compression ratio.

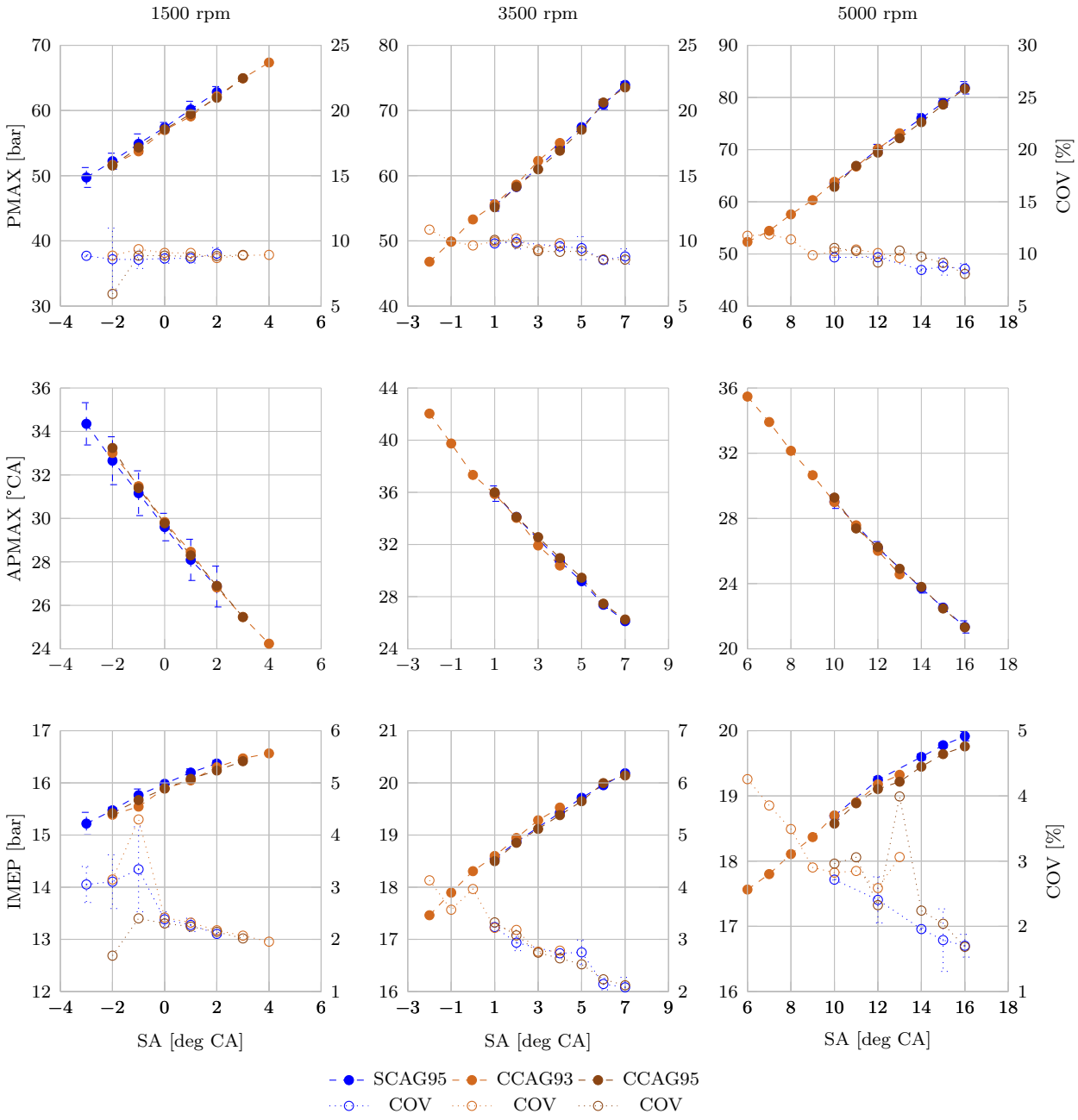

Figure 5.8: *PMAX, APMAX and IMEP vs SA sweeps for SCAG fuel and CCAG fuels*

The crank duration for the 10% and 50% mass fraction burn combustion parameters were also found to be similar between the different CAG fuels as shown in figure 5.9. The combustion duration was defined as the difference between 90% MFB and 10% MFB positions and also showed no significant variation between the fuels.

The specific fuel consumption and regulated emissions were calculated using the indicated performance as shown in figure 5.10. With increased spark advance a reduction in specific

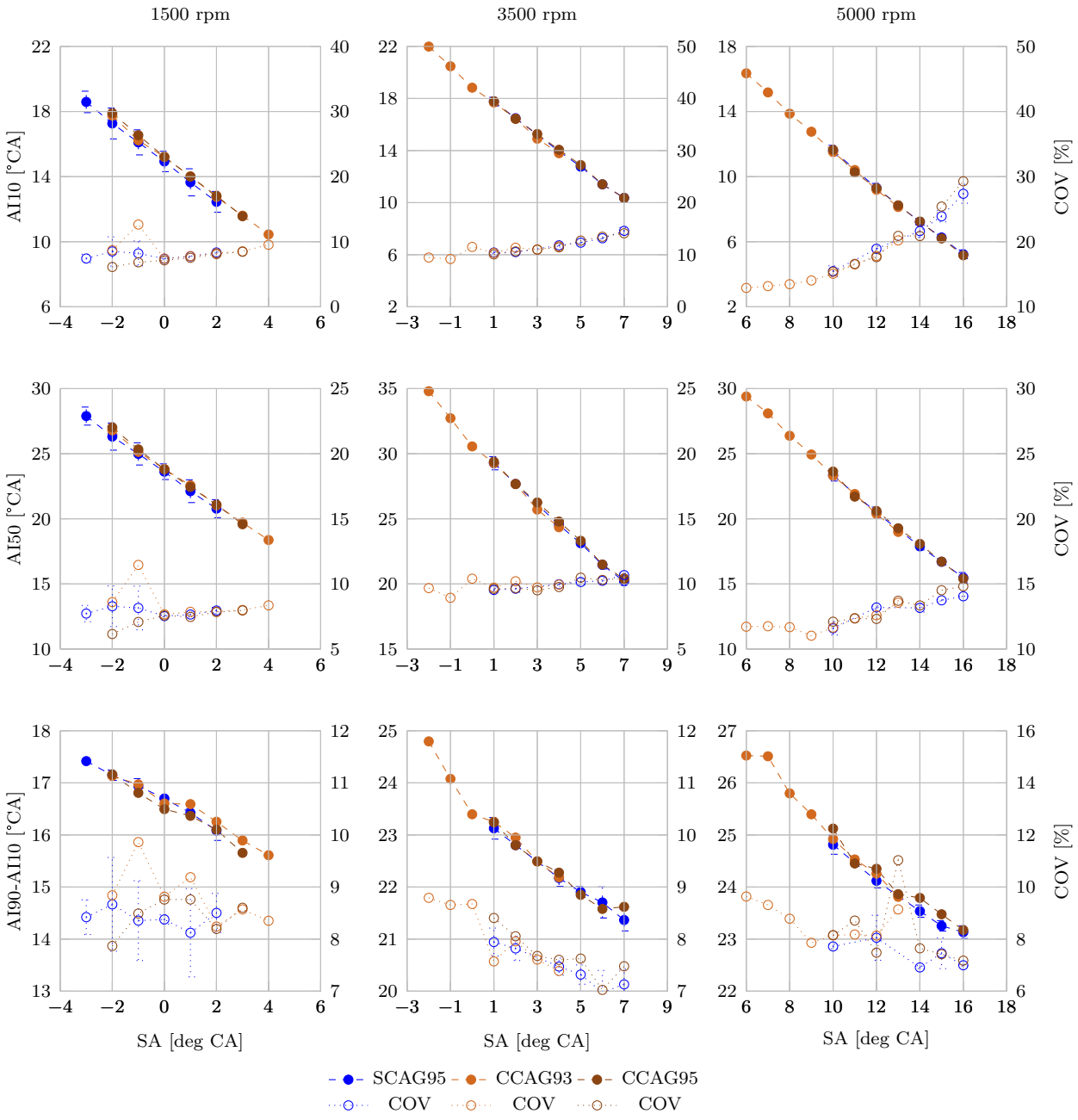

Figure 5.9: *AI10, AI50 and AI90-AI10 vs SA sweeps for SCAG fuel and CCAG fuels*

fuel consumption was seen as expected due to an improved thermal efficiency, while there was little effect as a result of the different fuels. Hydrocarbon emissions were found to be a bit higher with the 95 RON CCAG fuel whereas nitrous oxide and carbon monoxide emissions were marginally higher for both crude derived petrols.

5.4.2.2 Oxygenated synthetic gasoline blends

The ethanol and TAME blends resulted in a significantly higher knock limited spark advance with the 50% ethanol blend resulting in the peak combustion pressure limit being reached at all engine speeds before any appreciably knock activity was noted. As seen in Figure 5.11 at 1500 rpm the 50% ethanol blends resulted in a higher KLSA than TAME, which indicates the benefit of ethanols inherent charge cooling effect in GDI engines as found by other researchers [6, 116, 117]. A distinguishable offset in the IMEP was also found for the 50% ethanol blend at various spark advance settings, suggesting that an improved filling due to the charge cooling was taking place. This effect was not seen at 5000 rpm however, which is assumed to be due to the restricted time available for evaporation at the elevated engine speed. The location of peak cylinder pressure was the same for all the fuels which implies that there was no increase in burn rate. In fact the burn duration of the ethanol blend was found to be marginally slower at 1500 and 3500 rpm as shown by AI90-AI10 in figure 5.12. The 10% and 50% mass fraction burned points were nominally the same for the oxygenated fuels in comparison with the SCAG fuel. This was unexpected since ethanol has a high laminar flame speed as shown in Chapter 4. Beeckmann et. al. [83] reported in their experiments that a 10% blend of ethanol and gasoline resulted in a lower laminar flame speed than for pure gasoline. The authors stated that this results was surprising and that further experiments needed to be conducted. Furthermore, it can be surmised that the higher heat of vaporisation of the ethanol blends could have a profound effect on lowering the in-cylinder temperature conditions which could hamper the laminar flame speed at the onset of spark. This issue will be addressed in more detail in Chapter 6.

Due to the lower heating value of ethanol a significantly higher specific fuel consumption was measured for the 50% ethanol blend as shown in figure 5.13. It was found that the lower heating values of the 20% ethanol blends and the TAME blends were in part compensated for by the improved knock limited spark advance thereby resulting in similar specific fuel consumption. The unburned hydrocarbon emissions of the oxygenated fuel blends was found to be within the repeatability of the reference fuel although there was a clear trend of lower HC emissions using the 50% blends at higher engine speeds. Nitrous oxide emission also tended to be lower with increasing TAME and ethanol content. The carbon monoxide was found to be within the repeatability band.

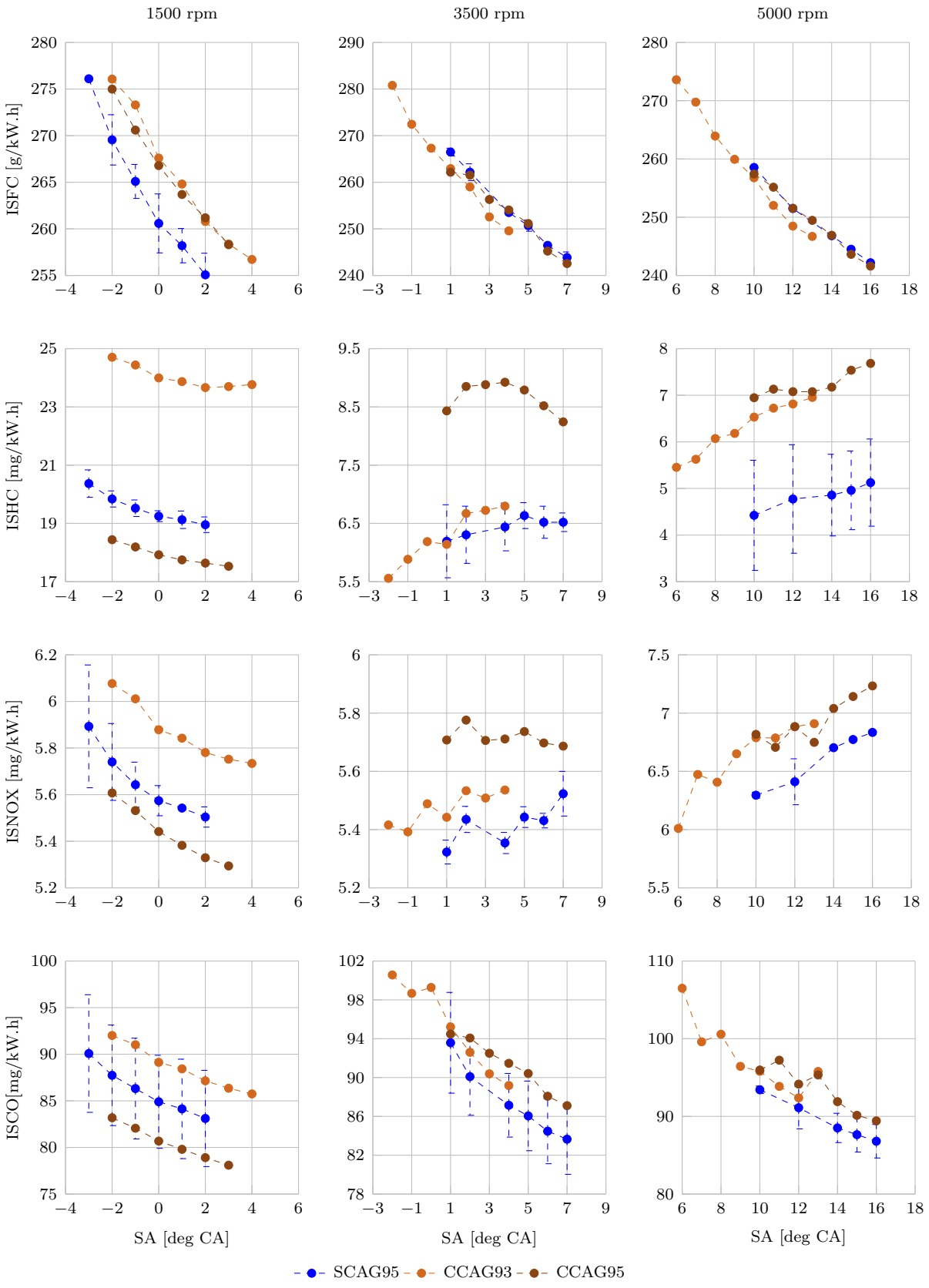

Figure 5.10: *ISFC, ISHC, ISNOx and ISCO vs SA sweeps for SCAG fuel and CCAG fuels*

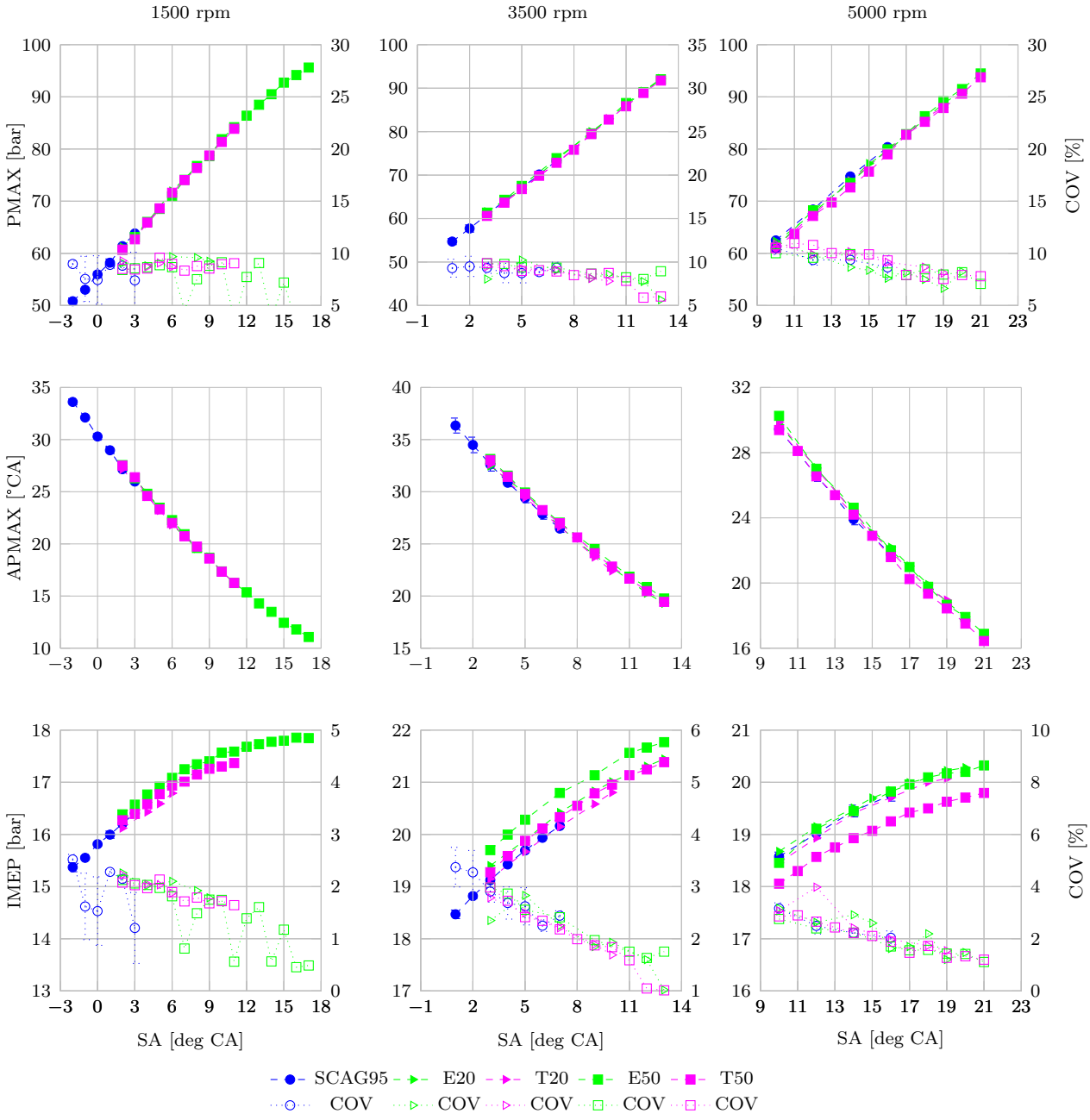

Figure 5.11: *PMAX, APMAX and IMEP vs SA sweeps for SCAG fuel and synthetic oxygenate test blends*

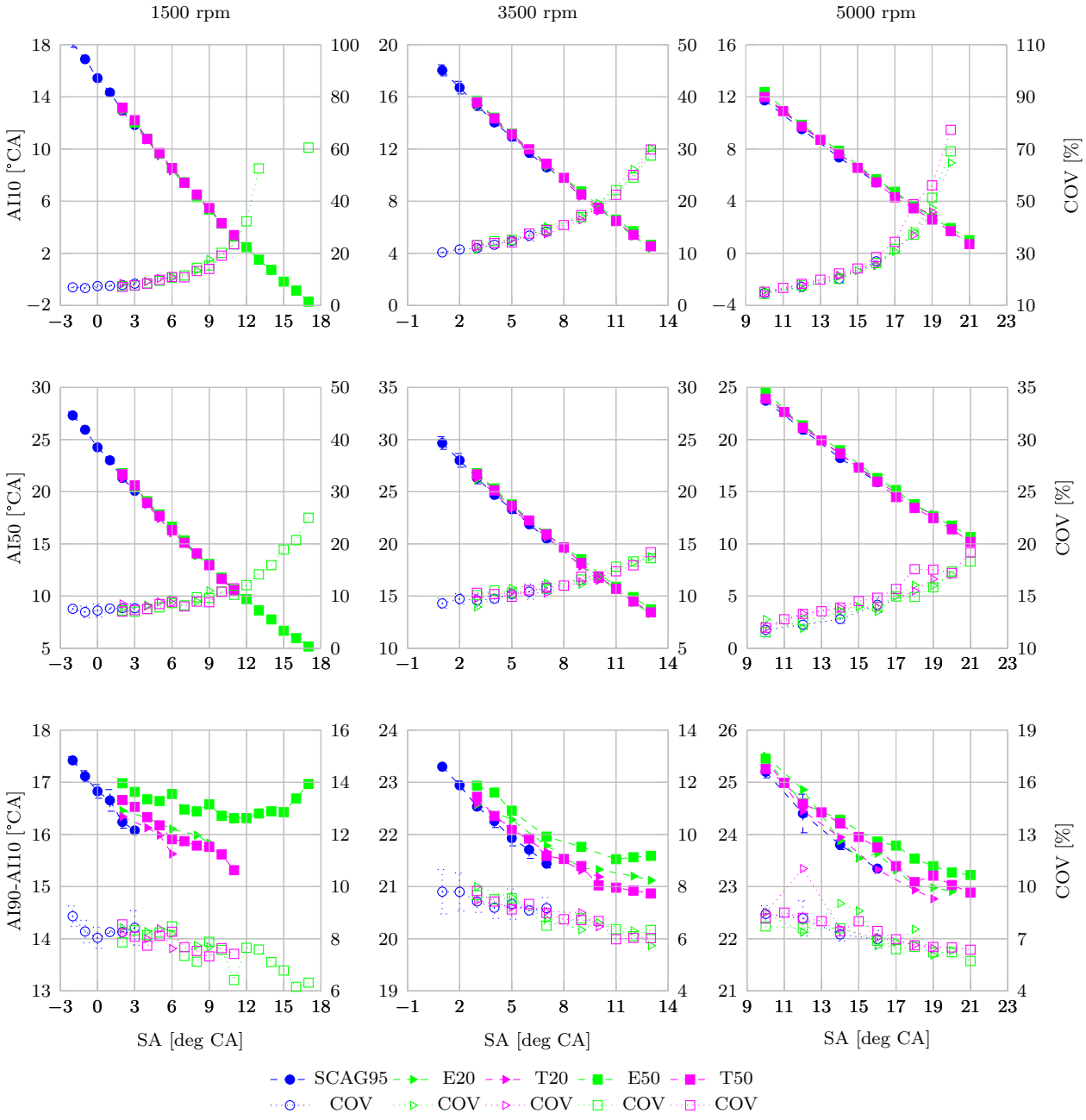

Figure 5.12: *AI10, AI50 and AI90-AI10 vs SA sweeps for SCAG fuel and synthetic oxygenate test blends*

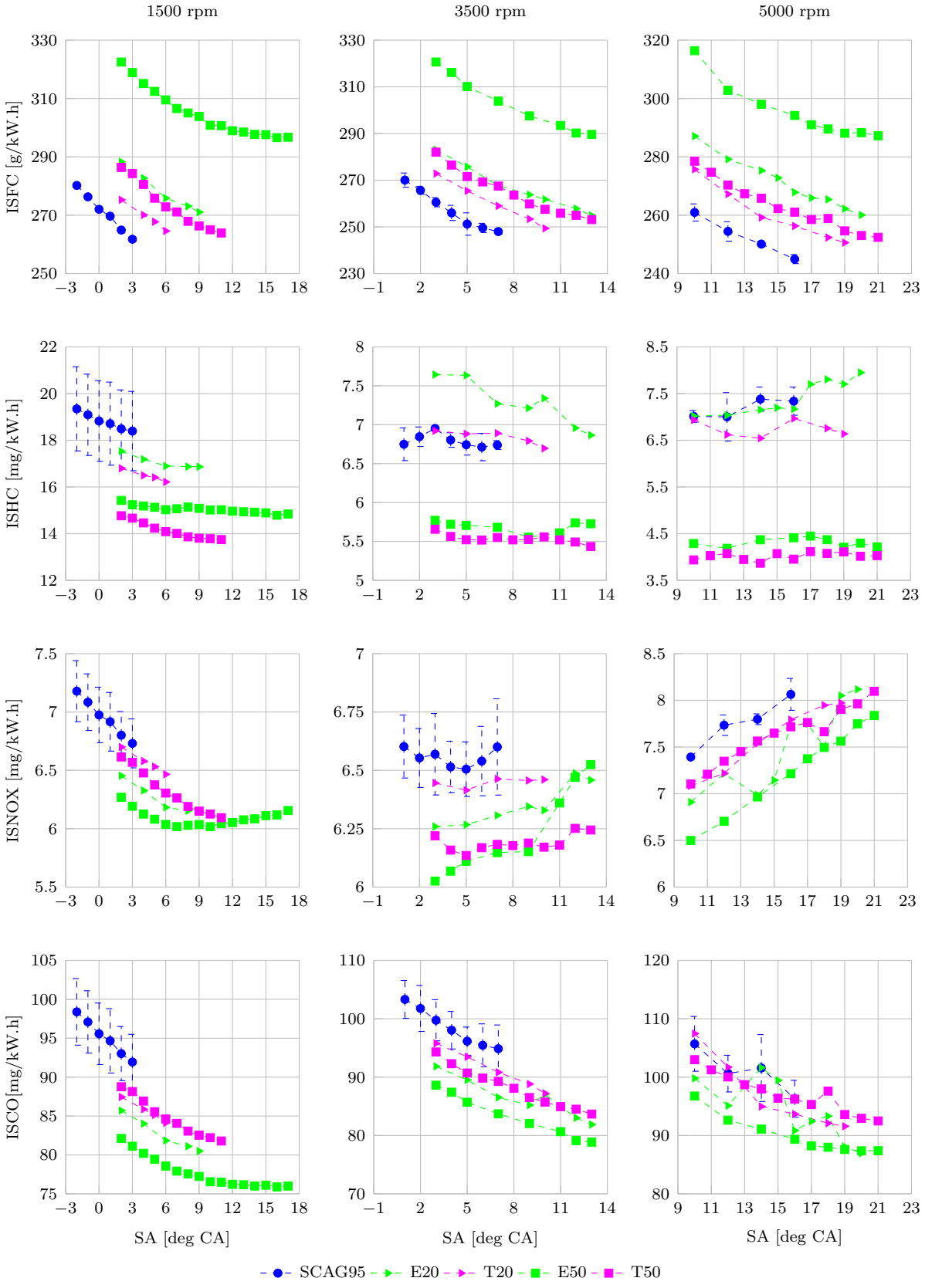

Figure 5.13: *ISFC, ISHC, ISNOx and ISCO vs SA sweeps for SCAG fuel and synthetic oxygenate test blends*

5.4.2.3 Olefinic synthetic gasoline blends

In figure 5.14 the peak pressure and the crank angle location show that synthetic blending component F increases the burn rate with optimal combustion phasing and subsequently results in a higher indicated mean effective pressure. At a set spark advance, an IMEP increase of over 2% was realised using 50% blend of synthetic blending component F. Due to the relatively poor octane rating of blending component F the peak performance is limited in comparison to the SCAG fuel, therefore suggesting its potential as a blending component with higher octane fuel blends. The olefinic blend component B has a higher octane rating but does not exhibit the same improvements in burn rate which correlates with the laminar flame speed findings in chapter 4.

From the combustion duration shown in figure 5.15 it becomes evident that for blending component F the flame kernel growth period is noticeably shorter as shown by the 10% mass fraction burned crank duration. Furthermore the location of the 50% mass fraction burn point suggests that combustion predominantly takes place at a more optimised crank position and the AI90-AI10 crank duration indicates a shorter overall combustion period. Synthetic component B was found to behave similar to the SCAG fuel, although the overall combustion duration at 3500 and 5000 rpm was found to be marginally shorter for the SBB50.

The indicated specific fuel consumption in figure 5.16 clearly shows an improved efficiency for the synthetic fuel blend component F which correlates well with the improvement in combustion phasing. This further results in lower specific hydrocarbon emissions as a result of more complete burn although no improvement in carbon monoxide emission was found. The effect on nitrous oxide emissions was found to be inconclusive as there was no clear trend visible over the three engine speeds.

The olefinic blend component B did not show an improvement in ISFC although the improved knock resistance allowed a more optimal spark advance which improved overall specific fuel consumption. Hydrocarbon emissions were found to be similar to the SCAG fuel while the carbon monoxide was not found to be fuel specific. However, a clear trend showing a reduction in emissions with respect to spark advance was evident.

5.4.2.4 Aromatic synthetic gasoline blends

The predominantly aromatic synthetic blending components were compared in terms of peak cylinder pressure characteristics and indicated mean effective pressure in figure 5.17. Little difference was found with respect to the location of peak pressure or the absolute peak pressure measured. The performance of the aromatic synthetic fuel blends, as indicated by the mean effective pressure, was generally shown to be lower than the SCAG

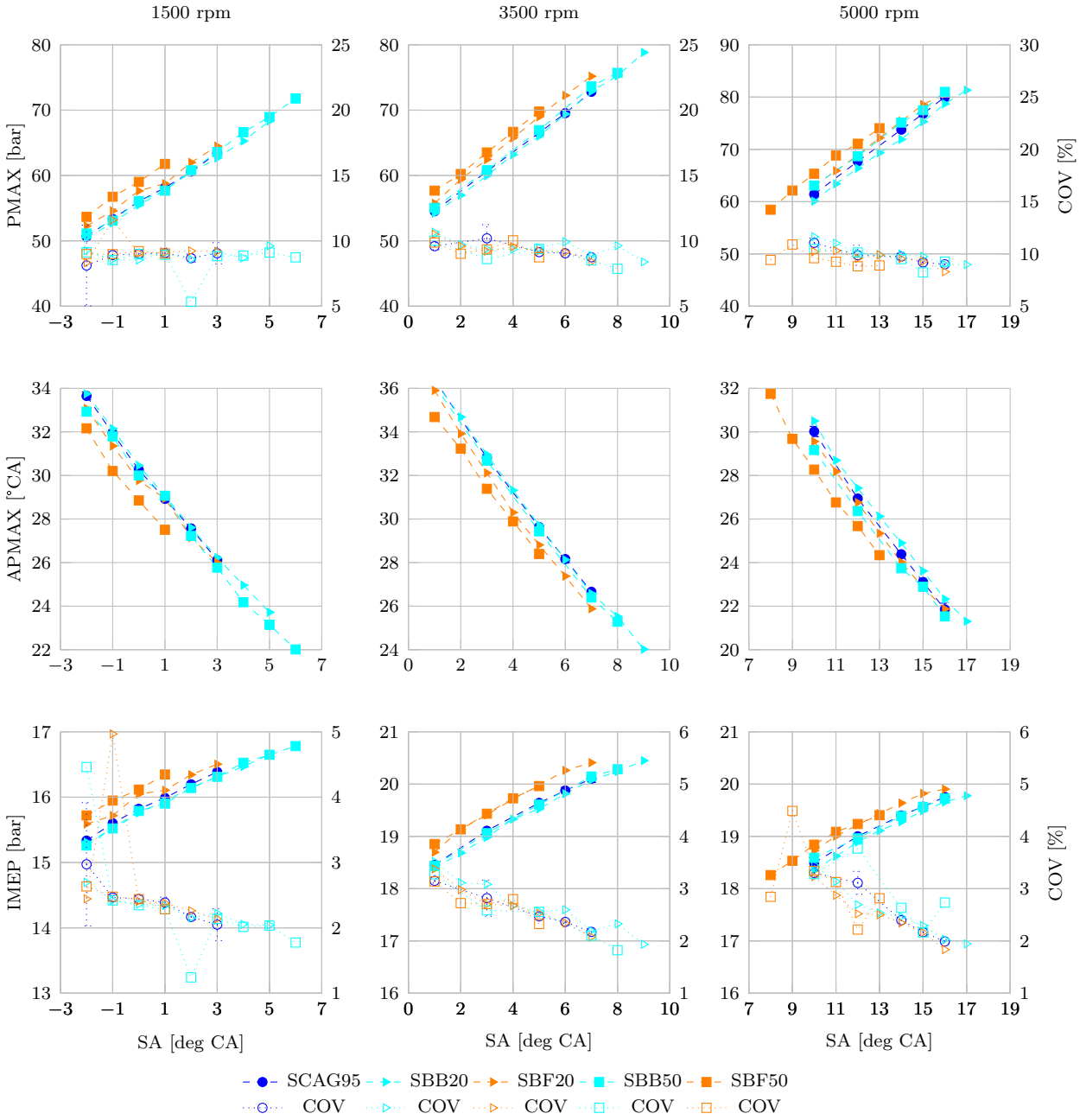

Figure 5.14: *PMAX, APMAX and IMEP vs SA sweeps for SCAG fuel and synthetic olefin test blends*

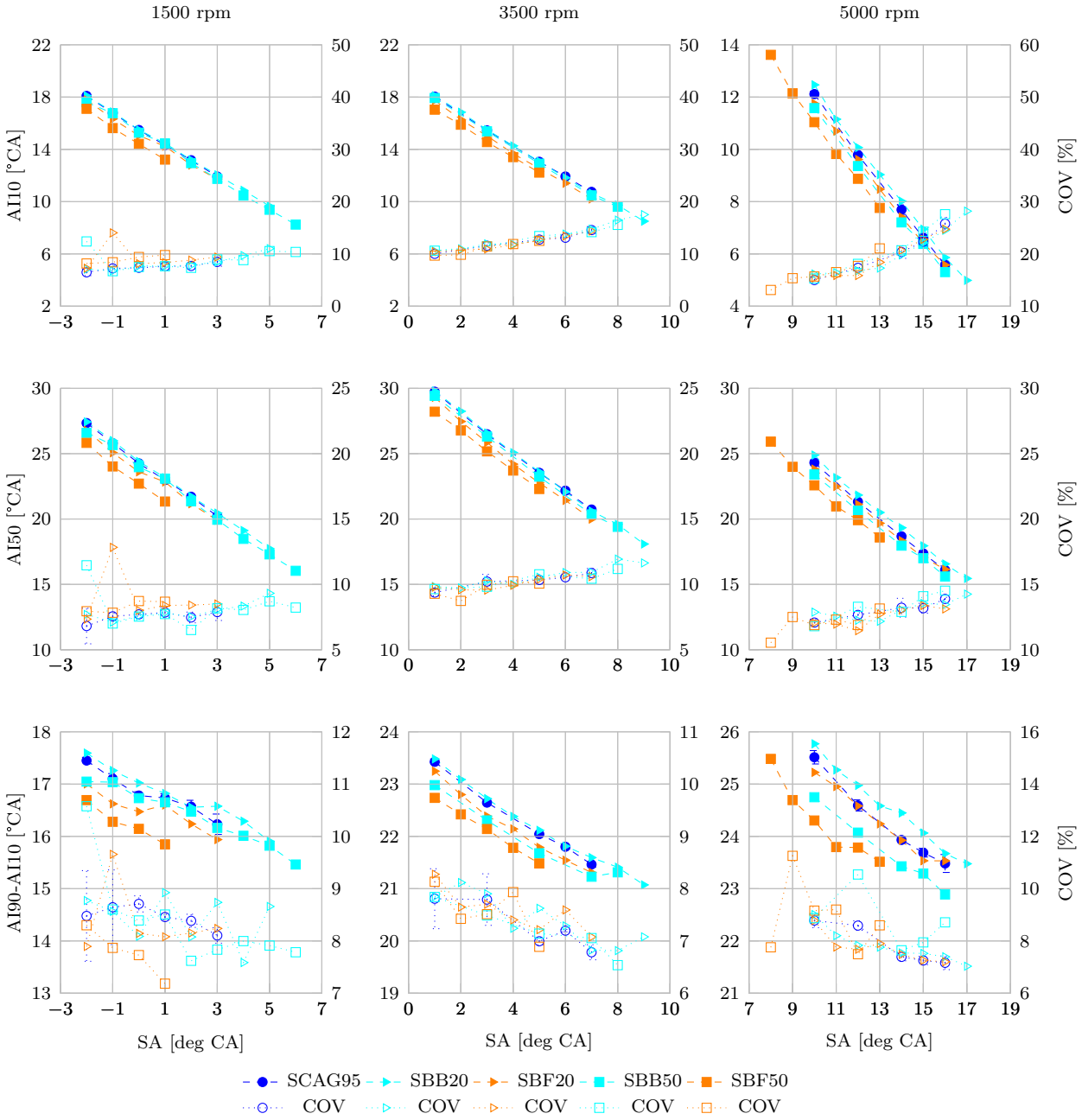

Figure 5.15: *AI10, AI50 and AI90-AI10 vs SA sweeps for SCAG fuel and synthetic olefin test blends*

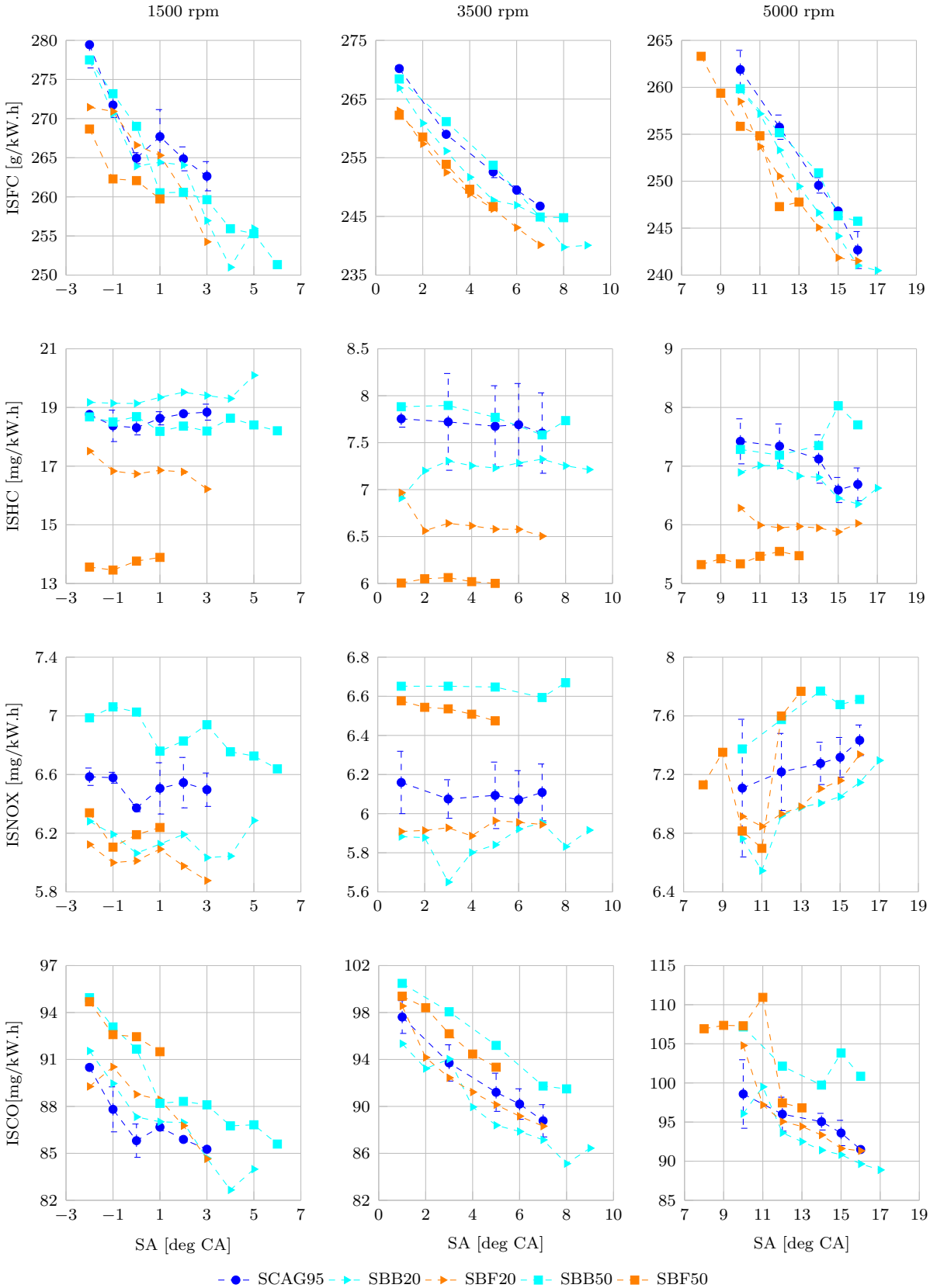

Figure 5.16: *ISFC, ISHC, ISNOx and ISCO vs SA sweeps for SCAG fuel and synthetic olefin test blends*

fuel. Synthetic blend E showed a slight improvement in performance by virtue of its higher knock resistance thereby allowing improved ignition advance while blend component C resulted in similar performance to the SCAG fuel. Blending component A was shown to be rich in iso-paraffin and aromatic content, but had very poor octane resulting in retarded ignition timing. Blending component D similarly required significant ignition retard.

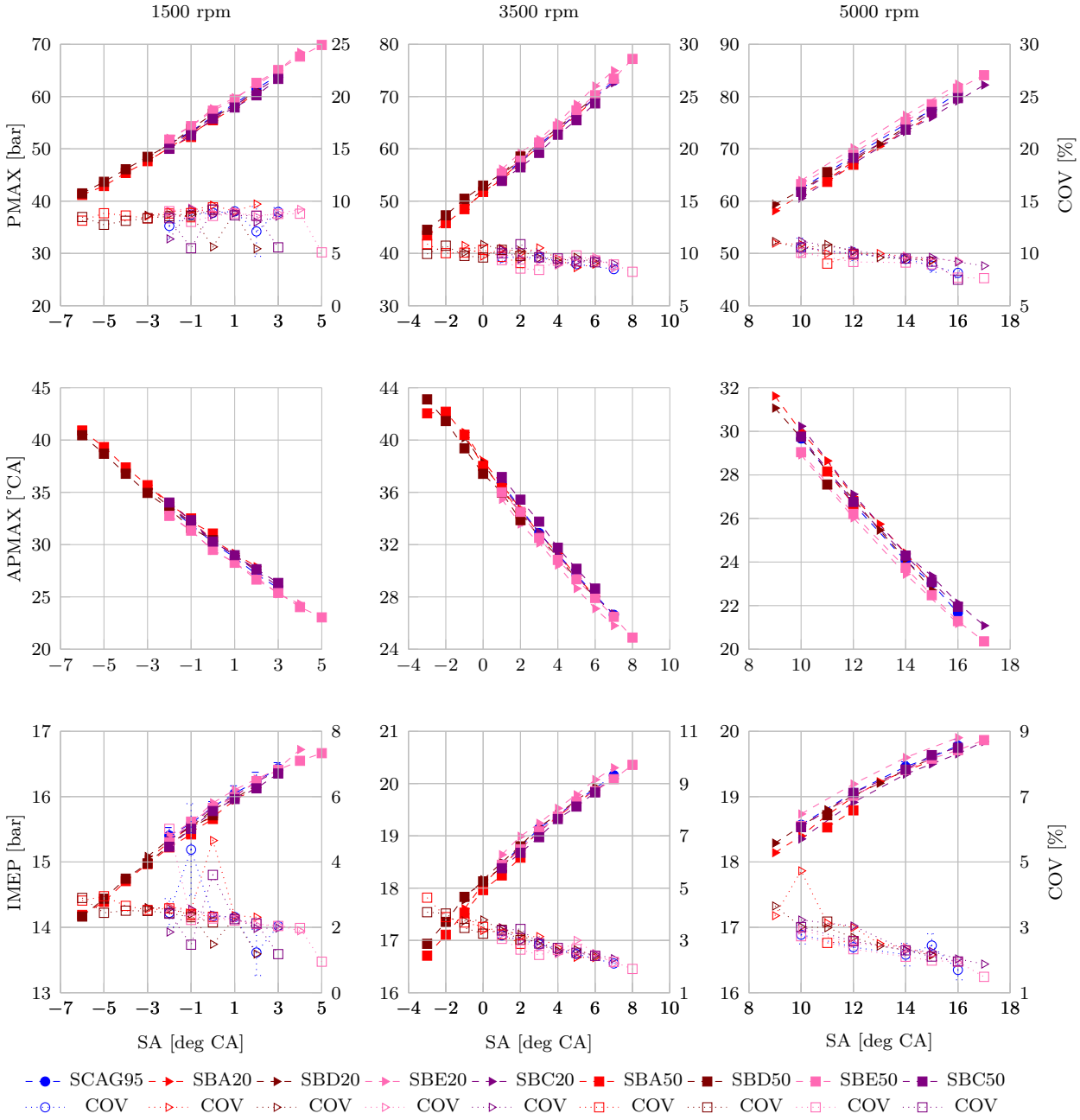

Figure 5.17: *PMAX, APMAX and IMEP vs SA sweeps for SCAG fuel and synthetic aromatic test blends*

Combustion durations of the different fuel blends was also found to be very similar as can

be seen in figure 5.18. The early flame kernel development (AI10) was the same for all the fuel blends with very little difference distinguishable in terms of the 50% mass fraction crank position. The overall burn duration indicated that 50% blends of components SBD and SBE resulted in a slightly higher burn rate as shown by the shorter AI90-AI10 crank duration at 1500 rpm. However, this behaviour was not clearly evident at the higher engine speeds as the turbulence effect on flame speed became more dominant.

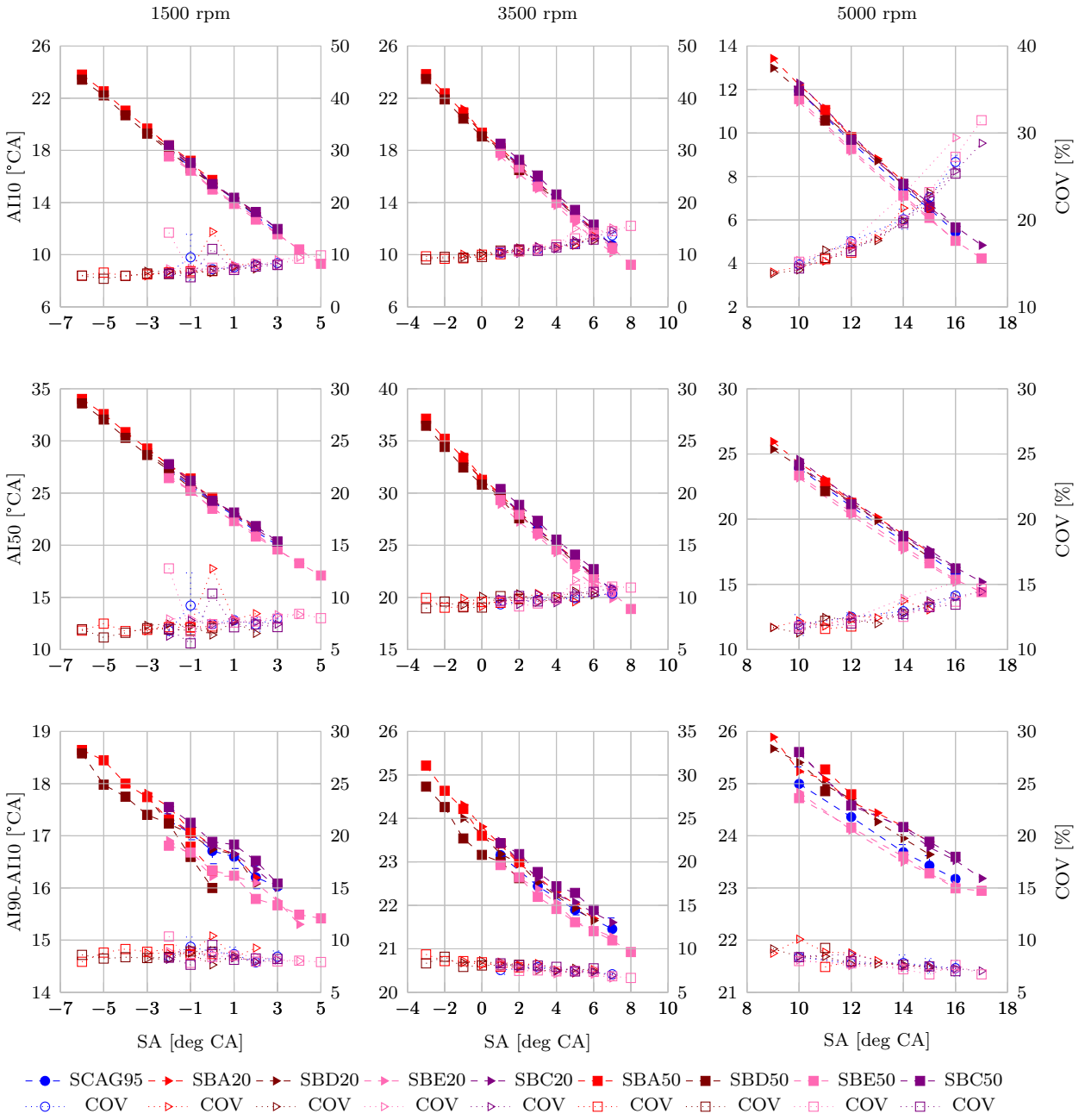

Figure 5.18: *AI10, AI50 and AI90-AI10 vs SA sweeps for SCAG fuel and synthetic aromatic test blends*

From figure 5.19 it is evident that the lower octane rating of blending component A

and D resulted in a clear reduction in efficiency as is shown by the poor specific fuel consumption while components C and E resulted in similar efficiency to the SCAG fuel. No clear distinction was observed between the emission behaviour of the synthetic blend components and the reference fuel.

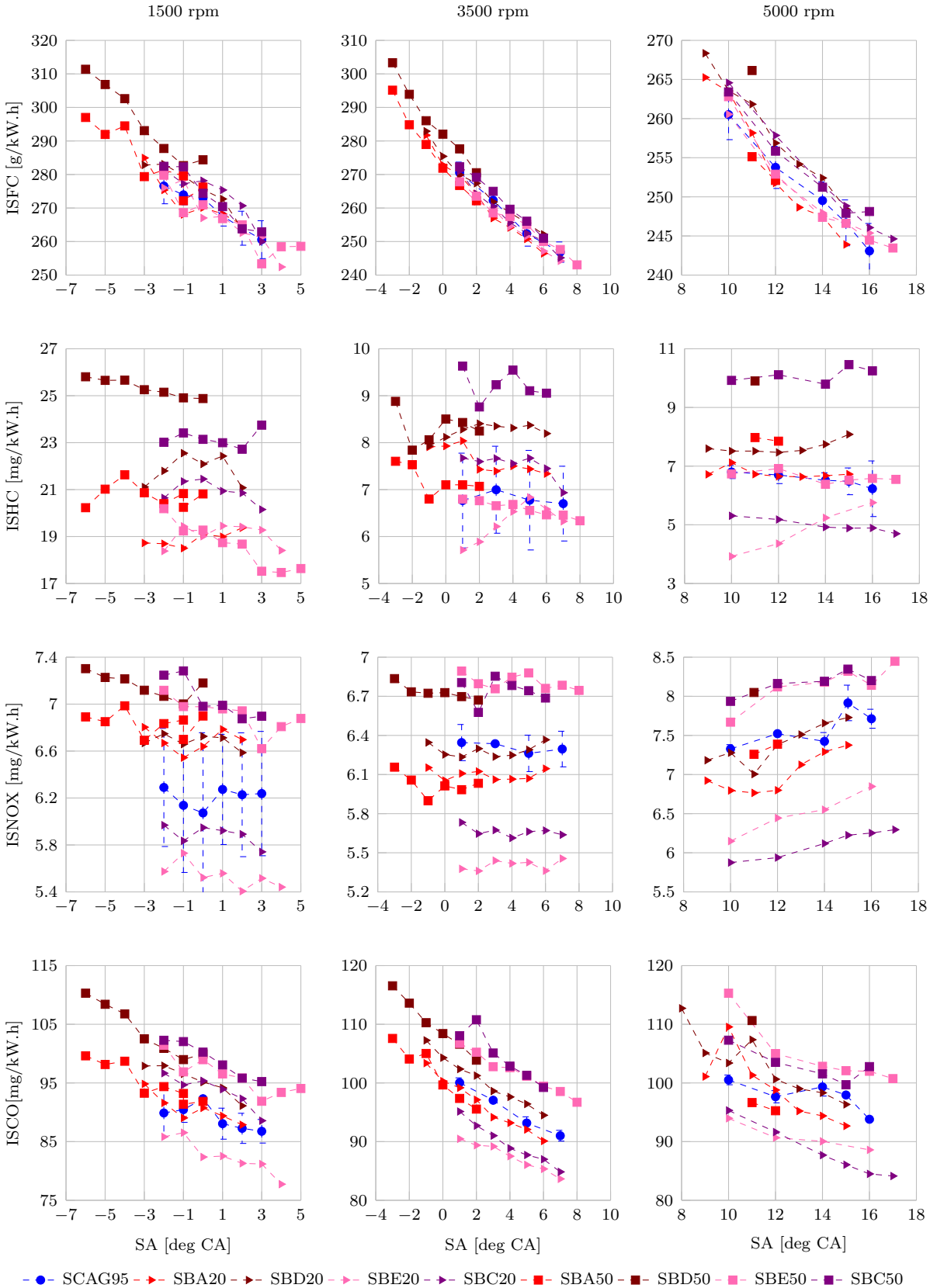

Figure 5.19: *ISFC, ISHC, ISNOx and ISCO vs SA sweeps for SCAG fuel and synthetic aromatic test blends*

5.4.3 EGR analysis

The exhaust gas recirculation rate was restricted at 1500 rpm by the available difference in positive pressure between the exhaust and the intake manifold under boosted conditions. The misfire limit could therefore not be reached, however a comparison on the effect of cyclic variation with regards to the test fuels was conducted. At 3500 rpm sufficient EGR rate was achieved to allow maximum brake torque timing to be reached with all fuels.

5.4.3.1 Crude derived gasoline

In figure 5.20 the effect of EGR rate shows a consistent increase in allowable knock limited spark advance and a subsequent reduction in specific fuel consumption is shown. At 3500 rpm the MBT timing, at approximately 50 degrees before top dead centre (TDC), was reached at an EGR rate of about 15% for all fuels, with a slight offset distinguishable for the 93 RON CCAG fuel due to its lower knock resistance. EGR rates greater than 16% therefore resulted in an increase in specific fuel consumption due to less optimal combustion phasing.

The lower knock limited spark advance of the 93 RON fuel resulted in a lower peak cylinder pressure and delayed phasing as shown by APMAX. At 3500 rpm the optimal location of the peak cylinder pressure was found at about 15 degree after top dead centre (ATDC) which agrees with literature findings [17]. At 1500 rpm a slightly lower IMEP was measured for the 93 RON and crude derived 95 RON fuel while at 3500 rpm no difference was found. At 1500 rpm the combustion variability was found to be consistently between 2 and 3% until the maximum EGR rate was reached. At the higher speed point, the EGR limit was reached at approximately 16% after which cyclic variation increased resulting in misfire.

The influence of EGR rate on exhaust gas temperature and combustion phasing is shown in figure 5.21. As expected an increase in EGR rate with the subsequent advance in allowable knock limited spark timing, resulted in a consistent reduction in exhaust gas temperature. At 3500 rpm the exhaust gas temperature reduction was found to plateau in accordance with the MBT spark timing. Early flame kernel development, 50% mass fraction burned and the overall combustion duration showed no correlation with the fuel used. The 93 RON crude derived fuel was found to be offset slightly in relation with the lower allowable spark advance.

At 3500 rpm and an EGR rate of 14% the optimal location of AI50 was found to be between 10 and 14 degrees after top dead centre (ATDC) which is supported by findings in standard literature [17]. Increasing the EGR rate further, again resulted in retarded

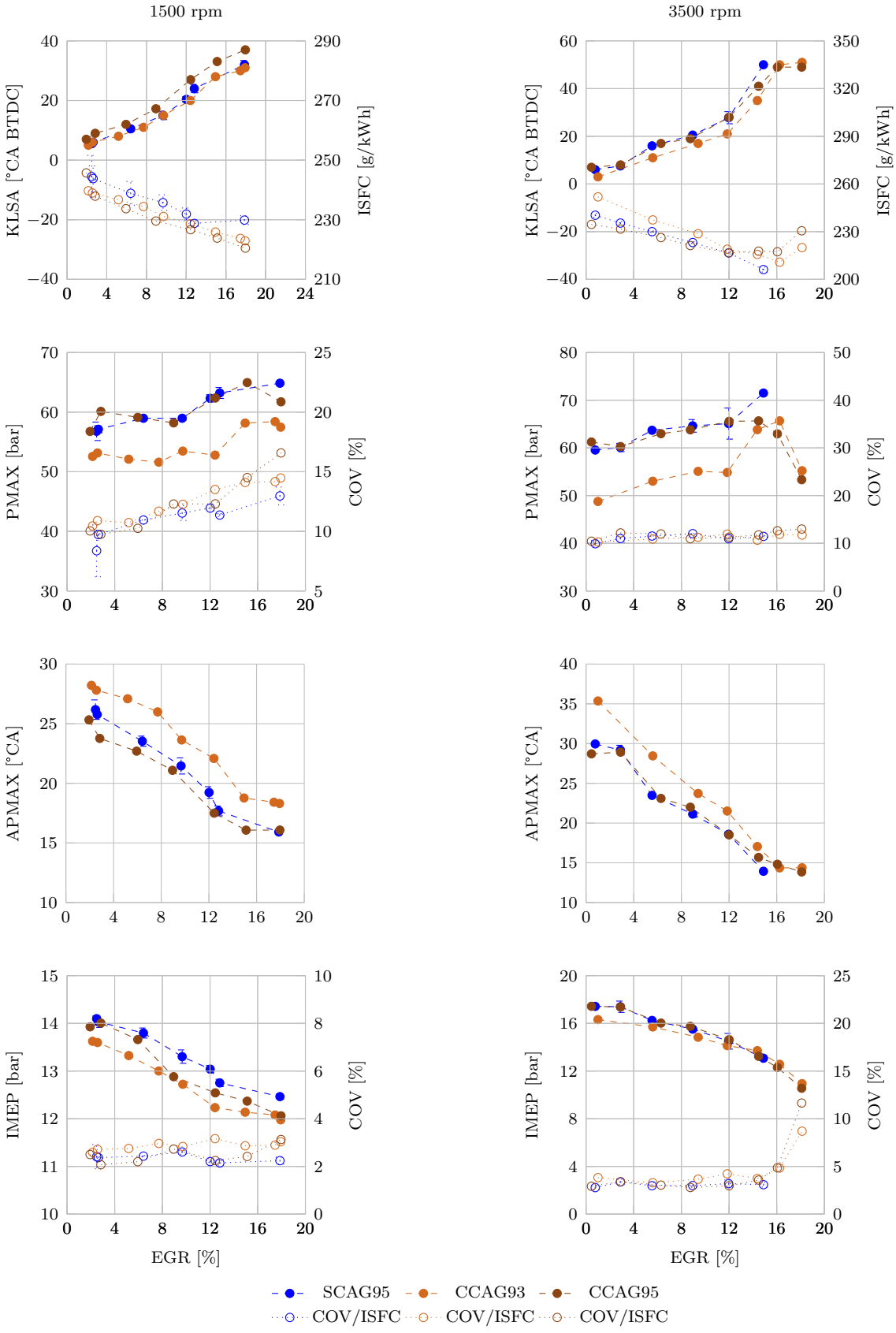

Figure 5.20: *PMAX, APMAX and IMEP vs EGR sweeps for SCAG fuel and CCAG fuels*

combustion phasing and reduced efficiency as shown by the increase in specific fuel consumption in figure 5.20.

5.4.3.2 Oxygenated synthetic gasoline blends

A similar trend in allowable knock limited spark advance was observed for the EGR sweep shown in figure 5.22, with the higher knock resistance of the oxygenated fuels showing a clear offset. The increased spark advance of the oxygenated fuels resulted in elevated peak cylinder pressure and more optimal combustion phasing thereby improving the power output as indicated by the higher mean effective pressure. This effect was most pronounced for the 50% ethanol blend while the 20% ethanol blend resulted in similar IMEP as the 50% TAME blend. At 3500 rpm the MBT timing was again found to be at a spark advance of 50 degrees BTDC which was obtainable at 12% EGR for the 50% ethanol blend. Once the MBT timing was reached, further addition of exhaust gas resulted in a deterioration of the specific fuel consumption. At 16% EGR rate the SCAG gasoline was no longer knock limited thereby resulting in the same IMEP as the oxygenated fuel components.

The more optimal spark advance of the oxygenated fuel blends resulted in lower cyclic variation when compared to the SCAG fuel as shown by the COV of the IMEP. At 3500 rpm an EGR rate above 16% was found to induce significant cyclic variation subsequently resulting in misfires.

Increased EGR rate and a more optimal spark advance gradually reduced the exhaust gas temperature for all the test fuels as shown in figure 5.23. The 50% oxygenate blends were found to exhibit lower exhaust gas temperature while the 20% blends were found to be similar to the SCAG fuel.

The early flame kernel development for the oxygenated fuels at 1500 rpm was significantly earlier than the SCAG fuel due to the increased spark advance. This also resulted in an overall earlier combustion phasing as shown by the 50% mass fraction burned (AI50). It was found however that for the 50% ethanol blend the overall combustion duration was generally longer than for the SCAG fuel. At 3500 rpm a similar offset in AI10 and AI50 was found until the 95 RON reference gasoline was no longer knock limited at an EGR rate of about 15%. Further increasing the EGR rate resulted in significant retarding of the combustion phasing (AI50) and increased combustion duration (AI90-AI10) for all the fuels.

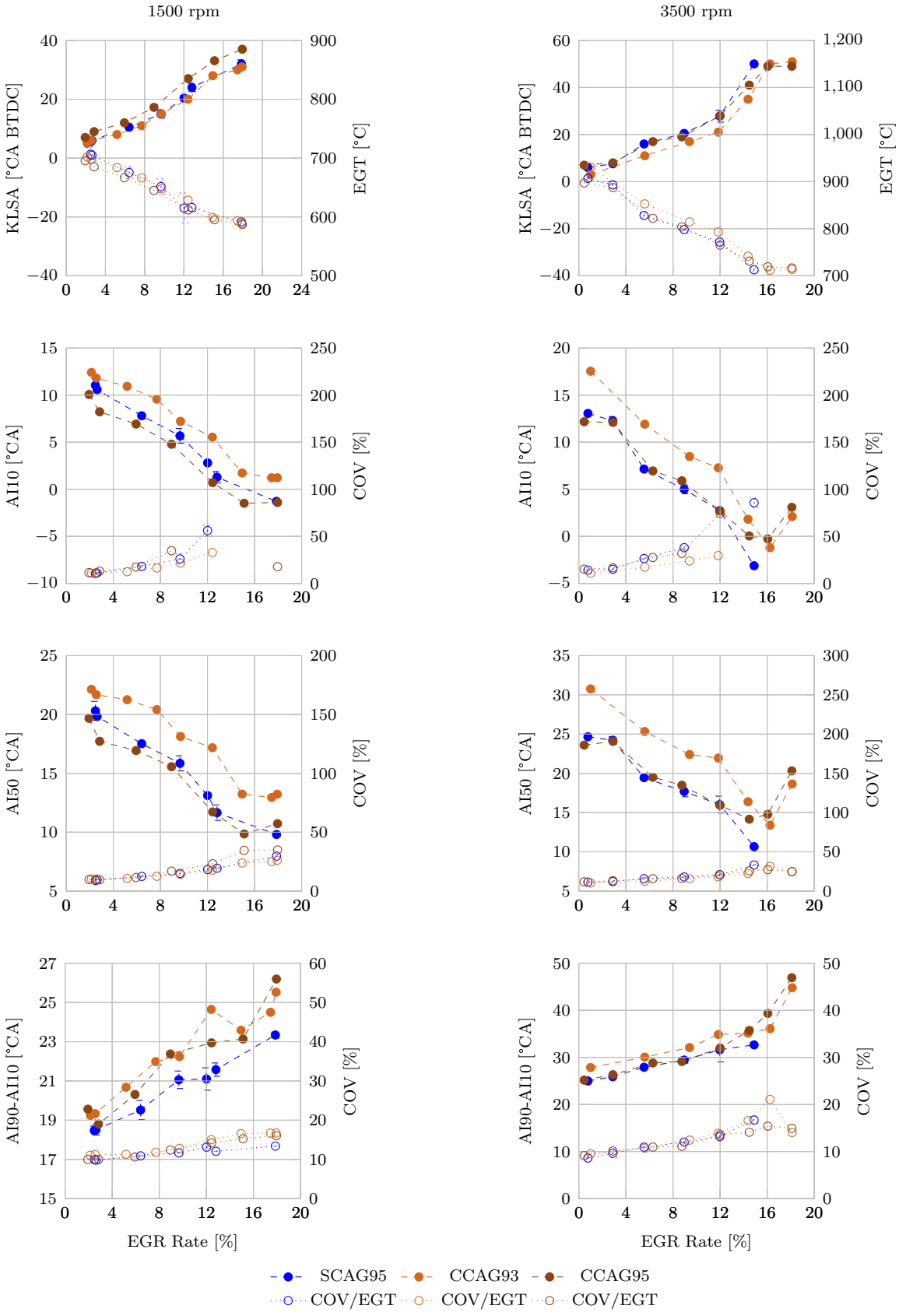

Figure 5.21: *AI10, AI50 and AI90-AI10 vs EGR sweeps for SCAG fuel and CCAG fuels*

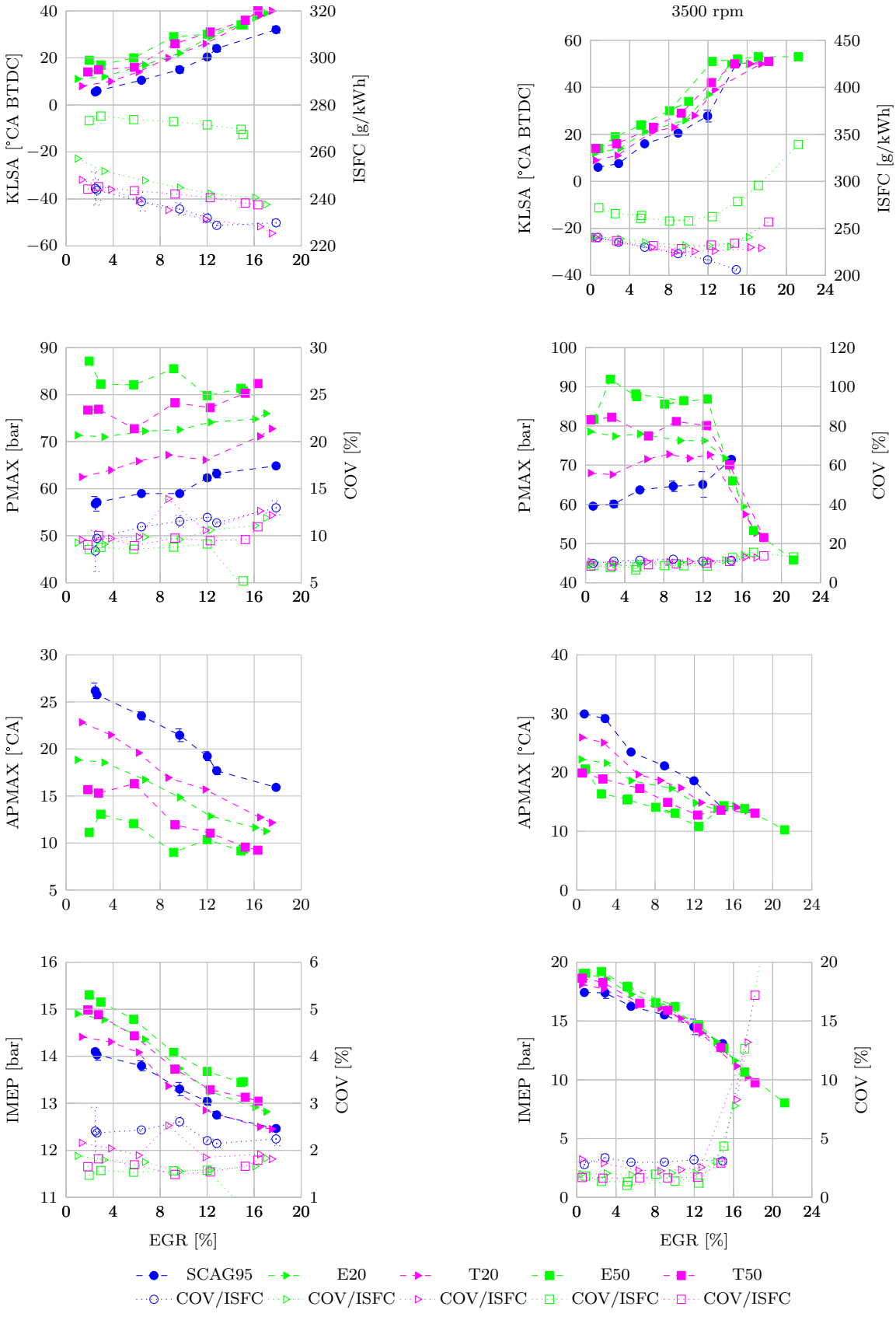

Figure 5.22: *PMAX, APMAX and IMEP vs EGR sweeps for SCAG fuel and synthetic oxygenate test blends*

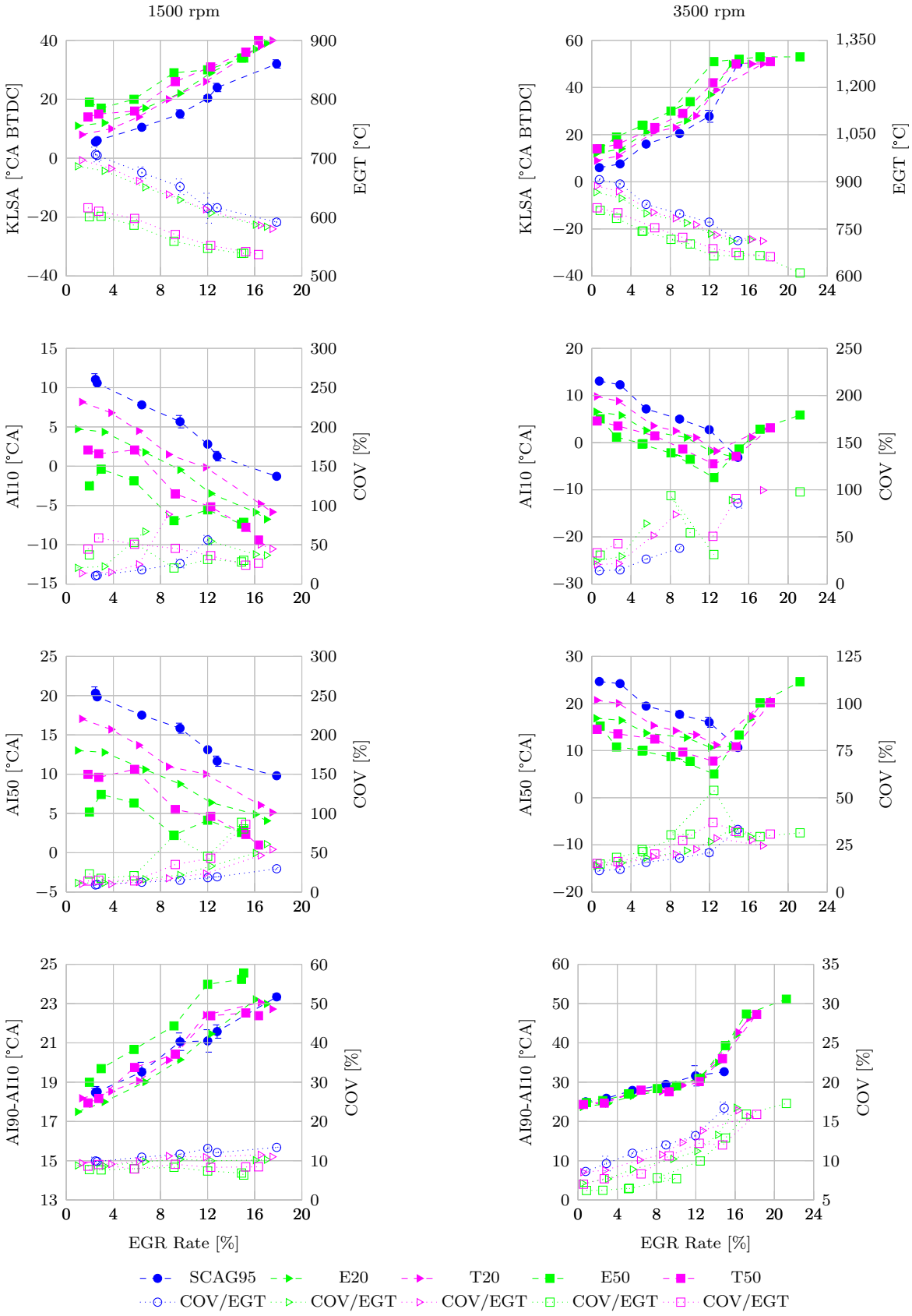

Figure 5.23: *AI10, AI50 and AI90-AI10 vs EGR sweeps for SCAG fuel and synthetic oxygenate test blends*

5.4.3.3 Olefinic synthetic gasoline blends

The olefinic synthetic blending component B exhibits a moderately higher RON and more sensitivity which benefits the knock limited spark advance as seen in figure 5.24. At 1500 rpm this results in a noticeably higher maximum combustion pressure and earlier phasing while the effect is less pronounced at the higher engine speed. Synthetic blending component F reduces the allowable spark advance slightly due to a lower octane rating. The effect on peak cylinder pressure and phasing were found to be marginal however, while the IMEP at both engine speeds was not affected by the fuel used.

At 1500 rpm the specific fuel consumption gradually reduced with increasing EGR rate and advanced spark advance until the maximum achievable EGR rate of approximately 18% was reached. The cyclic variation was found to be steady at about 2%. At 3500 rpm, the MBT spark timing for the SCAG fuel and the SBB blends was reached at approximately 14% EGR while the SBF blends required exhaust gas recirculation at a rate of 17% to attain MBT spark timing. However, the cyclic variation for all fuels increased drastically above 16%, accompanied by misfires.

The exhaust gas temperature was found to reduce in accordance with the EGR rate and spark advance but independent of the fuel type used as seen in figure 5.25.

A distinctly shorter flame kernel growth phase at 1500 rpm was found using synthetic blend component B as a result of the improved ignition advance. This further resulted in more optimal combustion phasing as indicated by the 50% mass fraction burned. However, there was little difference in the overall combustion duration.

At 3500 rpm the retarded ignition timing of SBF50 similarly resulted in a minor retardation in AI10 and AI50. However, the overall combustion duration was again found to be similar for all fuels.

5.4.3.4 Aromatic synthetic gasoline blends

The significant variation in octane rating of the aromatic fuel blends, resulted in vastly different knock limited spark advance as seen in figure 5.26. For the 1500 rpm speed point the specific fuel consumption reduced in accordance with EGR rate and the allowable spark advance. At 3500 rpm it was found that the MBT spark timing was achievable for all fuels when using sufficient exhaust gas recirculation, thereby negating the knock resistance benefit of the higher octane fuels. However, at EGR rates above 16% the cyclic variation increased dramatically and the misfire limit was reached which resulted in fuel blends SBA50 and SBD50 being 'misfire limited' before MBT timing was reached.

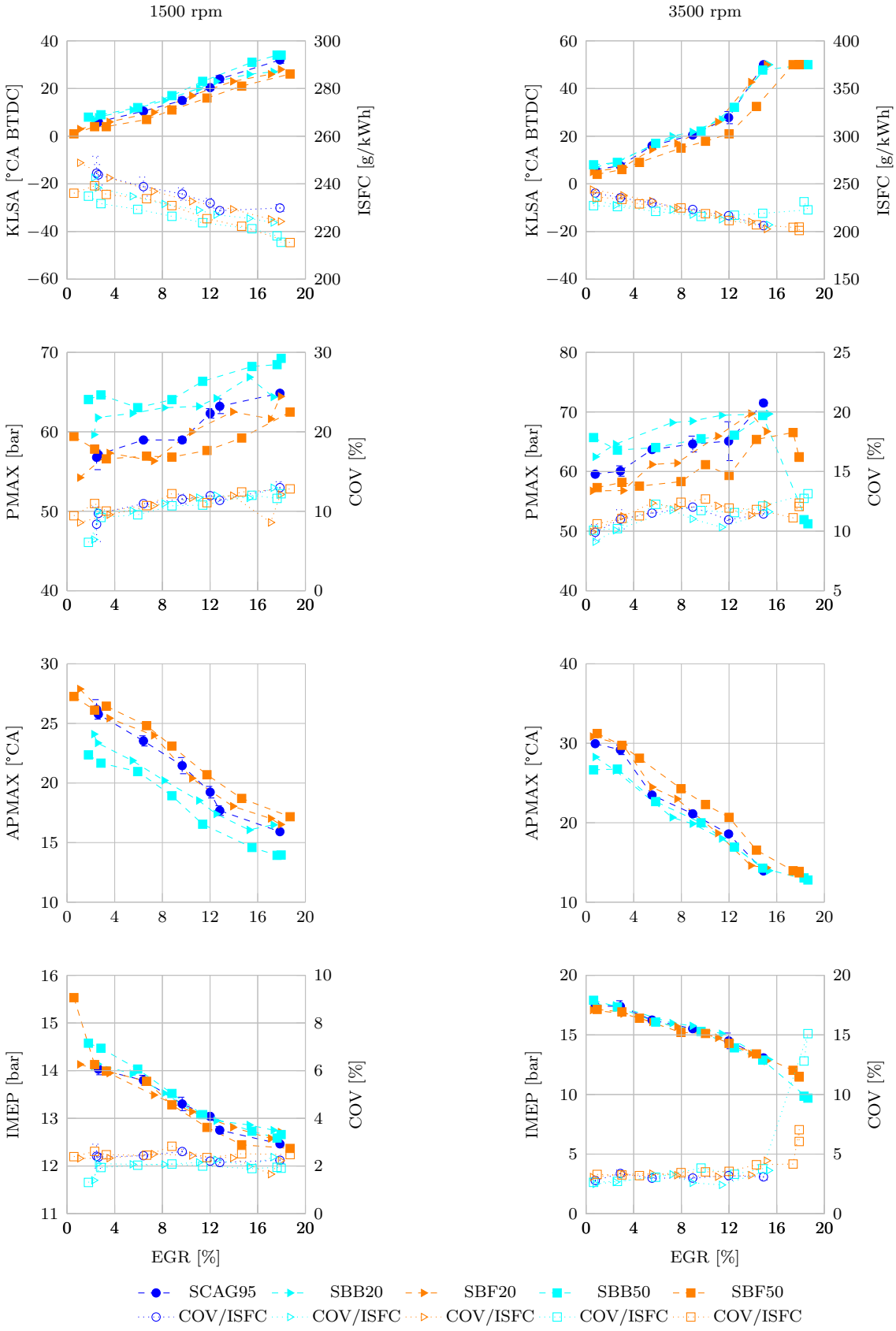

Figure 5.24: *PMAX, APMAX and IMEP vs EGR sweeps for SCAG fuel and synthetic olefin test blends*

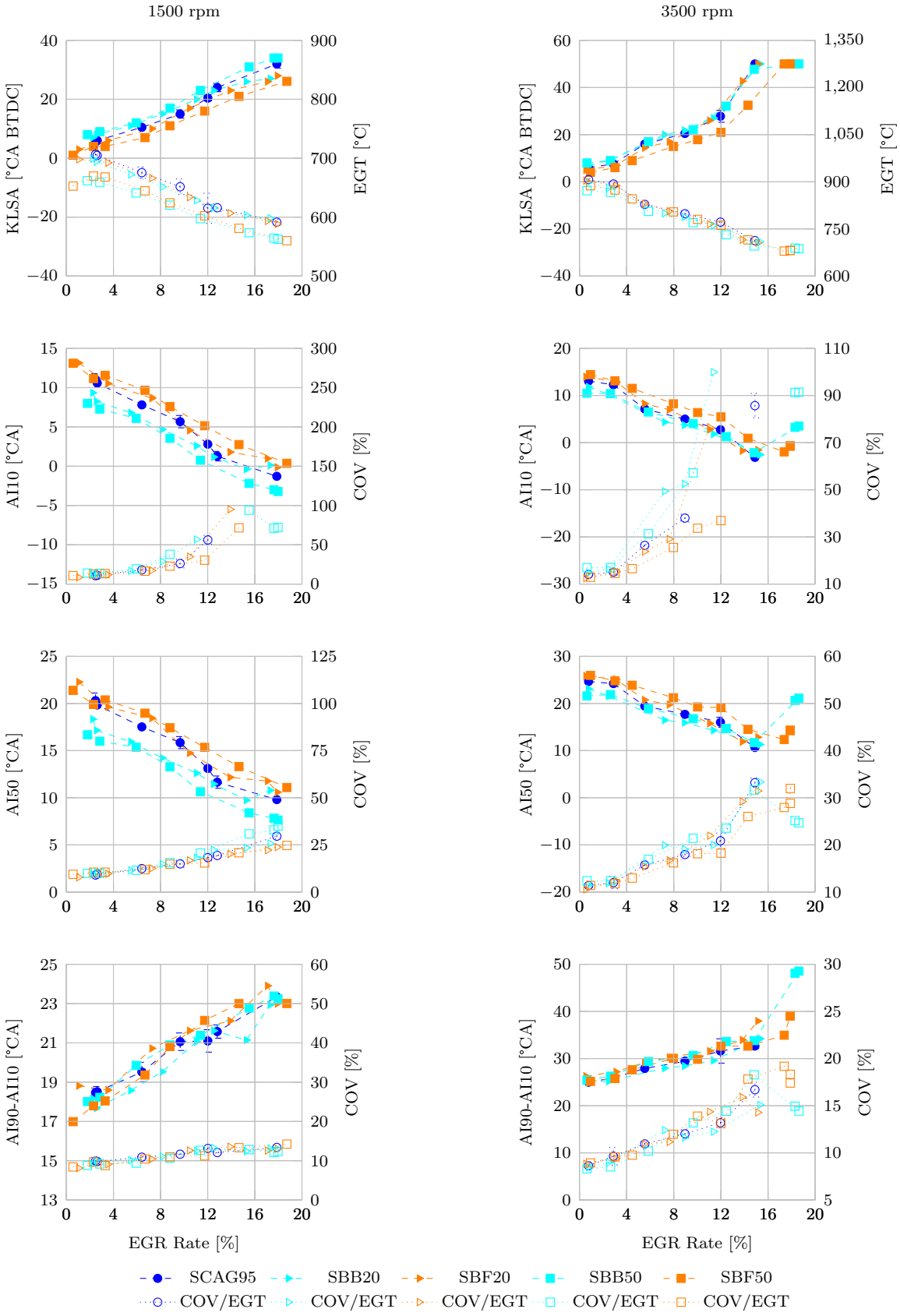

Figure 5.25: *AI10, AI50 and AI90-AI10 vs EGR sweeps for SCAG fuel and synthetic olefin test blends*

The low octane rating of the SBA50 and SBD50 blends resulted in significantly lower maximum combustion pressure and delayed peak pressure phasing due to the retarded ignition timing. Synthetic blend component E improved the octane rating of the SCAG fuel thereby allowing more spark advance which resulted in higher peak combustion pressure and more optimal combustion phasing.

Synthetic components SBA50 and SBD50 resulted in significantly lower IMEP due to the spark advance limitation while only marginal differences were found between the other components and the reference fuel.

Exhaust gas temperature decreased consistently with increased EGR and spark advance plateauing slightly from an EGR rate of 16% at both engine speeds as seen in figure 5.27.

At low EGR rates the early flame kernel development and combustion phasing (AI50) in this case is dependent on the octane rating of the fuel due to its knock limited spark advance. For the higher octane component E and the reference SCAG fuel, optimal combustion phasing could be achieved at 1500 rpm with AI50 at about 10 degrees after top dead centre. For all fuels AI50 approached the optimal combustion phasing of about 10 deg ATDC at 3500 rpm with an EGR rate of about 14%.

Overall combustion duration was found to be mainly dependent on the knock resistance of the fuel due to the knock limited spark advance.

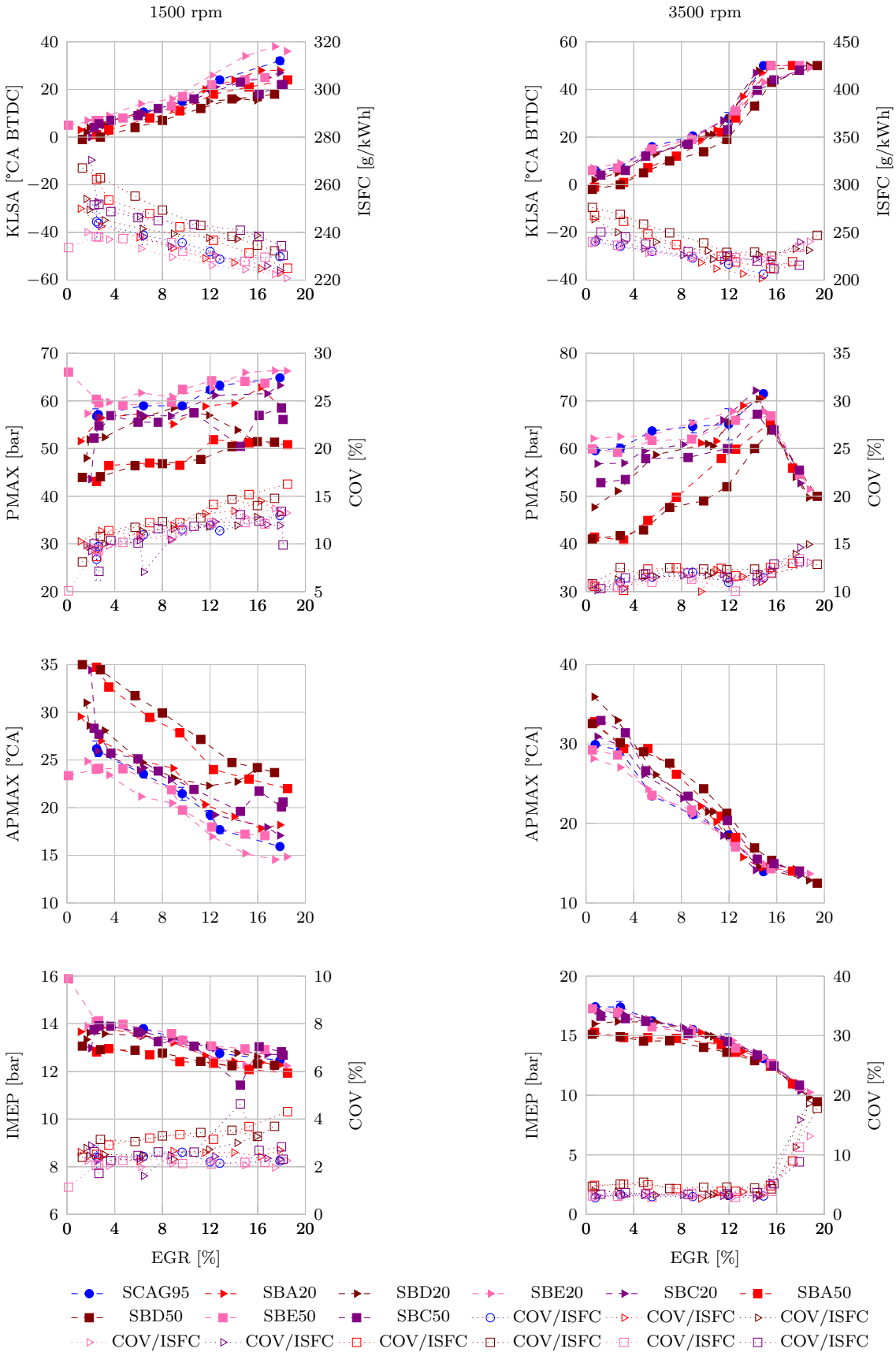

Figure 5.26: *PMAX, APMAX and IMEP vs EGR sweeps for SCAG fuel and synthetic aromatic test blends*

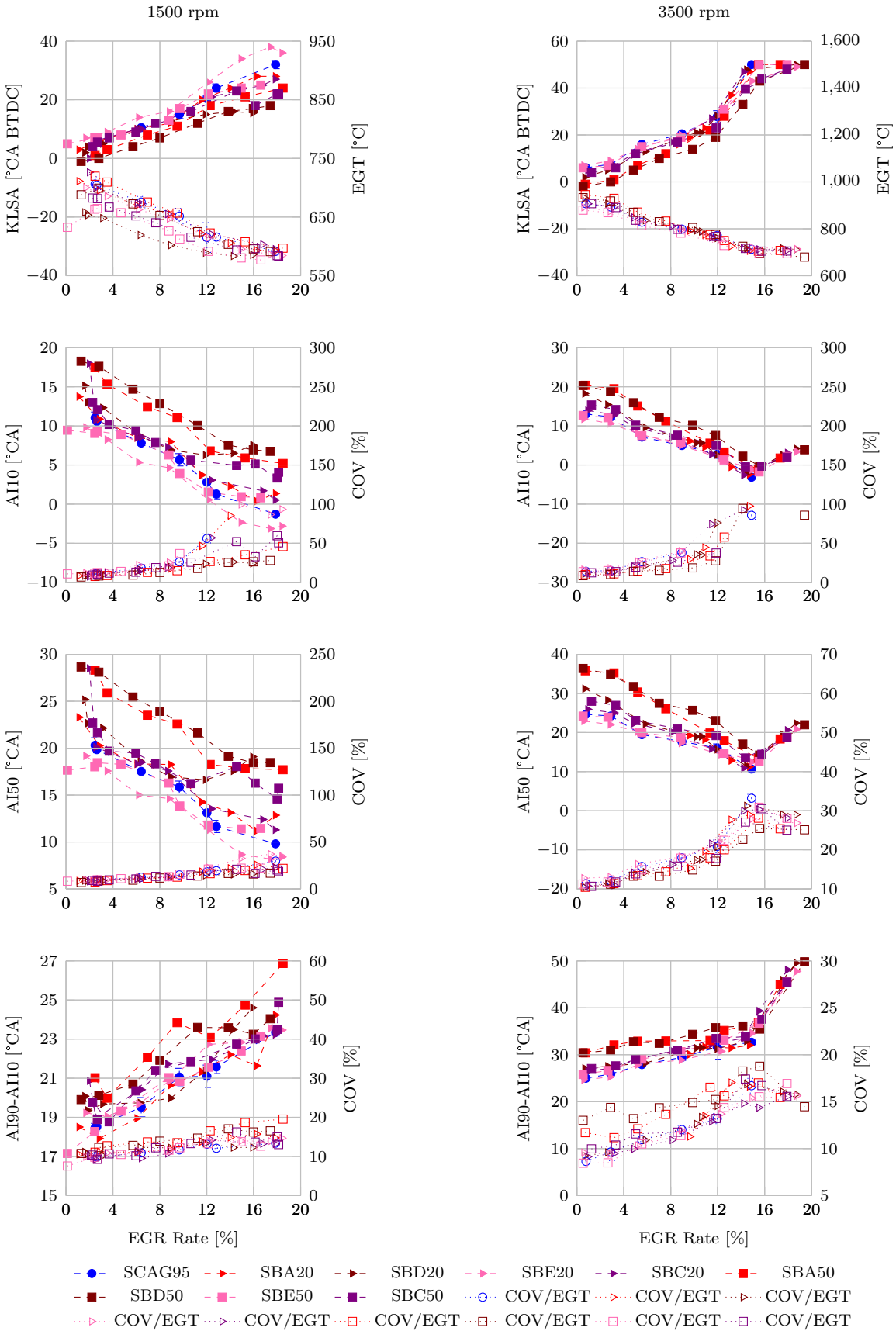

Figure 5.27: *AI10, AI50 and AI90-AI10 vs EGR sweeps for SCAG fuel and synthetic aromatic test blends*

5.4.4 Summary and discussion

The evaluation of the knock limited spark advance and the octane index revealed that while the engine was operating well "beyond RON", the K value showed some dependence on the fuel type used. While a reasonable correlation between KLSA and OI was found using PRF, TSF and CAG fuels, synthetic blends consisting of predominantly aromatic components resulted in a poor fit. A particularly poor agreement between KLSA and the OI was found when using the synthetic olefin blend components.

The performance analysis revealed that no distinguishable difference was found in the indicated mean effective pressure between 95 RON SCAG fuel and the comparable crude derived gasoline. Key combustion properties such as peak cylinder pressure, location of peak pressure, early flame kernel development and combustion phasing indicated by the 50% mass fraction burned were found to be similar. Indicated specific fuel consumption and indicated specific emissions were also found to be on par. The EGR tolerance was also found to be similar.

Evaluation of the oxygenated fuel components indicated that a significant performance benefit could be gained from ethanol due to its very high knock resistance. Similar findings have been shown in literature [6, 96, 184]. TAME was not found to exhibit the same octane benefit although a significant increase in KLSA was possible with the TAME blends. The combustion phasing was found to be similar for the oxygenated fuel blends and the SCAG fuel, however the overall combustion duration was slightly longer for the oxygenates in particular the ethanol blends. Specific fuel consumption at a given spark advance increased at elevated oxygenate content while TAME blends were less affected due to their higher heating value. Indicated emissions improved slightly with increasing oxygenate content. EGR tolerance improved at low EGR rates due to an increased knock limited spark advance.

The olefinic synthetic blending component F was found to increase the burn rate which resulted in improved combustion phasing, higher peak combustion pressure and higher IMEP at a given spark advance. However, due to a lower octane number the performance benefit was limited in comparison to the SCAG gasoline. Synthetic component B exhibited an improved octane rating which allowed a higher spark advance than the reference fuel although the burn rate and combustion phasing were found to be similar. Despite the lower knock resistance of SBF its faster burn rate resulted in improved specific fuel consumption which would be beneficial when operating the engine under low IMEP conditions such as those experienced during homologation cycles. SBB did not provide any advantages in terms of fuel efficiency in comparison to the SCAG fuel and specific emissions were found to be similar between SBB and SBF. The faster burn rate of component SBF did not provide an advantage in terms of EGR tolerance due to the

lower knock resistance. SBB allowed a higher spark advance resulting in more optimal combustion phasing.

Cracknell et al. reported a 1.5% performance increase using 20% of a specific aromatic in their fuel blends [5].

Synthetic aromatic blending components were found to either provide lower performance, due to very low octane number, or similar to the SCAG fuel. At a given spark advance there was little distinction in terms of combustion phasing and burn rate. No improvements in specific emissions were found. The low octane aromatic blends provided poor combustion stability at lower EGR rates due to the limited spark advance where MBT spark advance could not be achieved before the misfire limit was reached. The aromatic blends with similar octane number to the SCAG fuel also had a similar combustion stability under EGR conditions.

The performance evaluation revealed that subtle differences exist between the synthetic blending components which suggests that there is potential to formulate an optimal blend to maximise these benefits. From the preceding analysis, the best performance could be related to the blending components as follows:

- Peak IMEP was found to strongly correlate with knock resistance with ethanol allowing the highest spark advance resulting in the best engine performance. Additionally ethanol provided a performance benefit due to charge cooling resulting in improved cylinder filling. Synthetic components B and E as well as TAME also provided a performance benefit over the commercial synthetic gasoline owing to improved knock resistance
- Synthetic blending components B and E provided the lowest specific fuel consumption at their optimal spark advance setting. Blend component F was knock constrained due to a lower octane rating but was found to have the best fuel consumption over the spark advance curve as a result of the faster burn rate resulting in a higher thermodynamic efficiency.
- EGR tolerance in terms of cycle-to-cycle variation of IMEP was found to improve with the oxygenate blend components

Using the data and insights gained from the analysis presented in this chapter, an attempt was made to formulate an optimised synthetic gasoline adhering to stipulated specifications and performance criteria. This will be the subject of discussion in the following chapter.

Chapter 6

Optimised synthetic fuel blend analysis

This chapter provides details on the optimization process and the performance results.

6.1 Optimisation model

Based on the findings from chapter 5 a blend optimisation was conducted to define an optimised synthetic fuel by making use of the eight synthetic blending components used throughout this investigation. A holistic model with a data derived scoring system was developed which included non linear blending rules and specified constraints to predict an optimised fuel blend to fulfil any one or several performance parameters.

6.1.1 Optimisation modelling approach

6.1.1.1 Optimisation criteria

The following optimisation category criteria were used:

- IMEP - used as an assessment for power only
- gravimetric ISFC - to provide a comprehensive measure of thermal efficiency
- volumetric ISFC - to provide a customer focussed fuel efficiency
- indicated specific emissions - since exhaust emissions are legislated

6.1.1.2 Numerical scoring

The test results from the 50% fuel blends in the engine combustion analysis was used to define the respective peak IMEP, lowest ISFC and lowest indicated specific emissions. Using the average of the three engine speeds, the parameters were scored numerically from 1 for the worst performing fuel to 10 for the best performance. The remaining fuels were then scored between this band in proportion to their performance as shown in table 6.1.

Due to the benefit of improved knock resistance, the highest IMEP was found with the oxygenated fuel blending components, with ethanol providing the best performance. The olefinic fuel blend B and the predominantly aromatic blending component E also provided good performance as indicated by the scoring, while components A and D were particularly poor. Although blending component F provided a high performance at set spark advance due to its fast burn rate, the low octane rating limited the overall performance at KLSA. However, due to its high gravimetric heating value, it resulted in a high rating in terms of specific fuel consumption on mass basis, which was only surpassed by synthetic blending component B. Ethanol was found to have a particularly poor scoring with respect to specific fuel consumption, due to its low heating value, with TAME having a comparatively higher energy content. Blend components E and C were found to offer the best volumetric fuel consumption characteristics, due to their high heating value and high density, the latter being attributed to its aromatic content. Overall specific emissions were found to be lowest for the oxygenate blends, however NO_x emissions were high for the ethanol blend due to the very advanced spark timing resulting in higher peak combustion temperature. In comparison, synthetic blending component A had the lowest NO_x emissions due to a low octane rating which required substantial spark retard. The aromatic components had a high emissions rating overall, with only synthetic blend E providing good HC emissions. Olefinic blending components B and F exhibited lower overall emissions than the aromatic components.

Characteristic	SBA	SBB	SBC	SBD	SBE	SBF	TAME	Ethanol
IMEP (bar)	1	6.81	5.06	1.87	6.75	5.65	8.55	10
ISFC (g/ikWh)	6.44	10	7.27	5.10	8.78	8.90	7.34	1
ISFC (l/ikWh)	3.19	6.75	7.94	6.42	10	1	5.58	1.92
HC Emission (mg/ikWh)	6.18	5.33	1	3.89	8.02	8.99	10	9.24
NOx Emission (mg/ikWh)	10	4.82	1.62	3.53	1	5.52	7.26	3.73
CO Emission (mg/ikWh)	4.48	6.98	1.71	1	3.13	5.52	8.56	10

Table 6.1: *Numerical scoring of performance characteristics of synthetic gasoline blending components*

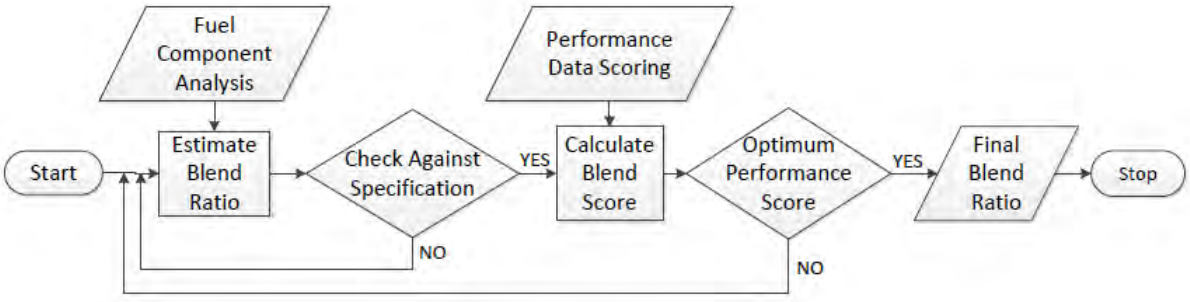

Figure 6.1: *Flow chart of blending model*

6.1.1.3 Modelling approach

The model was structured as shown in the flow chart in figure 6.1. Input parameters to the model include the specification relevant fuel component analysis results of the blending components and the numerical performance scoring values from table 6.1. In the first process a volumetric blend ratio is estimated from which the blend analysis is calculated. If the specification constraints are met the blend score is calculated. With the current South African fuel specification providing the boundary conditions, the blend score was refined with the generalised reduced gradient (GRG) solver in Microsoft Excel 2010 until the optimum was reached.

Linear blending rules on mass or volume basis were applied when applicable. The octane number was predicted on the basis of molar mass as previously defined by Anderson et al. [185, 186]. The method was tested with the octane test results of the 20 and 50% blends used for the evaluation described in chapter 5. While the prediction was found to be very accurate for the oxygenate blends, the prediction for the other synthetic blending components was not as good and resulted in similar accuracy when using a linear prediction by volume. Reid vapor pressure (RVP) was calculated using the blending index method according to the Petrofine physical properties manual [187].

6.1.1.4 Optimised blends

Four optimised test fuel blends were established as listed below:

1. Synthetic blend with highest IMEP - SB-IMEP
2. Synthetic blend with lowest ISFC by mass - SB-ISFCM
3. Synthetic blend with lowest ISFC by volume - SB-ISFCV
4. Synthetic blend with highest IMEP not adhering to specification - SB-PP

Test fuels 1 to 3 adhered to the current fuel specification while test fuel 4 was optimised purely for performance while only regarding the RVP limit to enable favourable cold start characteristics. A blend for a fuel with optimised performance, ISFC and specific emission was modelled by applying equal weighting factors to all performance criteria. This resulted in the same fuel blend as the fuel optimised for ISFC on a mass basis (SB-ISFCM).

6.1.2 Optimisation modelling results

The volumetric concentration of the synthetic blending components in the optimised fuel blends is shown in table 6.2. Although ethanol was found to be most beneficial for a high IMEP, the optimisation method resulted in TAME being used for the SB-IMEP blend. Since the oxygenate content is limited on a mass basis, it allowed more addition of TAME which was predicted to provide more benefit in terms of allowable spark advance than a smaller concentration of ethanol would. For all the synthetic blends, blend component A and D were not used due to their poor octane rating whereas blend component D was automatically eliminated due to its high benzene content. The allowable quantity of blend component F was limited by the density and RVP specification, while in SB-ISFCV there was additional need to increase the volumetric energy density. This resulted in more aromatic components being added than for the other fuels. The prediction for the SB-PP blend resulted in almost a quarter of the fuel being blend component F in order to increase the RVP.

Optimised blend	SBA	SBB	SBC	SBD	SBE	SBF	TAME	Ethanol	%
SB-IMEP	0	26.6	3.1	0	27.2	25.6	17.5	0	
SB-ISFCM	0	31.8	4.4	0	26.4	24.6	11.9	0.8	
SB-ISFCV	0	0	66.5	0	20.5	13	0	0	
SB-PP	0	0	0	0	0	22.2	0	77.8	

Table 6.2: *Volumetric concentration of synthetic blending components in optimised test fuel blends*

The test fuels were analysed and the key parameters are shown in table 6.3 along with the model results and the South African fuel specifications SANS:342:2006. The octane number and RVP prediction were found to be quite accurate but the oxygen mass of the SB-IMEP fuel was noted to be just outside the specification limit. A significant difference between the measured and predicted values was noted for the aromatic and olefin content. As discussed in chapter 3, the detailed chemical analysis showed that there was significant error when using the FIA test method, hence the analysis results were considered dubious. Considering the relative simplicity of the model exercise and the academic rather than commercial nature of this study, the overall accuracy and directionality was considered

to be acceptable and the engine performance tests were therefore conducted using these blends.

Table 6.3: *Key fuel analysis results for optimised synthetic fuel blends compared to model predicted values and South African fuel specification SANS 342:2006*

Analysis	Units	SB-IMEP-Measured	SB-IMEP-Model	SB-ISFCM-Measured	SB-ISFCM-Model	SB-ISFCV-Measured	SB-ISFCV-Model	SANS 342:2006
Density[a]	kg/l	0.74	0.73	0.75	0.73	0.755	0.77	0.73 – 0.785
RON[b]		97.9	98.18	97.5	97.99	95.8	95.84	min 95
MON[b]		84.7	85	84.4	84.10	84.8	84.97	min 85
RVP[c]	kPa	55	56.34	53	56.76	51	56.70	45 – 75
IBP[d]	° C	36.4	47.5	37.4	45.32	36.1	38.57	
10% [d]	° C	55.6	65	55.4	65	56.6	65	max 65
50% [d]	° C	88.2	83	92.4	85.25	103.0	102.50	77 – 115
90% [d]	° C	129.5	103.7	131.6	106.93	152.6	140.64	max 185
FBP [d]	° C	180.9	136.27	185.1	141.02	194.1	180.39	max 215
Aromatics[e]	vol%	7.53	21.61	8.26	21.69	23.27	46.19	max 50
Benzene[f]	vol%	1.76	4	1.83	4	2.88	4	4
Oxygen[g]	mass%	2.93	2.7	1.967	2.13	0.087	0	2.7
Olefins[e]	vol%	60.54	46	62.64	50	11.84	15.28	

[a] ASTM D4052 - 11
[b] ASTM D2699-13b/ASTM D2700-14
[c] ASTM D323-08(2014)
[d] ASTM D86-12
[e] ASTM D1319-14
[f] ASTM D3606 - 10
[g] ASTM D5622-95(2011)

In table 6.4 the lower heating values (LHV) and specific energy on mass (SEM) and volumetric (SEV) basis is shown. The specific energy is calculated by dividing the LHV by the air-to-fuel ratio thereby providing a means of comparing the actual energy supplied to the engine. It was noted that specific energy per unit mass was quite similar among the fuels, with the high ethanol content of SB-PP resulting in the highest energy due to the low stoichiometric air-fuel ratio. When considering the specific energy on a volume basis, SB-SFCV resulted in the highest energy content.

Analysis	Units	SCAG 95RON	SB-IMEP	SB-ISFCM	SB-ISFCV	SB-PP
LHV	MJ/kg	41.81	41.42	41.68	41.87	30.1
SE-G	MJ/kg	2.95	2.95	2.94	2.92	2.98
SE-V	MJ/l	2.17	2.15	2.15	2.25	2.23

Table 6.4: *Comparison of energy content of optimised fuel blends*

6.2 Test and data analysis method

The optimised test fuels were evaluated according to the same test method implemented for the initial engine test investigations discussed in 5.3.

A heat release analysis was done for the three engine speeds at the KLSA of the reference fuel in order to compare the heat release rate as well as the total heat released. The heat release was calculated with the commercial software Tiger using the average of 200 combustion cycles. In order to accurately calculate the heat release, the operator of Tiger needs to supply engine related information and make choices on sub-models that are used in the algorithm to calculate the gross heat release rate. These settings are listed below:

- The piezo-electric cylinder pressure signal was pegged to an absolute pressure value using the assumption of a point of zero heat transfer through the control volume during a given crank angle range during the compression phase. Since there was concern of the SB-PP fuel evaporating after inlet valve closing, the heat release analysis was also checked using the high temporal resolution inlet manifold absolute pressure measurement as a pegging reference.
- Internal residual gas was estimated by assuming that the cylinder was completely filled with exhaust gas at TDC during the gas exchange phase. The cylinder pressure, exhaust port temperature and compression volume were then used to calculate the mass using the ideal gas law.
- The cylinder-gas leakage was provided by the average blow-by meter readings from the test bench at the relevant operating point.
- The heat release analysis was calculated using a 2-zone combustion model
- In order to check the air and fuel mass parameters, the software calculates the A/F ratio and compares it to the A/F ratio provided in the operating point parameters.
- The thermodynamic properties of the burnt gas and fuel vapour were calculated using the model by Grill et al. [188]. In order to do this, the C/H/O ratio of the respective fuel was entered as obtained for each fuel by the 2D GC analysis.
- A wall heat transfer model by Bargende was used to calculate the heat transfer coefficient [189]. The cylinder wall temperature was estimated to be 200° C.

6.3 Results and discussion

6.3.1 Performance evaluation

In figure 6.2 the peak pressure, location of peak pressure and the IMEP are shown. Peak pressure was found to be mainly dependent on spark advance although fuel blend SB-ISFCM was found to exhibit a marginally higher peak pressure at 1500 and 5000 rpm, while SB-PP had a higher peak pressure at 3500 rpm. Apart from SB-ISFCV, a distinct improvement in IMEP over the reference fuel was noted for all optimised fuel blends, in particular the SB-PP. The same fuels also had an improved octane rating along with higher octane sensitivity which resulted in higher KLSA and thereby significantly increased performance. However, it was clearly evident that the fuel blends SB-IMEP and SB-ISFCM had a higher IMEP than the SCAG95 at the same spark advance.

The crank duration for the 10% and 50% mass fraction burn combustion parameters were found to be similar between the fuels as shown in figure 6.3. A small offset was noted for the fuel blend SB-PP at 5000 rpm implying a slightly longer burn duration. The same fuel blend was found to have a longer burn duration (AI90-AI10) at 1500 rpm and was also noted to 'plateau' as the spark advance neared the MBT spark timing. This behaviour was unexpected since ethanol is known to have a high laminar flame speed and some researchers have reported shorter burn durations with ethanol [184, 190, 191]. The other fuels exhibited fairly similar burn durations while fuel blend SB-ISFCM was found to have slightly shorter burn duration at 3500 and 5000 rpm.

Due to a significant oxygenate content, SB-PP resulted in a higher specific volumetric and gravimetric fuel consumption as shown in figure 6.4. The improvement in fuel consumption of fuel blend SB-SFCM was not as pronounced as expected, however a distinct offset in comparison to the commercial reference fuel was noted which was further improved due to a higher KLSA. SB-IMEP showed a similar improvement.

Lower specific hydrocarbon emissions were found for fuel blend SB-SFCM while SB-SFCV resulted in slightly higher emissions. At 5000 rpm the oxygenated fuel blend resulted in higher HC emissions, which reduced as the spark advance was adjusted towards MBT.

Specific NO_x emissions were found to be highest for the SB-PP fuel blend, indicating that peak combustion temperatures were higher than for the other fuels. A subtle increase in NO_x emissions was also noted to correlate with an increased spark advance which results in higher peak combustion temperatures. The lowest specific NO_x emissions were measured for the SB-SFCM fuel blend. A similar ranking was found for the specific CO emissions.

The highest performance increase was obtained using the SB-PP fuel blend as defined

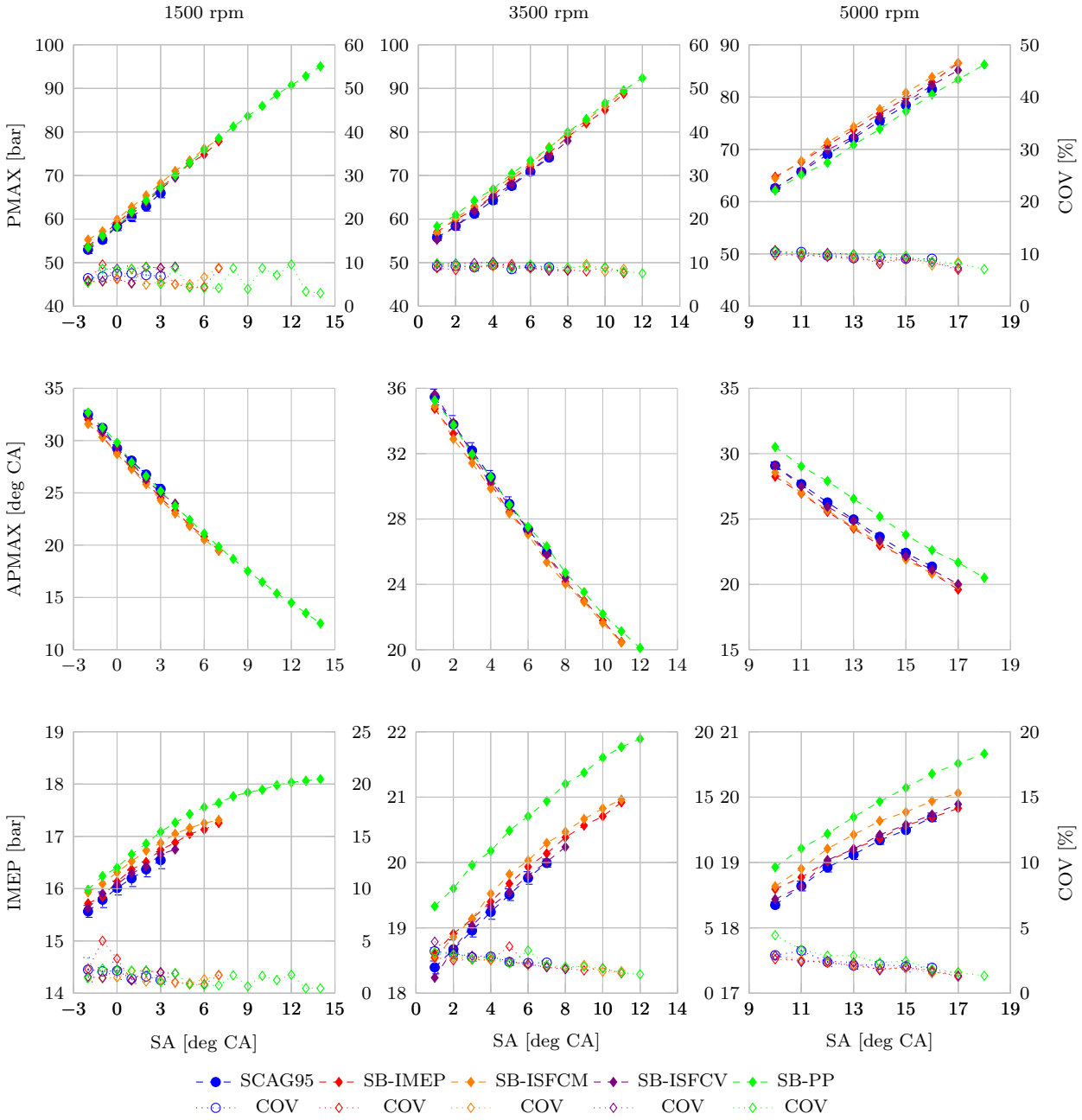

Figure 6.2: *PMAX, APMAX and IMEP vs SA sweeps for SCAG fuel and optimised synthetic fuel blends*

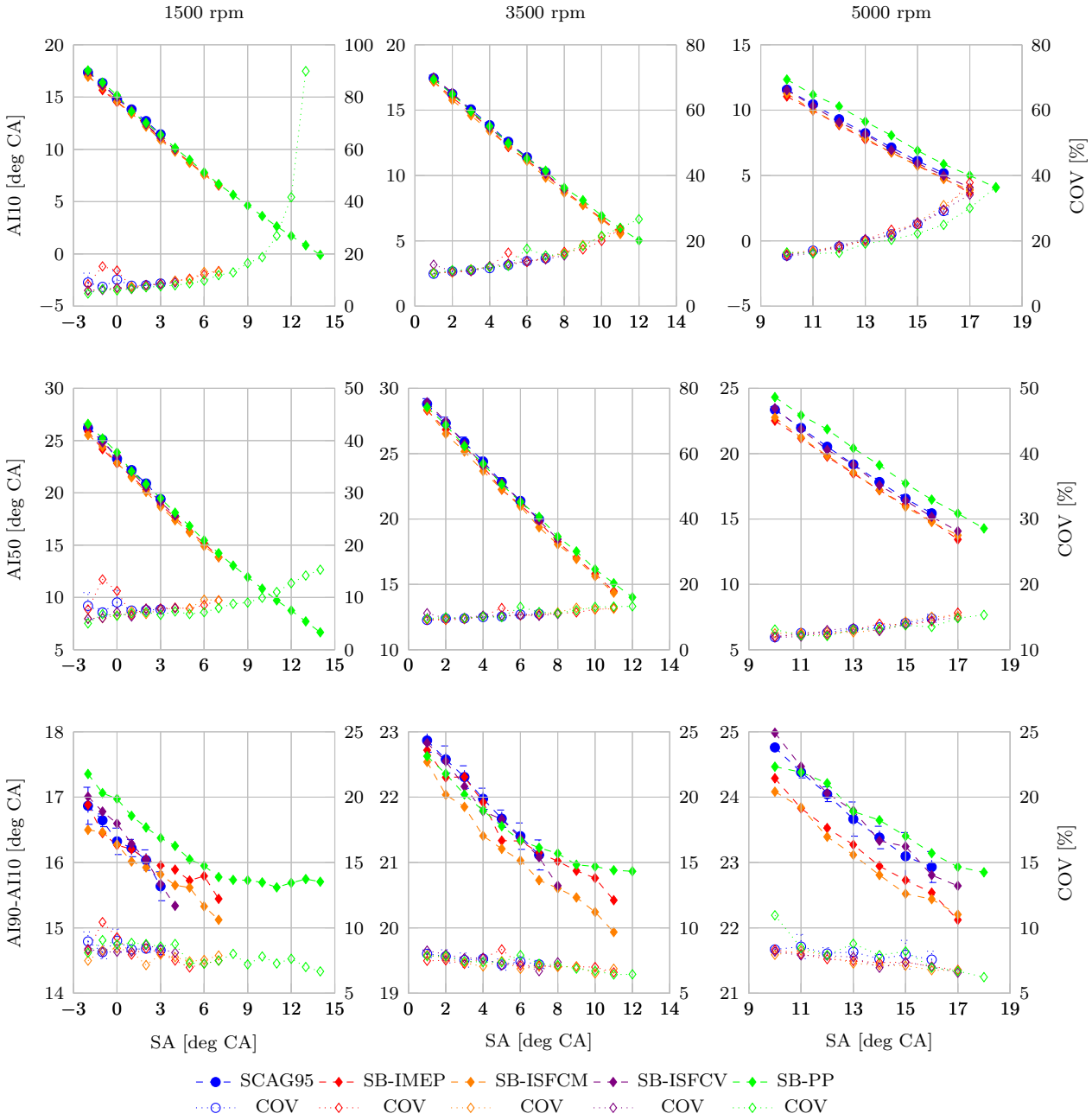

Figure 6.3: *AI10, AI50 and AI90-AI10 vs SA sweeps for SCAG fuel and optimised synthetic fuel blends*

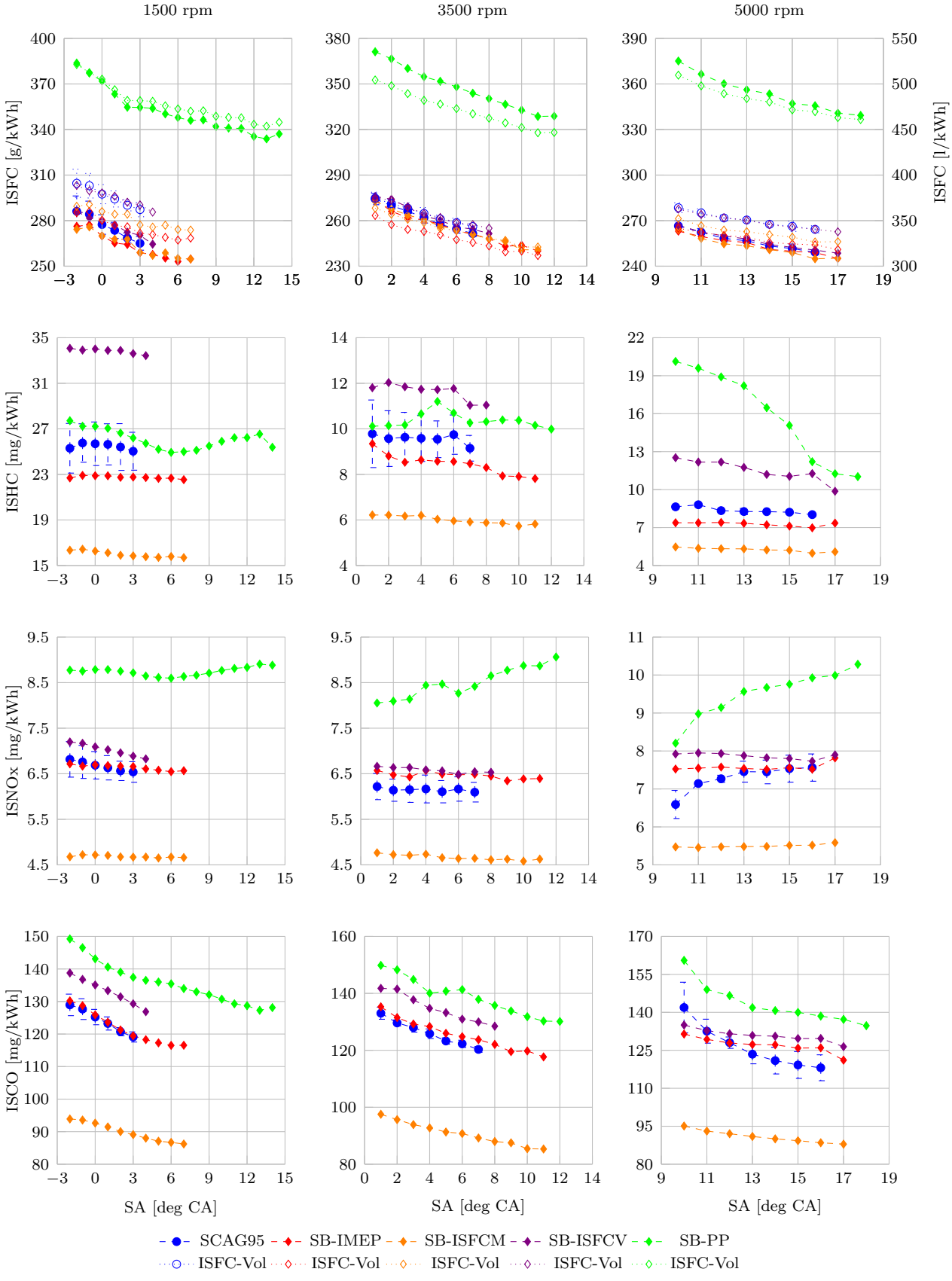

Figure 6.4: *ISFC, ISHC, ISNOx and ISCO vs SA sweeps for SCAG fuel and optimised synthetic fuel blends*

by the modelling exercise. The synthetic blend for optimal performance (SB-IMEP) was found to improve the power output over the reference fuel mostly due to a higher knock resistance that allowed more optimal spark advance. The SB-ISFCM fuel resulted in an even higher IMEP than the SB-IMEP, although this was not too surprising since thermal efficiency directly impacts engine power and the modelling results indicated that their performance would be similar. As predicted by the modelling exercise, fuel blend SB-SFCM was found to exhibit the lowest emissions and fuel consumption while offering an improved performance in comparison with the commercial synthetic reference fuel.

6.3.2 Heat release analysis

The heat release analysis at 1500 rpm shown in figure 6.5 indicates that the SB-PP fuel blend had the highest peak heat release rate as well as the highest cumulative heat released. For the other optimised fuels a higher peak heat release rate than the reference fuel was noted, while the total heat release was found to be similar.

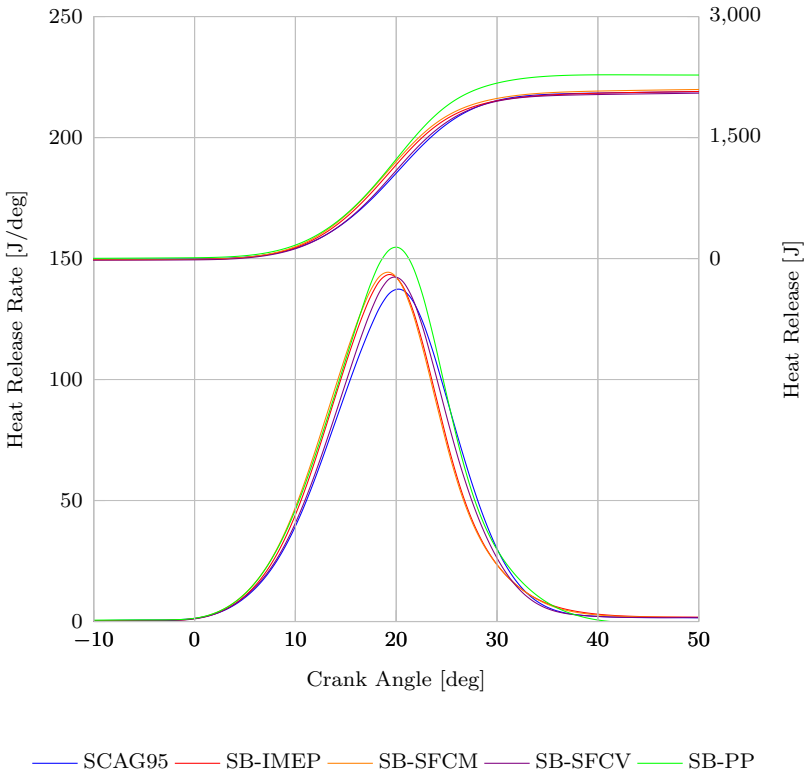

Figure 6.5: *Comparison of heat release analysis at 1500 rpm, SA3 BTDC for SCAG fuel and optimised synthetic fuel blends*

At 3500 rpm the difference in heat release rate as well as total heat release for the SB-PP fuel blend was less pronounced but still notable as shown in figure 6.6. Again the remaining optimised blends were also found to exhibit slightly higher heat release rate,

most notably the SB-SFCM blend. The same ranking was visible on the cumulative heat release curve.

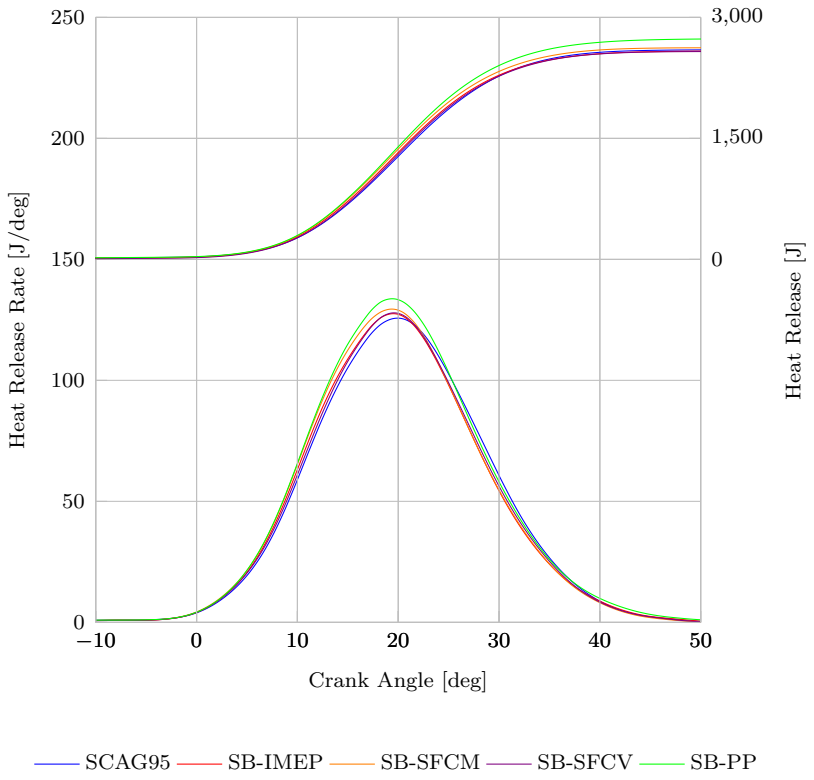

Figure 6.6: *Comparison of heat release analysis at 3500 rpm, SA7 BTDC for SCAG fuel and optimised synthetic fuel blends*

In figure 6.7 the heat release analysis at 5000 rpm is shown. Blends SB-SFCM and SB-PP have a similar peak heat release rate but the oxygenated fuel was found to have a noticeably lagging overall heat release rate. This was also evident in the flame kernel growth period (AI10) as well as the delayed 50% mass fraction burned point in figure 6.3. The overall heat release was still found to be highest for the SB-PP blend while an appreciable offset was also noted for the SB-SFCM blend. With increasing engine speed there was a noticeable reduction in variation between the different fuels presumed to be due to the increasingly dominant influence of turbulence on the combustion rate.

In order to try and investigate possible correlation between the peak heat release rate to the flame speed of the fuels, the laminar flame speeds of the final fuel blends was estimated using the flame speed data defined in chapter 4 and the energy fraction mixing rule proposed by [79]. While it is recognized that the in-cylinder conditions would not be the same for the different fuels, primarily due to charge cooling effects, some correlation was found as shown in figure 6.8. A slightly higher heat release rate or conversely lower laminar flame speed of the SB-PP fuel would have resulted in a better straight line fit. This implies that the charge cooling of the predominantly ethanol containing fuel blend SB-PP has a significant effect on its laminar flame speed and burn rate which could

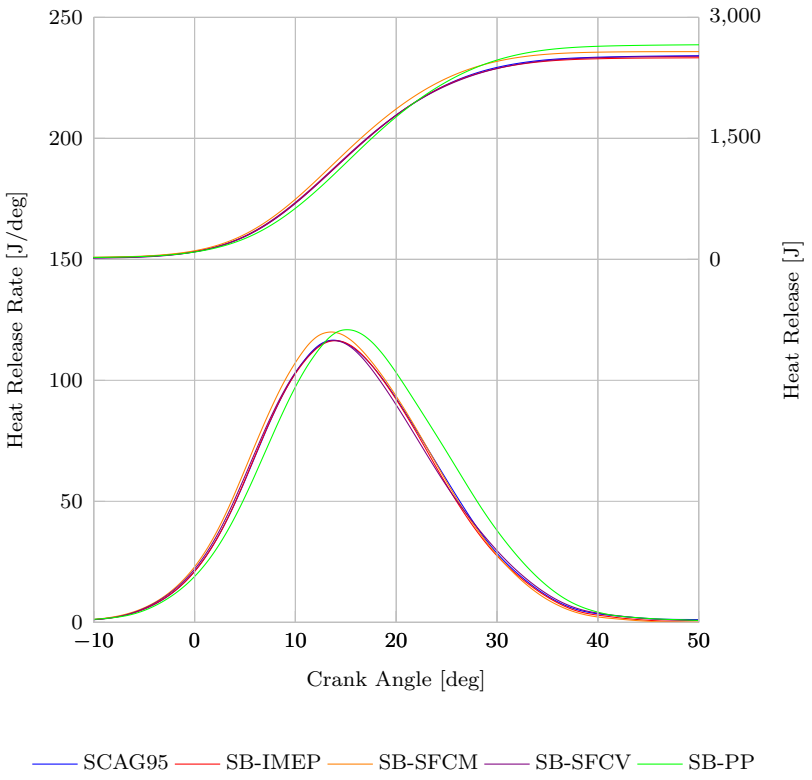

Figure 6.7: *Comparison of heat release analysis at 5000 rpm, SA16 BTDC for SCAG fuel and optimised synthetic fuel blends*

explain the slightly longer overall burn duration shown in figure 6.3. In order to evaluate the effects of differing fuel evaporation rates, latent heats and air fuel ratio effects on charge cooling, charge densification and heat transfer rates and to elucidate these effects on end of compression temperatures, simulations were conducted on the GT-Power model of the single cylinder engine.

6.3.3 GT-Power model interpretation

A predictive GT-Power model of the single cylinder engine described in chapter 2 was used to estimate the in-cylinder conditions at the end of compression. GT-Power has a limited library of fuels to choose from for the fluid object in the injector and combustion model. Ethanol was chosen to represent the SB-PP fuel while iso-octane was used as a surrogate for the synthetic CAG reference fuel. The cylinder evaporation model makes use of a simple phenomenological method to estimate the rate of evaporation in the cylinder with the following equation:

$$EvaporationRate = \frac{4.16 * RPM_{ref}}{CA50}(\frac{T}{T_{ref}})^{TMPEXP}(\frac{RPM}{RPM_{ref}})^{RPMEXP} \tag{6.1}$$

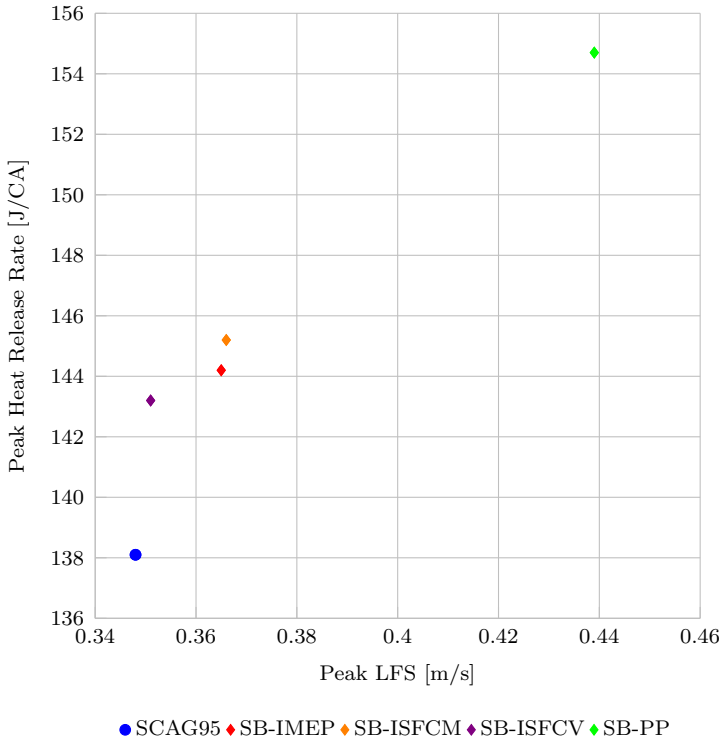

Figure 6.8: *Comparison of laminar flame speed at λ=0.9 (at reference conditions, P = 1bar, T = 25 ° C) and peak heat release rate at 1500 rpm, SA3 BTDC for SCAG fuel and optimised synthetic fuel blends*

where:

CA50 = 50% Evaporation duration in degree crank angle
TMPEXP = Exponent for temperature dependence
RPMEXP = Exponent for engine speed (rpm) dependence
RPM = Engine speed in rpm
RPMref = Reference speed (4000 rpm)
T = Temperature in K
Tref = Reference temperature (600 K)
4.16 is a constant that is used to scale the integrated evaporation to be equal to 50% at the reference conditions

CA50 is defined as the time scale for evaporation of 50% of the liquid at a cylinder temperature of 600 K and an engine speed of 4000 rpm. This value needs to be estimated by the operator and entered in crank angle degrees. In order to make a reasonable assumption, a recent PhD thesis by Kasseris from the Massachusetts Institute of Technology was consulted [192]. Kasseris made use of computational fluid dynamics (CFD) to quantify the charge cooling of ethanol and iso-octane in a 2.0 litre 4 cylinder turbocharged GDI engine operated in homogeneous charge mode. The engine was run at 2000 rpm with a compression ratio of 9.2:1, the manifold pressure was 1.8 bar absolute and the fuel was

injected at 55 CAD after TDC with a pressure of 100 bar. Although the engine in question was fitted with a side mounted injector operated at stoichiometric air-fuel ratio, the in-cylinder conditions were deemed to be comparable with the operating point at 1500 rpm of this investigation. It was shown by Kasseris that ethanol resulted in a significant amount of wall wetting while for iso-octane it was found to be negligible. Furthermore the results indicated that while 90% of iso-octane evaporated within 80 CAD, ethanol took 180 CAD. If these results are carried over to the operating conditions of the single cylinder engine, then a start of injection at 60 degree ATDC would likely result in some evaporation taking place just after the inlet valve closes at 126 degree BTDC. For the single cylinder engine model in GT-Power, the CA50 duration for ethanol was therefore assumed to be approximately 2.5 times longer than for iso-octane. In an attempt to predict the maximum charge cooling potential of ethanol, Kasseris modified the CFD code to allow the fuel droplets to bounce off the cylinder walls in order to partake solely in cooling of the cylinder charge. It was found that approximately 22% remained in liquid form until TDC [192]. Since it can be expected that more than 22% of the heat of vaporisation (ΔH_{vap}) would be absorbed by the cylinder walls, the fraction was assumed to be roughly 30% for the GT-Power model.

In figure 6.9 the estimated cylinder temperatures for iso-octane and ethanol at 1500 rpm are depicted. The end of compression temperature for ethanol was found to be approximately 74 K lower than iso-octane. This result for rich mixtures is deemed to be reasonable in comparison to the CFD analysis of Kasseris which showed a difference of 52 K under stoichiometric air-fuel ratio conditions [192].

The synthetic CAG 95 RON fuel was found to have a ΔH_{vap} of 248 kJ/kg which is within 20% of the value of 307 kJ/kg for iso-octane. Due to the very high ethanol content (approximately 80%) in synthetic blend SB-PP, this should result in roughly 60 ° C lower charge temperature at the end of compression. As shown in figure 6.8, the peak laminar flame speed for SB-PP was estimated to be 0.439 m/s at standard conditions of 1 bar and 25 ° C. Using the methodology described in Appendix A, the laminar flame speed of the synthetic CAG 95 RON was re-calculated for a temperature of 85 ° C which resulted in a peak laminar flame speed of 0.473 m/s which exceeds the peak laminar flame speed of ethanol at 25 ° C. It can therefore be deduced that the slightly longer burn duration of SB-PP shown in figure 6.3 could be fully attributed to the slower flame speed as a result of the charge cooling.

Despite the obvious effect of charge cooling on the cylinder temperature, the simulation results indicate that pure ethanol does in fact result in a faster burn rate as indicated by the combustion phasing shown by the cylinder pressure in figure 6.10 and the heat release in figure 6.11. The laminar flame speed in GT-Power is calculated using the following equation [17]:

$$S_L = (B_m + B_\Phi(\Phi - \Phi_m)^2)(\frac{T_u}{T_{ref}})^\alpha(\frac{p}{p_{ref}})^\beta(1 - 2.06(Dilution)^{DEM-0.77}) \quad (6.2)$$

where:

S_L = Laminar flame speed in m/s
B_m = Maximum laminar flame speed in m/s (fuel specific)
B_Φ = Laminar flame speed roll-off value (fuel specific)
Φ = In-cylinder equivalence ratio
Φ_m = Equivalence ratio at maximum laminar flame speed
p = pressure in Pa
p_{ref} = 101325 Pa
T_{ref} = 298 K
T_u = Temperature of the unburned gas in K
Dilution = Mass fraction of the residuals in the unburned zone
α = Temperature exponent (fuel specific)
β = Pressure exponent (fuel specific)
DEM = Dilution Exponent Multiplier

The maximum laminar flame speed for iso-octane is given as 0.263 m/s in GT-Power, which is significantly lower than 0.348 m/s of the synthetic CAG 95 RON and would therefore influence the combustion phasing in relation to a fuel containing a significant amount of ethanol. However, the cylinder temperature profile of the iso-octane and ethanol implies that the SB-PP fuel could converge during the combustion process and thereby give it a higher flame speed as indicated by the faster heat release rate shown in figure 6.5.

As shown in figure 6.5 and in the simulation results in figure 6.11, total heat released is higher for a fuel with high ethanol content due to an increase in the molar ratio of product to reactants, resulting in extra water vapour in the exhaust. However, it needs to be borne in mind that it results in a reduction in the exhaust gas enthalpy as shown in figure 6.9. This would handicap the effectiveness of an exhaust gas turbocharger, implying that the performance gains shown for the SB-PP fuel with an externally charge boosted engine are somewhat artificial.

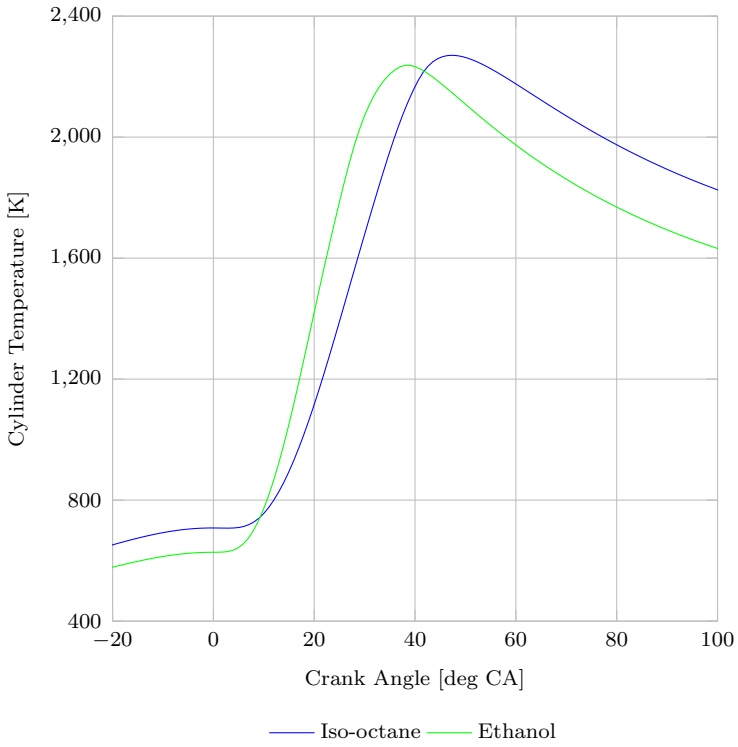

Figure 6.9: *Estimated cylinder temperature for iso-octane and ethanol at 1500 rpm, SA3 BTDC using GT-Power*

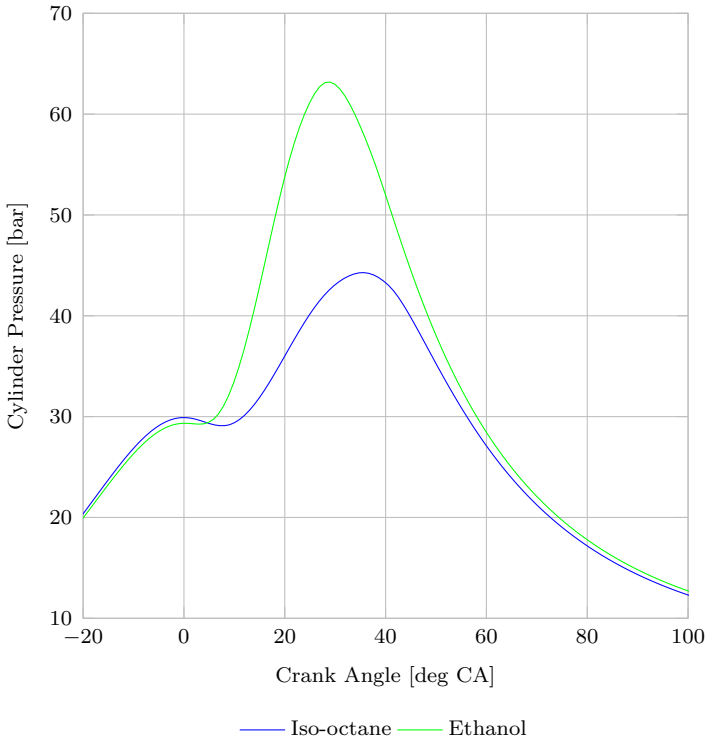

Figure 6.10: *Estimated cylinder pressure for iso-octane and ethanol at 1500 rpm, SA3 BTDC using GT-Power*

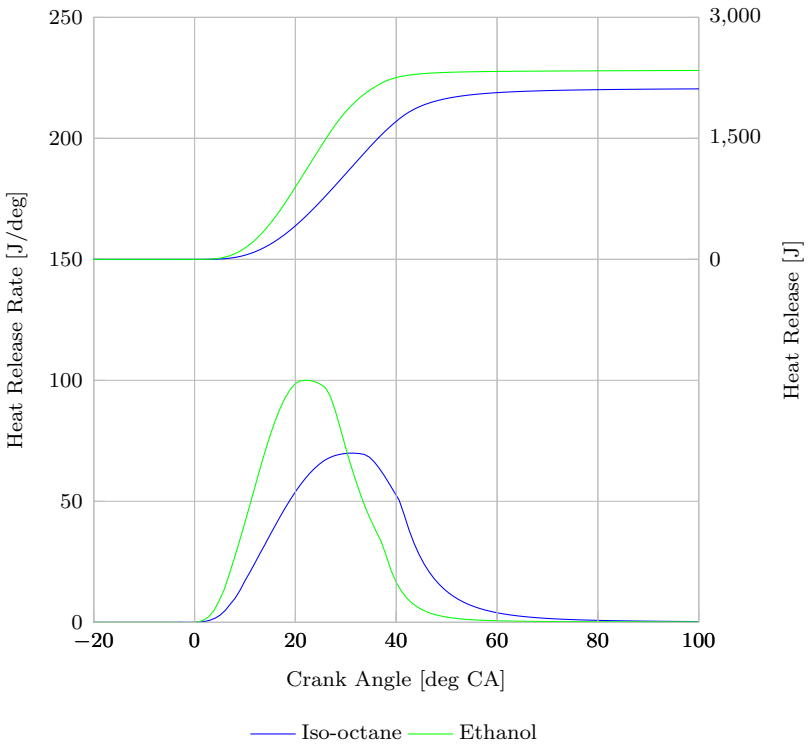

Figure 6.11: *Estimated heat release analysis for iso-octane and ethanol at 1500 rpm, SA3 BTDC using GT-Power*

6.3.4 EGR tolerance

In figure 6.12 a comparison of the combustion pressure parameters for the optimised blends with the reference fuels is shown. Due to a higher KLSA the specific fuel consumption improved with increasing EGR rate which can be seen in the peak pressure being maintained at an earlier crank angle. At 1500 rpm the maximum possible EGR flow rate was reached below 20% while at 3500 rpm the MBT spark timing was reached at about 16% EGR resulting in a associated reduction in peak cylinder pressure as well as IMEP. Overall the IMEP reduced with increasing EGR rate due to charge dilution. However, the cycle-to-cycle variation was fairly constant throughout at 1500 rpm but increased drastically at 3500 rpm when the EGR rate was increased once the MBT timing was reached.

The exhaust port temperature as well as combustion phasing parameters are shown in figure 6.13. Increasing the EGR rate resulted in a corresponding reduction of the exhaust gas temperature. Early flame kernel growth and combustion mid point (AI50) consistently advanced according to KLSA until the MBT timing was reached for 3500 rpm. Overall combustion duration increased however with EGR rate, which was exacerbated at 3500 rpm once the MBT timing was reached.

In figure 6.14 the KLSA at 0% EGR rate for each fuel was maintained throughout the

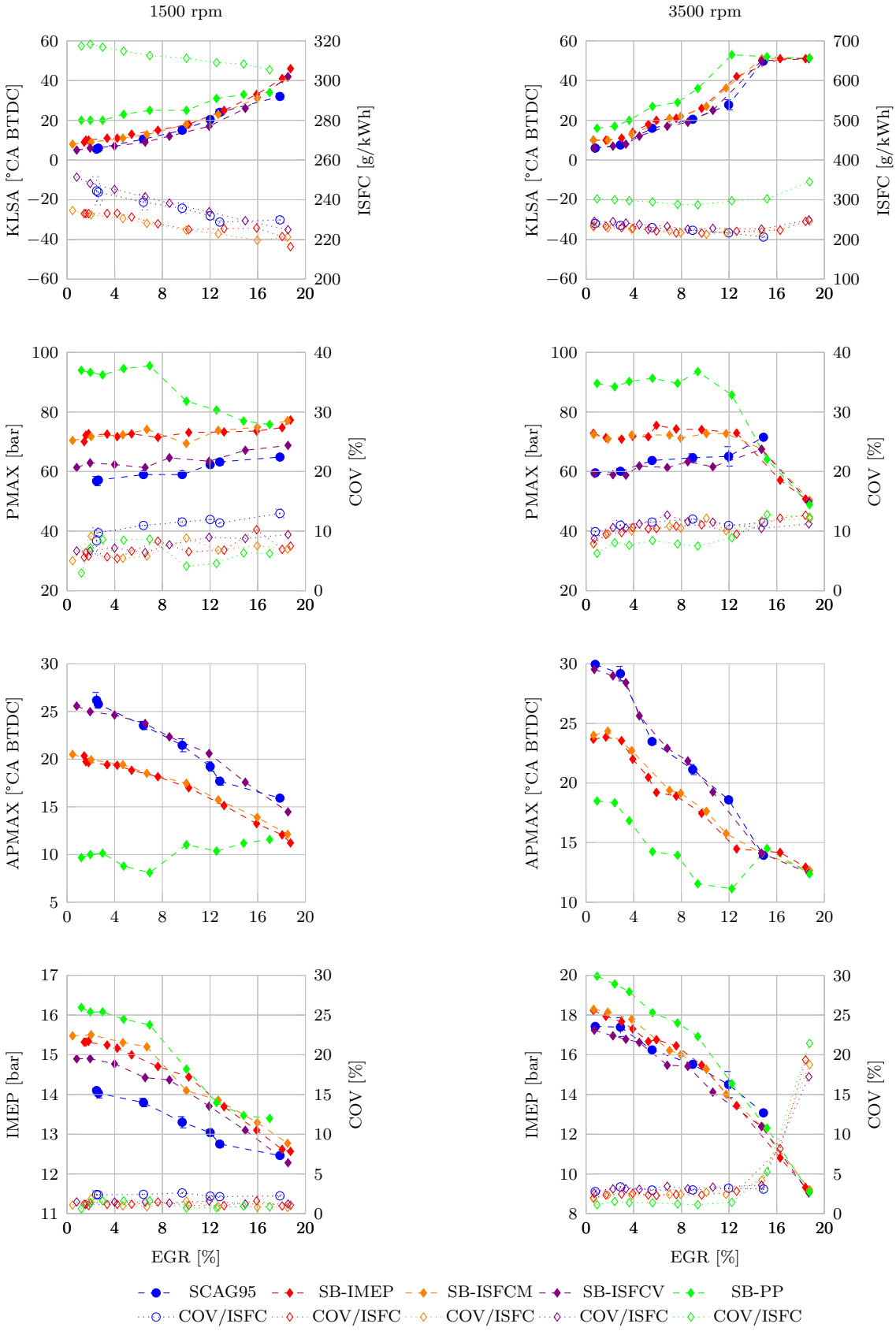

Figure 6.12: *PMAX, APMAX and IMEP vs EGR sweeps for SCAG fuel and optimised synthetic fuel blends at KLSA*

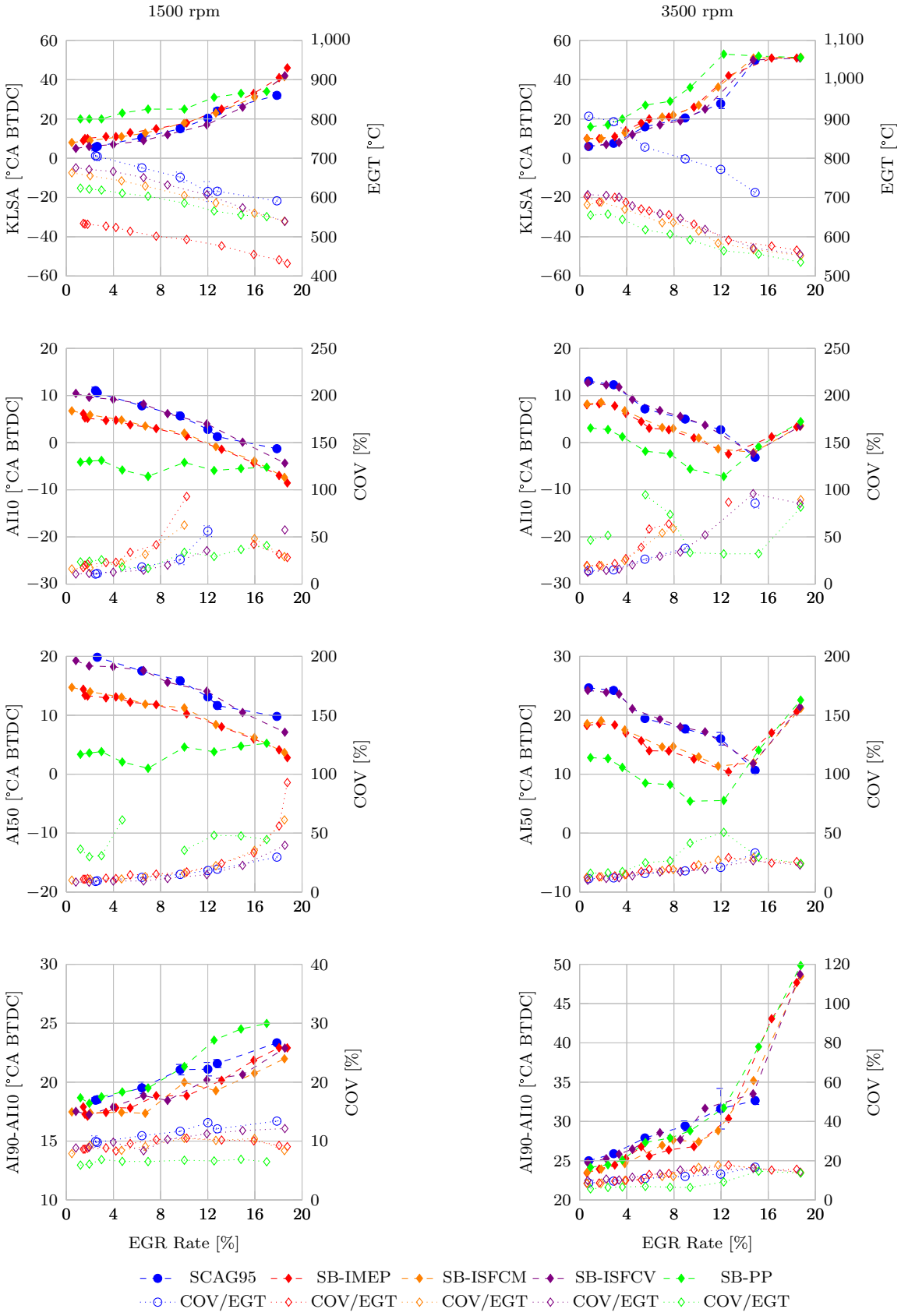

Figure 6.13: *AI10, AI50 and AI90-AI10 vs EGR sweeps for SCAG fuel and optimised synthetic fuel blends at KLSA*

EGR sweep. At 1500 rpm the ISFC remained fairly constant for the commercial reference fuel and the SB-ISFCV until approximately 10% EGR rate after which there was a sudden steep increase as the misfire limit was reached. This correlated with a lower peak cylinder pressure and sudden decrease in IMEP. A similar behaviour was observed for the SB-ISFCM and SB-IMEP fuel blends, but only at approximately 13%. The SB-PP blend was found to have a constant ISFC irrespective of the EGR rate since there was a steady reduction in IMEP which correlated with a lower fuel consumption.

At 3500 rpm all fuels exhibited a continuous increase in specific fuel consumption with increasing EGR. For all the fuels apart from SB-PP there was an associated reduction in IMEP from approximately 5% EGR rate, while SB-PP reduced suddenly at about 10%.

In figure 6.15 the exhaust gas temperature and combustion phasing is depicted. Due to the static spark advance, an increase in EGR rate resulted in delayed combustion phasing as shown by the initial kernel growth period (AI10) as well as the 50% MFB (AI50). The exhaust gas temperature was found to be fairly constant throughout the EGR sweep which can be attributed to the exhaust gas temperature increase as a result of delayed combustion, overshadowing the overall reduction in exhaust gas temperature due to mixture dilution and increased heat capacity of the exhaust gas compounds.

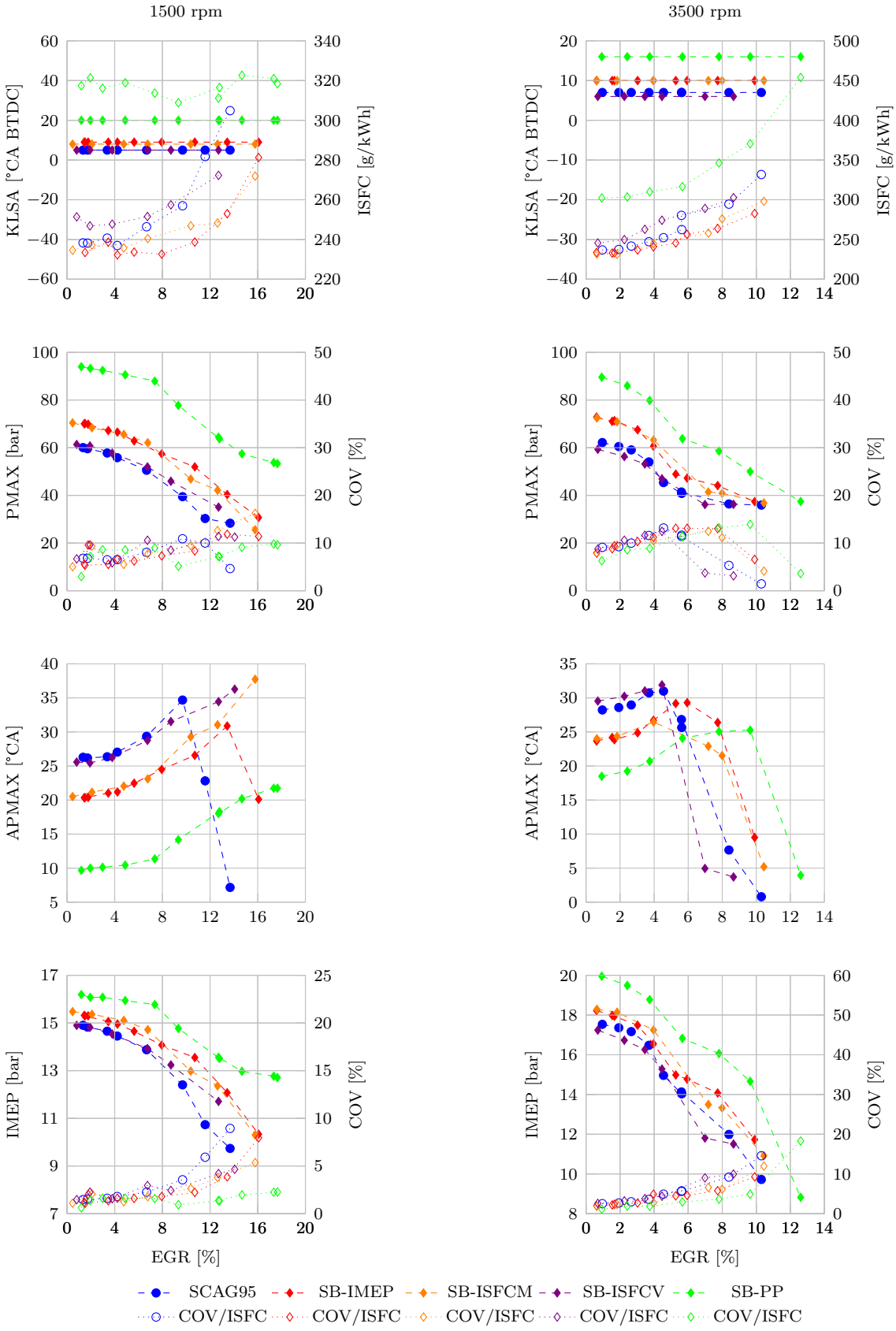

Figure 6.14: *PMAX, APMAX and IMEP vs EGR sweeps for SCAG fuel and optimised synthetic fuel blends at constant spark advance*

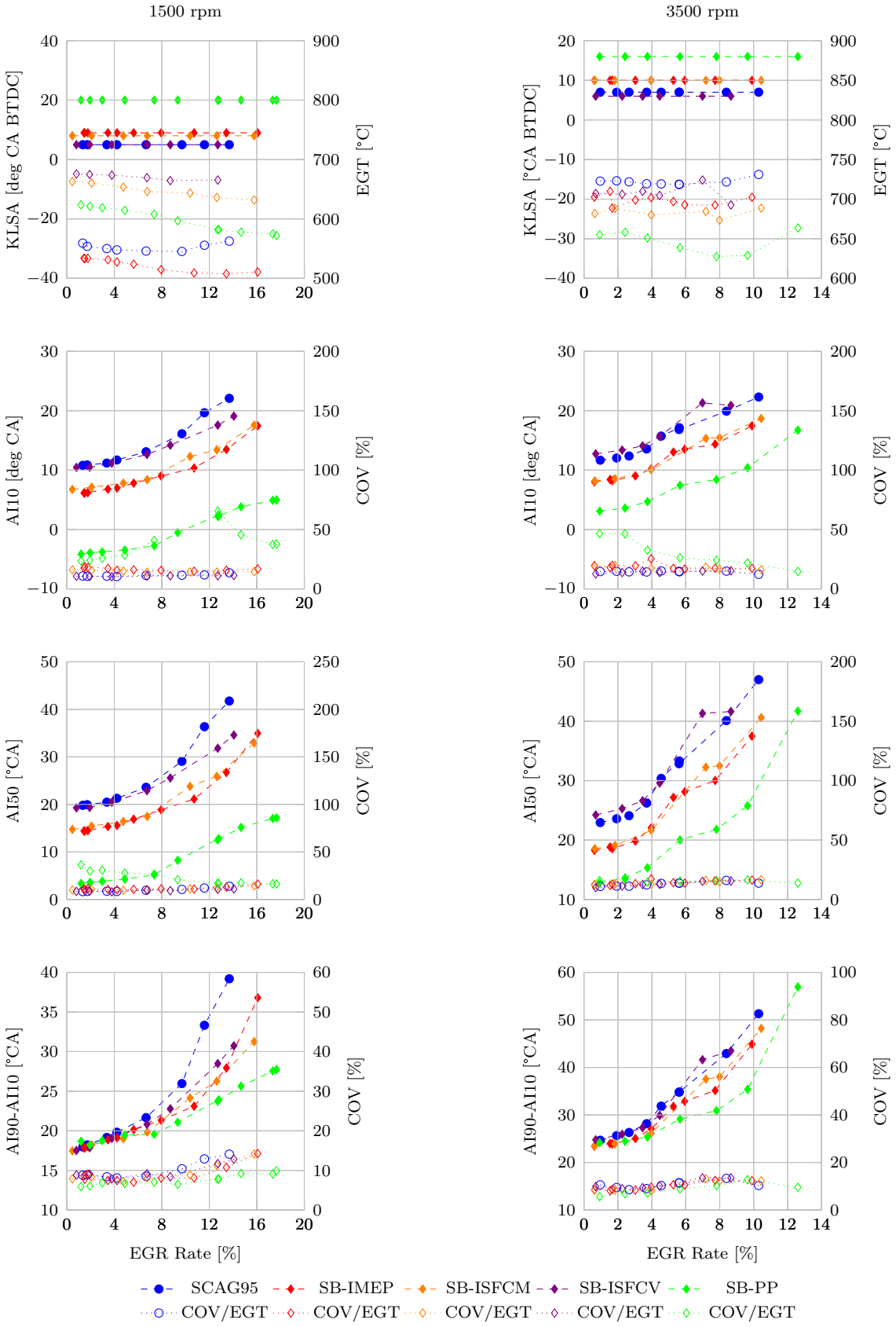

Figure 6.15: *AI10, AI50 and AI90-AI10 vs EGR sweeps for SCAG fuel and optimised synthetic fuel blends at constant spark advance*

6.4 Summary and discussion

Through the use of a novel modelling exercise, optimised synthetic fuel blends were defined to improve the IMEP as well as indicated specific fuel consumption both on a mass as well as volume basis, while adhering to the current South African fuel specification. An optimisation was also done for a blend with high IMEP, low fuel consumption and low raw emissions. The resulting blend ratio was found to be the same as the fuel blend optimised purely for SFC on a mass basis. An additional fuel blend was defined for optimal performance without regard for fuel specifications other than the RVP value.

The performance analysis revealed that the fuel blends for optimal IMEP (SB-IMEP) and ISFC on mass basis (SB-ISFCM) provided a 5% improvement in IMEP as a result of the higher KLSA. A distinctly higher IMEP was also noted at all spark advance settings, due to a higher heat release rate, with the SB-ISFCM providing even better performance than the SB-IMEP. The peak performance synthetic blend (SB-PP) exhibited a significant performance increase due to a higher heat release rate as well as much improved KLSA. The SB-ISFCM fuel blend was found to have the lowest specific raw emissions, which agreed with the predictions from the model of the optimisation process.

The optimised blends were also evaluated with regards to their EGR tolerance, where it was found that the improved KLSA resulted in a higher IMEP throughout the EGR sweep, but that the cycle-to-cycle variation was similar for all fuels. Due to the limitation on the available EGR rate at 1500 rpm, the misfire limit could not be reached. At 3500 rpm the improved octane rating of the SB-IMEP and SB-ISFCM test fuels allowed for an improved IMEP up to an EGR rate of approximately 14%, whereafter the MBT ignition timing of 50 deg BTDC was reached for all the test fuels. An increase in EGR rate from that point resulted in a drastic increase in cycle-to-cycle variation of the IMEP for all the test fuels. By fixing the spark advance to the respective KLSA of the fuel, it was found that the IMEP decreased consistently for all fuels, implying that there was no inherently higher EGR tolerance. This was expected, since the initial component blend testing had revealed no potential for enhanced EGR tolerance.

In order to prove its merits with regards to engine operation under part load, non-knock limited conditions, it would be interesting to populate the model with the relevant engine performance data in order to check the optimised fuel blends. It is believed that the blends presented here would perform similarly well. For example, blend component F, which was shown to also improve specific fuel consumption due to a more optimal burn angle, was already included within the realm of the current fuel specification, while selected aromatics with a high volumetric energy density formed the building blocks of fuel blend SB-ISFCV. Overall, a final commercial fuel blend would need to be optimised to cater for both part- and full load operation by assigning relevant weighting factors to the

optimisation routine.

Chapter 7

Conclusions

This chapter provides conclusions on the work presented in this thesis.

The chemical analysis of commercial crude derived gasoline and synthetic gasoline as well as blending components allows for the following conclusions to be drawn:

- Standard FIA chemical analysis indicated that the commercial synthetic gasoline had an equivalent and in some cases lower olefin content than some of the commercial crude derived gasoline
- Detailed chemical analysis revealed that the FIA method did not accurately identify the paraffin, aromatic and olefin content in a full boiling range gasoline. For the synthetic gasoline the FIA method over-predicted the aromatic content by 30% and the olefin concentration by over 80%. Similarly the olefin content of the crude derived gasoline was over-predicted by over 90%. This has important implications since the aromatic content in gasoline is restricted by South African legislation and the olefin content limit restriction is under discussion.
- Synthetic gasoline blending components were found to exhibit distinct chemical characteristics as a result of the refining processes.
- Two predominantly olefinic blending components were found to have significant differences in the olefin subclasses. Blend component B consisted predominantly of tertiary and quaternary olefins, while blend component F had a high concentration of α- and internal olefins. It has been shown in literature [41] and in this study that the subclasses have a significant influence on the combustion behaviour.

From the laminar flame speed analysis it can be concluded:

- The laminar flame speed behaviour of the commercial gasolines was found to be similar although the synthetic fuel was slightly higher than the crude derivatives.
- The synthetic gasoline blending components revealed distinct variation in laminar flame speed behaviour which were shown to be related to their chemical characteristics.
- Two fuel blend components (Blend B and Blend F) identified with a high olefin content were found to exhibit a higher flame speed than the aromatic and paraffinic components. Blend F had an exceptionally high laminar flame speed which could be related its high α-olefin content. The tertiary and quaternary olefins inherent to Blend B, do not exhibit such a high flame speed.
- The synthetic oxygenate components, ethanol and TAME, also exhibited significantly different laminar flame speed behaviour. Ethanol was shown to have a very fast flame speed while TAME exhibited a slow flame speed. Since both oxygenates have a very high octane rating this finding had important implications on the choice of oxygenate as a blending component for a final product.

The combustion analysis on the GDI engine yielded the following conclusions:

- Using PRF, TSF commercial gasoline it was found that the operating conditions of the charge boosted GDI engine were "beyond RON". However the K value was found to be somewhat dependent on the fuel type used, since a poor correlation between KLSA and OI was found with the aromatic blending components and even less correlation with the olefinic blending components.
- The performance analysis revealed that there was no significant power output difference between the synthetic and crude derived gasoline. Similarly the specific fuel consumption and emissions were found to be comparable. The combustion analysis also did not reveal any appreciable differences while the EGR tolerance was also found to be similar.
- Due to their high octane rating, the oxygenate components resulted in a significant performance increase as a result of a higher KLSA. Ethanol was found to exhibit an even higher knock resistance and higher performance throughout the spark advance sweep while TAME offered a lower fuel consumption due to its inherently higher heating value. The improved KLSA of both fuels improved the EGR tolerance at low EGR rates. At elevated EGR rates the performance was similar to lower octane fuels since the spark advance was no longer knock limited.

- The olefinic synthetic blend component F increased the burn rate due to its high laminar flame speed, thereby improving the combustion phasing and duration which subsequently improved performance. However, there was a performance trade off due to the low octane rating of the blend, which also resulted in poorer EGR tolerance. The other olefinic blending component (Blend B), was found to have a similar combustion phasing to the commercial pump fuel. Performance was improved in comparison to the reference fuel due to a higher KLSA as a result of improved octane rating.
- The predominantly aromatic synthetic blending components were not found to provide any performance benefit over the commercial synthetic gasoline. Aromatic blend components with low octane rating naturally reduced the performance potential.

From the analysis of the optimised synthetic blends it can be concluded:

- Using a novel modelling exercise it was possible to define optimised synthetic gasoline blends using the eight synthetic blend components used in this study.
- A fuel optimised for peak IMEP resulted in up to 4% higher performance than the commercial gasoline while the fuel blend optimised for ISFC on a mass basis, provided an even higher performance increase of up to 5%, with an improvement in specific fuel consumption of up to 5%.
- Without regard for current fuel specification a fuel blend was optimised purely for peak performance while controlling the RVP for acceptable cold start characteristics. It resulted in a blend of approximately 25% blend component F and the rest being ethanol. The improvement in IMEP was measured to be up to 8.5%.
- A synthetic blend optimisation was done to obtain a fuel adhering to current fuel specification with improved IMEP, ISFC and specific raw emissions. The blend ratio was found to be the same as the fuel blend for optimal IMEP on a mass basis, thereby resulting in 5% improvement of IMEP and ISFC with up to 30-40% lower specific raw emissions.

General conclusions:

- The unique chemical characteristics of the synthetic blending components were found to influence their laminar flame speed and in some cases this could be carried over into the combustion regime of the GDI engine

- Octane number was the predominant driver in improved performance characteristics due to a higher KLSA resulting in more optimal combustion phasing. Under common spark timing conditions, an improvement of up to 2% in IMEP was measurable using a synthetic blending component with high laminar flame speed characteristic.
- It was possible to optimise the blend ratio for a commercial synthetic gasoline using eight existing blending components thereby substantiating the hypothesis of the thesis.

Chapter 8

Recommendations

This chapter provides recommendations for future work.

From the conclusions drawn the following recommendations can be made:

- Although mixing rules have been established to calculate the LFS of fuel mixtures from the LFS characteristics of the individual components it would be interesting to experimentally quantify the LFS of the optimised fuel blends.
- The laminar flame speed rig has subsequently been equipped with optical analysis tools which allows for more accurate determination of Markstein length. The relationship of stretched to un-stretched flame velocity could be re-evaluated.
- The LFS of the synthetic blending components should be analysed with respect to their sensitivity on exhaust gas residuals
- Due to the limitations of the engine restricting the peak combustion pressure to 100 bar, the boost pressure was limited to 0.5 bar which is not on par with most modern highly boosted GDI engines. The combustion analysis should therefore be conducted under these more stringent in-cylinder conditions.
- Modern GDI engines employ variable valve timing which allows over-scavenging and thereby cooling of the combustion chamber. This can have a profound effect on the in-cylinder conditions to which the charge is subjected and should therefore be investigated.
- The GDI combustion analysis investigation should be conducted at part load conditions with emphasis on fuel consumption.
- The low speed pre-ignition (LSPI) characteristics of the synthetic blending components would need to be defined, especially for blend components with intrinsically

high laminar flame speed. It has been shown in literature that an increase in LSPI propensity can be correlated to fuel streams with elevated laminar flame speed characteristics [8].

- An investigation into the behaviour of the synthetic blending components at low engine speed under EGR rates exceeding 20% would be of interest due to the ongoing development in this area [145, 146].

References

[1] C. F. Taylor, *Internal Combustion Engine in Theory and Practice, second edition, revised, Volume 2*. The MIT Press, 1985. (Cited on pages 1, 3 & 41).

[2] V. Mittal and J. Heywood, "The shift in relevance of fuel RON and MON to knock onset in modern SI engines over the last 70 years," *SAE International*, no. SAE2009-01-2622, 2009. (Cited on page 1).

[3] G. Kalghatgi, "Fuel anti-knock quality-Part II. Vehicle Studies-how relevant is Motor Octane Number (MON) in modern engines?," no. SAE2001-01-3585, 2001. (Cited on pages 2, 44 & 55).

[4] A. Yates, A. Swarts, and C. Viljoen, "Correlating auto-ignition delays and knock-limited spark-advance data for different types of fuel," *SAE Technical Paper*, no. SAE2005-01-2083, 2005. (Cited on pages 2, 3, 44 & 55).

[5] R. Cracknell, A. Prakash, and R. Head, "Influence of Laminar Burning Velocity on Performance of Gasoline Engines," *SAE International*, no. SAE2012-01-1742, 2012. (Cited on pages 2, 3, 4, 55 & 93).

[6] R. Stein, D. Polovina, K. Roth, M. Foster, M. Lynskey, T. Whiting, J. E. Anderson, M. H. Shelby, T. G. Leone, and S. VanderGriend, "Effect of Heat of Vaporization, Chemical Octane, and Sensitivity on Knock Limit for Ethanol - Gasoline Blends," *SAE International*, vol. 2012, no. SAE2012-01-1277, pp. 823–843, 2012. (Cited on pages 2, 43, 67 & 92).

[7] O. Welling, J. Moss, J. Williams, and N. Collings, "Measuring the Impact of Engine Oils and Fuels on Low-Speed Pre-Ignition in Downsized Engines," *SAE International*, no. SAE2014-01-1219, 2014. (Cited on page 2).

[8] G. T. Kalghatgi and D. Bradley, "Pre-ignition and 'super-knock' in turbo-charged spark-ignition engines," *International Journal of Engine Research*, vol. 13, pp. 399–414, Feb. 2012. (Cited on pages 2, 45 & 124).

[9] E. Chapman, R. Davis, W. Studzinski, and P. Geng, "Fuel Octane and Volatility Effects on the Stochastic Pre-Ignition Behavior of a 2.0L Gasoline Turbocharged DI Engine," *SAE International*, no. SAE2014-01-1226, 2014. (Cited on page 2).

[10] Y. Okada, S. Miyashita, Y. Izumi, and Y. Hayakawa, "Study of Low-Speed Pre-Ignition in Boosted Spark Ignition Engine," *SAE International*, no. SAE2014-01-1218, 2014. (Cited on page 2).

[11] A. de Klerk, *Fischer-Tropsch Refining*. Weinheim, Germany: Wiley-VCH Verlag GmbH & Co. KGaA, 2011. (Cited on pages x, xii, 2, 15, 16, 17, 18, 19, 20, 21 & 26).

[12] A. Yates and C. Cilliers, "A Fundamental Study of the Relationship Between Altitude and Research Octane Number," *SAE Technical Paper*, no. SAE2002-01-1662, 2002. (Cited on page 2).

[13] A. Swarts, *Insights relating to octane rating and the underlying role of autoignition*. PhD thesis, University of Cape Town, 2006. (Cited on pages 2, 42 & 44).

[14] S. G. Bryce, R. Lindsay, I. Galliard, and A. R. Glover, "Fuels Development for Formula One," *SAE International*, no. SAE942540, 1994. (Cited on page 3).

[15] G. E. Jones, I. S. Myburgh, and J. J. Botha, "The Sasol Oil Racing Fuels and Lubricants Research Facility," *SAE International*, no. SAE942542, 1994. (Cited on page 3).

[16] R. Stanglmaier, C. Roberts, and D. Mehta, "Measurement of laminar burning Velocity of multi-component fuel blends for use in high-performance SI engines," *SAE Technical Paper*, no. SAE2003-01-3185, 2003. (Cited on pages 3 & 29).

[17] J. Heywood, *Internal combustion engine fundamentals*. Mc Graw Hill, 1988. (Cited on pages 3, 22, 39, 40, 41, 50, 51, 64, 80 & 108).

[18] P. Richards, *Automotive Fuels Reference Book*. SAE International, 3rd ed., 2014. (Cited on page 3).

[19] "World Wide Fuel Charter," 2013. (Cited on page 3).

[20] J. Farrell, W. Weissman, and R. Johnston, "Fuel effects on SIDI efficiency and emissions," *SAE Technical Paper*, no. SAE2003-01-3186, 2003. (Cited on page 3).

[21] T. Rockstroh, V. Burger, A. Yates, and D. Smit, "Laminar Flame Speed Characterization of Synthetic Gasoline Components," *SAE International*, no. SAE2014-01-2616, 2014. (Cited on pages xii, xv, 4, 7, 28, 34, 35, 37, 147 & 148).

[22] A. Yates, V. Burger, and C. Viljoen, "A method for determining the laminar flame speed of jet fuels," *ASME*, 2012. (Cited on pages 7, 30, 33, 143, 144, 146 & 147).

[23] "Thermodynamic analysis software Tiger," 2014. (Cited on page 13).

[24] "GT-Power V7.5," 2014. (Cited on page 14).

[25] A. de Klerk, *Fischer-Tropsch Refining*. PhD thesis, University of Pretoria, 2008. (Cited on page 15).

[26] A. de Klerk, "Environmentally friendly refining: Fischer-Tropsch versus crude oil," *Green Chemistry*, vol. 9, no. 6, p. 560, 2007. (Cited on pages x, 16, 17, 18 & 19).

[27] J. G. Speight, *The Chemistry and Technology of Petroleum, Fourth Edition*. CRC Press, 2006. (Cited on page 17).

[28] P. M. Maitlis and A. de Klerk, eds., *Greener Fischer-Tropsch Processes for Fuels and Feedstocks*. John Wiley & Sons, 2013. (Cited on page 17).

[29] B. Kamara and J. Coetzee, "Overview of High-Temperature Fischer Tropsch Gasoline and Diesel Quality," *Energy & Fuels*, no. 2, pp. 2242–2247, 2009. (Cited on pages 17, 18, 19 & 20).

[30] P. C. Weinert and G. Egloff, "Catalytic polymerization and its commercial application," *Petroleum Processing*, vol. 3, 1948. (Cited on page 19).

[31] S. A. Tabak, F. J. Krambeck, and W. E. Garwood, "Conversion of propylene and butylene over ZSM-5 catalyst," *AIChE Journal*, vol. 32, pp. 1526–1531, Sept. 1986. (Cited on page 19).

[32] F. Nierlich, "Oligomerize for better gasoline," *Hydrocarbon processing*, vol. 71, no. 2, pp. 45–46, 1992. (Cited on page 19).

[33] S. Ozmen, H. Abrevaya, P. Barger, M. Bentham, and M. Kojima, "Skeletal isomerization of C4 and C5 olefins for increased ether production," *Fuel Reformulation*, vol. 3, no. 5, p. 54, 1993. (Cited on page 19).

[34] J. Duplan, P. Amigues, J. Verstraete, and C. Travers, "Kinetic Studies of the skeletal isomerization of npentenes over the ISO-5 Process Catalyst," in *Proceedings of the 5th Ethylene Producers Conference*, pp. 429–449, 1996. (Cited on page 19).

[35] F. M. Floyd, M. F. Gilbert, M. Perez, and E. Koehler, "Light naphtha isomerization," *Hydrocarbon Eng.*, vol. September, no. 42, 1998. (Cited on page 19).

[36] P. J. Kuchar, R. Gillespie, C. Gosling, W. Martin, and M. Cleveland, "Developments in isomerisation," *Hydrocarbon Eng.*, vol. March, no. 50, 1999. (Cited on page 19).

[37] P. Tamm, D. Mohr, and C. Wilson, "Octane enhancement by selective reforming of light paraffins," *Stud.Surf.Sci Catal*, vol. 38, no. 335, 1988. (Cited on page 19).

[38] T. Hughes, R. Jacobsen, and P. Tamm, "Catalytic processes for octane enhancement by increasing the aromatics content of gasoline," *Stud.Surf.Sci Catal*, vol. 38, no. 317, 1988. (Cited on page 19).

[39] R. Peer, R. Bennett, D. E. Felch, and E. von Schmidt, "UOP Platforming leading octane technology into the 1990's," *Catal Today*, vol. 18, no. 473, 1993. (Cited on page 19).

[40] "Standard Test Method for Hydrocarbon Types in Liquid Petroleum Products by Fluorescent Indicator Adsorption," 2013. (Cited on page 22).

[41] J. Farrell, R. Johnston, and I. Androulakis, "Molecular structure effects on laminar burning velocities at elevated temperature and pressure," *SAE Technical Paper*, no. SAE2004-01-2936, 2004. (Cited on pages 22, 29, 34, 37, 45 & 119).

[42] S. G. Davis and C. Law, "Determination of and Fuel Structure Effects on Laminar Flame Speeds of C 1 to C 8 Hydrocarbons," *Combustion Science and Technology*, vol. 140, pp. 427–449, Dec. 1998. (Cited on pages 22, 28, 29 & 37).

[43] R. Johnston and J. Farrell, "Laminar burning velocities and Markstein lengths of aromatics at elevated temperature and pressure," *Proceedings of the Combustion Institute*, vol. 30, pp. 217–224, Jan. 2005. (Cited on pages 22, 29 & 37).

[44] C. Viljoen, A. Yates, and R. Coetzer, "A Molecular Modelling Investigation of Selected Gasoline Molecules to Relate Oxidation Pathways to their Autoignition Behaviour," *SAE International*, no. SAE2007-01-0005, 2007. (Cited on page 22).

[45] C. L. Viljoen, A. D. B. Yates, A. Swarts, G. Balfour, and K. Möller, "An Investigation of the Ignition Delay Character of Different Fuel Components and an Assessment of Various Autoignition Modelling Approaches," *SAE International*, no. SAE2005-01-2084, 2005. (Cited on page 22).

[46] J. Beens, H. T. Feuerhelm, J.-C. Fröhling, J. Watt, and G. Schaatsbergen, "A comparison of ten different methods for the analysis of saturates, olefins, benzene, total aromatics, and oxygenates in finished gasolines.," *Journal of chromatographic science*, vol. 41, no. 10, pp. 564–9, 2003. (Cited on pages 23 & 27).

[47] "Standard Test Method for Bromine Numbers of Petroleum Distillates and Commercial Aliphatic Olefins by Electrometric Titration," 2012. (Cited on page 23).

[48] R. Bekker, "Personal communication (29 July 2014)," 2014. (Cited on pages 23, 24, 25 & 149).

[49] "Standard Test Method for Determination of Individual Components in Spark Ignition Engine Fuels by 100 Metre Capillary High Resolution Gas Chromatography," 2014. (Cited on page 23).

[50] R. van der Westhuizen, M. Ajam, P. De Coning, J. Beens, A. de Villiers, and P. Sandra, "Comprehensive two-dimensional gas chromatography for the analysis of synthetic and crude-derived jet fuels.," *Journal of chromatography. A*, vol. 1218, pp. 4478–86, July 2011. (Cited on page 25).

[51] T. Al-Mughanam, D. Bradley, M. Lawes, G. Sharpe, and N. Tripathi, "Laminar Burning Velocities and Markstein Lengths of Iso-Octane, n-Heptane, 1-Hexene, Toluene and Ethanol and their Binary, Tertiary and Quaternary Blends." University of Leeds Colloquium, 2012. (Cited on page 28).

[52] D. Bradley, R. Hicks, M. Lawes, C. G. W. Sheppard, and R. Woolley, "The measurement of laminar burning velocities and Markstein numbers for iso-octaneair and iso-octanen-heptaneair mixtures at elevated temperatures and pressures in an explosion bomb," *Combustion and Flame*, vol. 144, pp. 126–144, 1998. (Cited on pages 28 & 30).

[53] J. van Lipzig, E. Nilsson, L. de Goey, and A. Konnov, "Laminar burning velocities of n-heptane, iso-octane, ethanol and their binary and tertiary mixtures," *Fuel*, vol. 90, pp. 2773–2781, Aug. 2011. (Cited on pages xii, 28, 32, 33 & 38).

[54] M. Metghalchi and J. Keck, "Burning velocities of mixtures of air with methanol, isooctane, and indolene at high pressure and temperature," *Combustion and flame*, vol. 210, pp. 191–210, 1982. (Cited on page 28).

[55] C. Ji, E. Dames, Y. L. Wang, H. Wang, and F. N. Egolfopoulos, "Propagation and extinction of premixed C5C12 n-alkane flames," *Combustion and Flame*, vol. 157, pp. 277–287, Feb. 2010. (Cited on page 28).

[56] S. Jerzembeck, N. Peters, P. Pepiotdesjardins, and H. Pitsch, "Laminar burning velocities at high pressure for primary reference fuels and gasoline: Experimental and numerical investigation," *Combustion and Flame*, vol. 156, pp. 292–301, Feb. 2009. (Cited on pages 28 & 29).

[57] B. Galmiche, F. Halter, and F. Foucher, "Effects of high pressure, high temperature and dilution on laminar burning velocities and Markstein lengths of iso-octane/air mixtures," *Combustion and Flame*, vol. 159, pp. 3286–3299, Nov. 2012. (Cited on page 28).

[58] Z. Zhao, J. Conley, A. Kazakov, and F. Dryer, "Burning velocities of real gasoline fuel at 353 K and 500 K," *SAE Technical Paper*, no. SAE2003-01-3265, 2003. (Cited on pages 28, 29 & 33).

[59] L. Sileghem, V. Alekseev, J. Vancoillie, K. Van Geem, E. Nilsson, S. Verhelst, and A. Konnov, "Laminar burning velocity of gasoline and the gasoline surrogate components iso-octane, n-heptane and toluene," *Fuel*, vol. 112, pp. 355–365, Oct. 2013. (Cited on pages 28, 30 & 32).

[60] S. Jerzembeck and N. Peters, "Measurements of Laminar Flame Velocity and Markstein Length for Standard Gasoline and a Corresponding Reference Fuel Mixture (PRF87)," *SAE International*, no. SAE2007-01-2006, pp. 448–455, 2007. (Cited on pages 28, 29 & 33).

[61] W. J. Pitz, N. P. Cernansky, F. L. Dryer, F. N. Egolfopoulos, J. T. Farrell, D. G. Friend, and H. Pitsch, "Development of an Experimental Database and Chemical Kinetic Models for Surrogate Gasoline Fuels," *SAE International*, no. SAE2007-01-0175, 2007. (Cited on pages 29 & 64).

[62] S. Davis, H. Wang, K. Breinsky, and C. Law, "Laminar flame speeds and oxidation kinetics of benene-air and toluene-air flames," *Symposium (International) on Combustion*, vol. 26, pp. 1025–1033, Jan. 1996. (Cited on page 29).

[63] T. Hirasawa, C. Sung, A. Joshi, Z. Yang, H. Wang, and C. Law, "Determination of laminar flame speeds using digital particle image velocimetry: Binary Fuel blends of ethylene, n-Butane, and toluene," *Proceedings of the Combustion Institute*, vol. 29, pp. 1427–1434, Jan. 2002. (Cited on pages 29 & 30).

[64] C. Ji, E. Dames, H. Wang, and F. N. Egolfopoulos, "Propagation and extinction of benzene and alkylated benzene flames," *Combustion and Flame*, vol. 159, pp. 1070–1081, Mar. 2012. (Cited on page 29).

[65] S. Marshall, S. Taylor, C. Stone, T. Davies, and R. Cracknell, "Laminar burning velocity measurements of liquid fuels at elevated pressures and temperatures with combustion residuals," *Combustion and Flame*, vol. 158, pp. 1920–1932, Oct. 2011. (Cited on pages 29 & 147).

[66] G. Gibbs and H. Calcote, "Effect of Molecular Structure on Burning Velocity," *Journal of Chemical and Engineering Data*, vol. 4, no. 3, pp. 226–237, 1959. (Cited on page 29).

[67] G. Andrews and D. Bradley, "Determination of burning velocities: A critical review," *Combustion and Flame*, vol. 18, pp. 133–153, Feb. 1972. (Cited on page 29).

[68] C. Law, "Dynamics of stretched flames," *Symposium (International) on Combustion*, vol. 22, pp. 1381–1402, Jan. 1989. (Cited on page 29).

[69] A. Rallis, C, Garforth, "The determination of laminar burning velocity," *Prog. Energy Combust. Sci*, vol. 6, pp. 303–329, 1980. (Cited on page 29).

[70] Y. Di, Z. Huang, N. Zhang, B. Zheng, X. Wu, and Z. Zhang, "Measurement of Laminar Burning Velocities and Markstein Lengths for Diethyl EtherAir Mixtures at Different Initial Pressure and Temperature," *Energy & Fuels*, vol. 23, pp. 2490–2497, May 2009. (Cited on page 30).

[71] T. Kitagawa, "Effects of Pressure on Burning Velocity and Instabilities of Propane-Air Premixed Flames," *JSME International Journal Series B*, vol. 48, no. 1, pp. 2–8, 2005. (Cited on pages 30 & 143).

[72] B. Lewis and G. von Elbe, *Combustion, Flames and Explosions of Gases*. Academic Press Inc., 1987. (Cited on page 30).

[73] F. Wu, A. P. Kelley, C. Tang, D. Zhu, and C. K. Law, "Measurement and correlation of laminar flame speeds of CO and C2 hydrocarbons with hydrogen addition at atmospheric and elevated pressures," *International Journal of Hydrogen Energy*, vol. 36, pp. 13171–13180, Oct. 2011. (Cited on page 30).

[74] C. K. Law, *Combustion Physics*. Cambridge University Press, 2006. (Cited on pages 30, 34 & 36).

[75] C. Tang, Z. Huang, and C. Law, "Determination, correlation, and mechanistic interpretation of effects of hydrogen addition on laminar flame speeds of hydrocarbonair mixtures," *Proceedings of the Combustion Institute*, vol. 33, no. 1, pp. 921–928, 2011. (Cited on page 30).

[76] V. Yumlu, "Prediction of burning velocities of saturated carbon monoxide-air flames by application of mixing rules," *Combustion and Flame*, vol. 11, pp. 389–396, Oct. 1967. (Cited on page 30).

[77] D. Spalding, "A mixing rule for laminar flame speed," *Fuel*, no. 35, pp. 347–51, 1956. (Cited on page 30).

[78] D. Bradley, S.-D. Habik, and S. El-Sherif, "A generalization of laminar burning velocities and volumetric heat release rates," *Combustion and Flame*, vol. 87, pp. 336–345, Dec. 1991. (Cited on page 30).

[79] L. Sileghem, J. Vancoillie, J. Demuynck, J. Galle, and S. Verhelst, "Alternative Fuels for Spark-Ignition Engines: Mixing Rules for the Laminar Burning Velocity of GasolineAlcohol Blends," *Energy & Fuels*, vol. 26, pp. 4721–4727, Aug. 2012. (Cited on pages 30 & 105).

[80] Y. Huang, C. Sung, and J. Eng, "Laminar flame speeds of primary reference fuels and reformer gas mixtures," *Combustion and Flame*, vol. 139, pp. 239–251, Nov. 2004. (Cited on page 31).

[81] T. Hara and K. Tanoue, "Laminar Flame Speeds of Ethanol, n-Heptane and iso-Octane Air Mixtures," 2006. (Cited on pages xii, 31 & 32).

[82] F. Egolfopoulos, D. Du, and C. Law, "A study on ethanol oxidation kinetics in laminar premixed flames, flow reactors, and shock tubes," *Symposium (International) on Combustion*, vol. 24, pp. 833–841, Jan. 1992. (Cited on pages 31 & 33).

[83] J. Beeckmann, S. Kruse, and N. Peters, "Effect of ethanol and n-butanol on standard gasoline regarding laminar burning velocities," *SAE International*, no. SAE2010-01-1452, 2010. (Cited on pages 33 & 67).

[84] J. Beeckmann, O. Röhl, and N. Peters, "Numerical and experimental investigation of laminar burning velocities of iso-octane, ethanol and n-butanol," *SAE International*, vol. 4970, no. SAE2009-01-2784, 2009. (Cited on page 34).

[85] R. van Basshuysen, ed., *Gasoline Engine with Direct Injection: Processes, Systems, Development, Potential*. Vieweg+Teubner Verlag, 2009. (Cited on pages 39, 40 & 51).

[86] H. Zhao, ed., *Advanced Direct Injection Combustion Engine Technologies and Development: Gasoline and Gas Engines*. Elsevier, 2014. (Cited on pages 39, 40, 41, 42 & 51).

[87] M. Wirth, U. Mayerhofer, W. F. Piock, and G. K. Fraidl, "Turbocharging the DI Gasoline Engine," *SAE International*, no. SAE2000-01-0251, 2000. (Cited on page 40).

[88] A. Ranini and G. Monnier, "Turbocharging a gasoline direct injection engine," *SAE International*, no. SAE2001-01-0736, 2001. (Cited on page 40).

[89] W. Bandel, G. Fraidl, and P. Kapus, "The turbocharged GDI engine: boosted synergies for high fuel economy plus ultra-low emission," *SAE International*, no. SAE2006-01-1266, 2006. (Cited on page 40).

[90] V. Korte, N. Fraser, J. Taylor, and R. Dingelstadt, "Efficient Downsizing for Future Gasoline Engines," *MTZ*, pp. 42–49, May 2011. (Cited on page 40).

[91] C. Luttermann and W. Mährle, "BMW High Precision Fuel Injectionin Conjunction with Twin-Turbo Technology: a Combination for Maximum Dynamic and High Fuel Efficiency," *SAE International*, no. SAE2007-01-1560, 2007. (Cited on pages 40, 44 & 46).

[92] B. Lechner, G. Kiesgen, J. Kriese, and J. Schopp, "The new Mini engine with Twin Power Turbo," *MTZ worldwide*, pp. 36–43, July 2010. (Cited on page 40).

[93] M. Kerkau, S. Knirsch, and H.-J. Neuß er, "The New 6-Cylinder Biturbo Engine with Variable Turbine Geometry for the Porsche 911 Turbo," in *27th INTERNATIONAL VIENNA MOTOR SYMPOSIUM*, 2006. (Cited on page 40).

[94] F. Schumann, F. Sarikoc, S. Buri, H. Kubach, and U. Spicher, "Potential of spray-guided gasoline direct injection for reduction of fuel consumption and simultaneous compliance with stricter emissions regulations," *International Journal of Engine Research*, vol. 14, pp. 80–91, Aug. 2012. (Cited on pages 41, 44, 48 & 49).

[95] R. Golloch and G. Merker, "Requirements and characteristics of downsizing-concepts," in *9th EAEC International Congress*, (Paris), 2003. (Cited on page 41).

[96] J. Turner, A. Popplewell, R. Patel, T. Johnson, N. Darnton, S. Richardson, S. Bredda, R. Tudor, C. Bithell, R. Jackson, S. Remmert, R. Cracknell, J. Fernandes, A. Lewis, S. Akehurst, C. Brace, C. Copeland, R. Martinez-Botas, A. Romagnoli, and A. Burluka, "Ultra Boost for Economy: Extending the Limits of Extreme Engine Downsizing," *SAE International*, no. SAE2014-01-1185, 2014. (Cited on pages 41, 49 & 92).

[97] S. Martin, C. Beidl, and R. Mueller, "Responsiveness of a 30 Bar BMEP 3-Cylinder Engine: Opportunities and Limits of Turbocharged Downsizing," *SAE International*, no. SAE2014-01-1646, 2014. (Cited on pages 41 & 49).

[98] L. Cruff, M. Kaiser, S. Krause, and R. Harris, "EBDI-application of a fully flexible high BMEP downsized spark ignited engine," *SAE International*, no. SAE2010-01-0587, 2010. (Cited on page 41).

[99] A. Boretti, "Towards 40% efficiency with BMEP exceeding 30bar in directly injected, turbocharged, spark ignition ethanol engines," *Energy Conversion and Management*, vol. 57, pp. 154–166, May 2012. (Cited on page 41).

[100] Y. Otobe, O. Goto, H. Miyano, M. Kawamoto, A. Aoki, and T. Ogawa, "Honda Formula One Turbo-charged V-6 1.5L Engine," *SAE Technical Paper*, no. SAE890877, 1989. (Cited on page 41).

[101] A. Swarts, A. Yates, C. Viljoen, and R. Coetzer, "A further study of inconsistencies between autoignition and knock intensity in the cfr octane rating engine," *SAE International*, no. SAE2005-01-2081, 2005. (Cited on page 41).

[102] S. Curry, "A Three-Dimensional Study of Flame Propagation in a Spark Ignition Engine," *SAE International*, Jan. 1963. (Cited on page 41).

[103] U. Spicher, H. Kröger, and J. Ganser, "Detection of Knocking Combustion Using Simultaneously High-Speed Schlieren Cinematography and Multi Optical Fiber Technique," *SAE International*, no. SAE912312, 1991. (Cited on page 41).

[104] R. Nates and A. D. B. Yates, "Knock Damage Mechanisms in Spark-Ignition Engines," *SAE International*, no. SAE942064, 1994. (Cited on page 42).

[105] R. Nates, *Knock damage in spark-ignition engines*. Phd, University of Cape Town, 1995. (Cited on page 42).

[106] J. Fitton and R. Nates, "Knock Erosion in Spark-Ignition Engines," *SAE International*, no. SAE962102, 1996. (Cited on page 42).

[107] R. J. Nates, "Thermal Stresses Induced by Knocking Combustion in Spark-Ignition Engines," *SAE International*, no. SAE2000-01-1238, 2000. (Cited on page 42).

[108] G. König, R. R. Maly, D. Bradley, A. K. C. Lau, and C. G. W. Sheppard, "Role of Exothermic Centres on Knock Initiation and Knock Damage," *SAE International*, no. SAE902136, 1990. (Cited on page 42).

[109] M. Schreiber, A. S. Sakak, C. Poppe, J. F. Griffiths, P. Halford-Maw, and D. J. Rose, "Spatial Structure in End-Gas Autoignition," *SAE International*, no. SAE932758, 1993. (Cited on page 42).

[110] X. Gu, D. Emerson, and D. Bradley, "Modes of reaction front propagation from hot spots," *Combustion and Flame*, vol. 133, pp. 63–74, Apr. 2003. (Cited on page 42).

[111] M. Rothe, T. Heidenreich, U. Spicher, and A. Schubert, "Knock Behavior of SI-Engines: Thermodynamic Analysis of Knock Onset Locations and Knock Intensities," *SAE International*, no. SAE2006-01-0225, 2006. (Cited on page 42).

[112] J. Livengood and P. Wu, "Correlation of autoignition phenomena in internal combustion engines and rapid compression machines," in *Fifth Symposium (International) on Combustion, The Combustion Institute*, pp. 347–356, 1955. (Cited on page 42).

[113] A. D. B. Yates and C. L. Viljoen, "An Improved Empirical Model for Describing Auto-ignition," *SAE International*, no. SAE2008-01-1629, 2008. (Cited on page 43).

[114] R. B. GmbH, *Ottomotor-Management*. Wiesbaden: Vieweg+Teubner Verlag, 2003. (Cited on page 43).

[115] T. Wallner and S. A. Miers, "Combustion Behavior of Gasoline and Gasoline/Ethanol Blends in a Modern Direct-Injection 4-Cylinder Engine," *SAE International*, no. SAE2008-01-0077, 2008. (Cited on page 43).

[116] E. Kasseris and J. B. Heywood, "Charge Cooling Effects on Knock Limits in SI DI Engines Using Gasoline/Ethanol Blends: Part 2-Effective Octane Numbers," *SAE International*, no. SAE2012-01-1284, pp. 844–854, 2012. (Cited on pages 43 & 67).

[117] E. Kasseris and J. B. Heywood, "Charge Cooling Effects on Knock Limits in SI DI Engines Using Gasoline/Ethanol Blends: Part 1-Quantifying Charge Cooling," *SAE International*, no. SAE2012-01-1275, 2012. (Cited on pages 43 & 67).

[118] E. A. Rivera, N. Mastro, J. Zizelman, J. Kirwan, and R. Ooyama, "Development of Injector for the Direct Injection Homogeneous Market using Design for Six Sigma," *SAE International*, no. SAE2010-01-0594, 2010. (Cited on pages 44 & 46).

[119] G. Kalghatgi, "Fuel anti-knock quality-Part I. Engine studies," *SAE Technical Paper*, no. SAE2001-01-3584, 2001. (Cited on pages 44, 45, 55, 58, 59 & 64).

[120] V. Mittal and J. Heywood, "The relevance of fuel RON and MON to knock onset in modern SI engines," *SAE International*, no. SAE2008-01-2414, 2008. (Cited on pages 44, 45, 55, 58 & 59).

[121] A. Bell, "Modern SI engine control parameter responses and altitude effects with fuels of varying octane sensitivity," *SAE International*, no. SAE2010-01-1454, 2010. (Cited on page 44).

[122] C. N. Orlebar, A. Joedicke, and W. Studzinski, "The Effects of Octane , Sensitivity and K on the Performance and Fuel Economy of a Direct Injection Spark Ignition Vehicle," *SAE International*, no. SAE2014-01-1216, 2014. (Cited on page 44).

[123] T. Davies, R. Cracknell, G. Lovett, L. Cruff, and J. Fowler, "Fuel effects in a boosted DISI engine," *SAE International*, vol. 2020, no. SAE2011-01-1985, 2011. (Cited on page 44).

[124] S. Remmert, R. Cracknell, R. Head, A. Schuetze, A. Lewis, S. Akehurst, J. Turner, and A. Popplewell, "Octane Response in a Downsized, Highly Boosted Direct Injection Spark Ignition Engine," *SAE International*, no. SAE2014-01-1397, 2014. (Cited on page 44).

[125] V. Mittal, *A study of the physics and chemistry of knock in modern SI engines and their relationship to the octane tests*. PhD thesis, Massachussetts Institute of Technology, 2009. (Cited on page 44).

[126] G. T. Kalghatgi, K. Nakata, and K. Mogi, "Octane Appetite Studies in Direct Injection Spark Ignition (DISI) Engines," *SAE Technical Paper*, no. SAE2005-01-0244, 2005. (Cited on pages 45 & 58).

[127] J. Willand, M. Daniel, E. Montefrancesco, B. Geringer, P. Hofmann, and M. Kieberger, "Limits on downsizing in spark ignition engines due to pre-ignition," *MTZ worldwide*, vol. 70, pp. 56–61, May 2009. (Cited on page 45).

[128] C. Dahnz, K. Han, U. Spicher, and M. Magar, "Investigations on pre-ignition in highly supercharged SI engines," *SAE International*, no. SAE2010-01-0355, 2010. (Cited on pages 45 & 46).

[129] C. Dahnz and U. Spicher, "Irregular combustion in supercharged spark ignition engines pre-ignition and other phenomena," *International Journal of Engine Research*, vol. 11, pp. 485–498, Dec. 2010. (Cited on page 45).

[130] A. Zahdeh, P. Rothenberger, W. Nguyen, M. Anbarasu, S. Schmuck-Soldan, J. Schaefer, and T. Goebel, "Fundamental Approach to Investigate Pre-Ignition in Boosted SI Engines," *SAE International*, no. SAE2011-01-0340, 2011. (Cited on page 45).

[131] M. Amann, D. Mehta, and T. Alger, "Engine Operating Condition and Gasoline Fuel Composition Effects on Low-Speed Pre-Ignition in High-Performance Spark

Ignited Gasoline Engines," *SAE International*, vol. 4, no. SAE2011-01-0342, 2011. (Cited on page 45).

[132] M. Amann, T. Alger, B. Westmoreland, and A. Rothmaier, "The Effects of Piston Crevices and Injection Strategy on Low-Speed Pre-Ignition in Boosted SI Engines," *SAE International Journal of Engines*, vol. 5, no. SAE2012-01-1148, pp. 1216–1228, 2012. (Cited on page 45).

[133] K. Takeuchi, K. Fujimoto, S. Hirano, and M. Yamashita, "Investigation of Engine Oil Effect on Abnormal Combustion in Turbocharged Direct Injection - Spark Ignition Engines," *SAE International Journal of Fuels and Lubricants*, vol. 5, no. SAE2012-01-1615, pp. 1017–1024, 2012. (Cited on page 45).

[134] S. Dingle, A. Cairns, H. Zhao, and J. Williams, "Lubricant Induced Pre-Ignition in an Optical SI Engine," *SAE International*, no. SAE2014-01-1222, 2014. (Cited on page 45).

[135] O. Welling, N. Collings, J. Williams, and J. Moss, "Impact of Lubricant Composition on Low-speed Pre-Ignition," *SAE International*, no. SAE2014-01-1213, pp. 4–8, 2014. (Cited on page 45).

[136] M. Braisher, R. Stone, and P. Price, "Particle Number Emissions from a Range of European Vehicles," *SAE International*, no. SAE2010-01-0786, 2010. (Cited on page 46).

[137] M. S. Peckham, A. Finch, B. Campbell, P. Price, and M. T. Davies, "Study of Particle Number Emissions from a Turbocharged Gasoline Direct Injection (GDI) Engine Including Data from a Fast-Response Particle Size Spectrometer," *SAE International*, no. SAE2011-01-1224, 2011. (Cited on page 46).

[138] R. Lindgren, M. Skogsberg, H. k. Sandquist, and I. Denbratt, "The Influence of Injector Deposits on Mixture Formation in a DISC SI Engine," *SAE International*, no. SAE2003-01-1771, 2003. (Cited on page 46).

[139] Y. Takei, Y. Kinugasa, M. Okada, T. Tanaka, and Y. Fujimoto, "Fuel Property Requirement for Advanced Technology Engines," *SAE International*, no. SAE2000-01-2019, 2000. (Cited on page 46).

[140] F. Parsinejad and W. Biggs, "Direct Injection Spark Ignition Engine Deposit Analysis: Combustion Chamber and Intake Valve Deposits," *SAE International*, no. SAE2011-01-2110, 2011. (Cited on page 46).

[141] D. C. Arters, E. A. Bardasz, E. A. Schiferl, and D. W. Fisher, "A Comparison of Gasoline Direct Injection Part I - Fuel System Deposits and Vehicle Performance," *SAE International*, no. SAE1999-01-1498, 1999. (Cited on page 46).

[142] J. Taylor, N. Fraser, and P. Wieske, "Water cooled exhaust manifold and full load EGR technology applied to a downsized direct injection spark ignition engine," *SAE International*, vol. 3, no. SAE2010-01-0356, pp. 225–240, 2010. (Cited on page 47).

[143] B. Grandin, H.-E. Å ngström, P. Stå lhammar, and E. Olofsson, "Knock Suppression in a Turbocharged SI Engine by Using Cooled EGR," *SAE Technical Paper*, no. SAE982476, 1998. (Cited on page 47).

[144] B. Grandin and H.-E. Å ngström, "Replacing Fuel Enrichment in a Turbo Charged SI Engine: Lean Burn or Cooled EGR," *SAE Technical Paper*, no. SAE1999-01-3505, 1999. (Cited on page 47).

[145] T. Alger, T. Chauvet, and Z. Dimitrova, "Synergies between high EGR operation and GDI systems," *SAE International*, vol. 1, no. SAE2008-01-0134, 2008. (Cited on pages 47, 48 & 124).

[146] T. Alger and B. Mangold, "Dedicated EGR: A New Concept in High Efficiency Engines," *SAE International*, no. SAE2009-01-0694, 2009. (Cited on pages 47 & 124).

[147] D. Roth, R. Sauerstein, M. Becker, and R. Meilinger, "Application of Hybrid EGR Systems to Turbocharged GDI Engines," *MTZ*, pp. 12–17, Apr. 2010. (Cited on pages 47 & 48).

[148] S. Diana, V. Giglio, B. Iorio, and G. Police, "A Strategy to Improve the Efficiency of Stoichiometric Spark Ignition Engines," *SAE Technical Paper*, no. SAE961953, 1996. (Cited on page 47).

[149] A. Cairns, H. Blaxill, and G. Irlam, "Exhaust Gas Recirculation for Improved Part and Full Load Fuel Economy in a Turbocharged Gasoline Engine," *SAE International*, no. SAE2006-01-0047, 2006. (Cited on page 47).

[150] A. Cairns, N. Fraser, and H. Blaxill, "Pre Versus Post Compressor Supply of Cooled EGR for Full Load Fuel Economy in Turbocharged Gasoline Engines," *SAE International*, no. SAE2008-01-0425, 2008. (Cited on page 47).

[151] J. Turner, R. Pearson, R. Curtis, and B. Holland, "Effects of Cooled EGR Routing on a Second-Generation DISI Turbocharged Engine Employing an Integrated Exhaust Manifold," *SAE International*, no. SAE2009-01-1487, 2009. (Cited on page 47).

[152] Y. Kawabata, T. Sakonji, and T. Amano, "The Effect of NOx on Knock in Spark-ignition Engines," *SAE International*, no. SAE1999-01-0572, 1999. (Cited on page 47).

[153] O. Stenlåå s, A. Gogan, R. Egnell, B. Sundén, and F. Mauss, "The Influence of Nitric Oxide on the Occurrence of Autoignition in the End Gas of Spark Ignition Engines," *SAE International*, no. SAE2002-01-2699, 2002. (Cited on page 47).

[154] D. Takaki, H. Tsuchida, T. Kobara, M. Akagi, and T. Tsuyuki, "Study of an EGR System for Downsizing Turbocharged Gasoline Engine to Improve Fuel Economy Comparison of EGR Systems," *SAE International*, no. SAE2014-01-1199, 2014. (Cited on page 47).

[155] G. Bourhis, J. Chauvin, X. Gautrot, and L. de Francqueville, "LP EGR and IGR Compromise on a GDI Engine at Middle Load," *SAE International*, no. SAE2013-01-0256, 2013. (Cited on page 48).

[156] B. Kaul, R. Wagner, and J. Green, "Analysis of Cyclic Variability of Heat Release for High-EGR GDI Engine Operation with Observations on Implications for Effective Control," *SAE International*, no. SAE2013-01-0270, pp. 132–141, 2013. (Cited on page 48).

[157] T. Alger, J. Gingrich, C. Roberts, B. Mangold, and M. Sellnau, "A High-Energy Continuous Discharge Ignition System for Dilute Engine Applications," *SAE International*, no. SAE2013-01-1628, 2013. (Cited on page 48).

[158] G. Ruan, D. Kienzle, D. Roth, and M. Becker, "Dual coil ignition for gasoline EGR engines," *MTZ*, pp. 18–21, Mar. 2013. (Cited on page 48).

[159] J. Wheeler, D. Polovina, S. Ramanathan, K. Roth, D. Manning, and J. Stein, "Increasing EGR Tolerance using High Tumble in a Modern GTDI Engine for Improved Low-Speed Performance," *SAE International*, no. SAE2013-01-1123, 2013. (Cited on page 48).

[160] F. Wu, A. Kelley, D. Zhu, and C. Law, "Further Study on Effects of Hydrogen Addition on Laminar Flame Speeds of Fuel-Air Mixtures," *7th US National Combustion Meeting Organized by the Eastern States Section of the Combustion Institute and Hosted by the Georgia Institute of Technology, Atlanta, GA*, pp. 8–23, 2011. (Cited on page 48).

[161] T. Alger, J. Gingrich, and B. Mangold, "The Effect of Hydrogen Enrichment on EGR Tolerance in Spark Ignited Engines Reprinted From : SI Combustion," *SAE Technical Paper*, no. SAE2007-01-0475, 2007. (Cited on pages 48 & 56).

[162] D. Fennell, J. M. Herreros, A. Tsolakis, H. Xu, K. Cockle, and P. Millington, "GDI Engine Performance and Emissions with Reformed Exhaust Gas Recirculation (REGR)," *SAE International*, no. SAE2013-01-0537, 2013. (Cited on page 48).

[163] J. Taylor, H. Marlok, J. Hall, and M. Warth, "Analysis of real world driving with an extreme downsizing engine," *MTZ*, pp. 24–31, May 2013. (Cited on page 49).

[164] H. Zellbeck, T. Ross, and C. Guhr, "The Turbocharged Direct-Injection Petrol Engine A Consistent Solution for Reducing CO 2 Emission," *MTZ*, vol. 68, 2007. (Cited on page 49).

[165] J. Gindele, T. Ramsteiner, J. Fischer, and B. Tschamon, "The new 2.0-L high-performance four-cylinder engine from Mercedes-AMG," *MTZ worldwide*, 2013. (Cited on page 49).

[166] A. Kneifel, S. Buri, A. Velji, U. Spicher, J. Pape, and M. Sens, "Investigations on Supercharging Stratified Part Load in a Spray-Guided DI SI Engine," *SAE International*, no. SAE2008-01-0143, 2008. (Cited on page 49).

[167] O. Lang, K. Habermann, K. Krebber-Hortmann, A. Sehr, M. Thewes, H. Kleeberg, and D. Tomazic, "Potential of the Spray-guided Combustion System in Combination with Turbocharging," *SAE International*, no. SAE2008-01-0139, 2008. (Cited on page 49).

[168] S. Buri, H. Kubach, and U. Spicher, "Effects of increased injection pressures of up to 1000bar opportunities in stratified operation in a direct-injection spark-ignition engine," *International Journal of Engine Research*, vol. 11, pp. 473–484, Dec. 2010. (Cited on page 49).

[169] C. Chadwell, T. Alger, J. Zuehl, and R. Gukelberger, "A Demonstration of Dedicated EGR on a 2.0 L GDI Engine," *SAE International*, no. SAE2014-01-1190, 2014. (Cited on page 50).

[170] A. L. GmbH, *Engine Indicating User Handbook*. AVL List GmbH, 2002. (Cited on pages 51, 52 & 54).

[171] A. Randolph, "Methods of processing cylinder-pressure transducer signals to maximize data accuracy," *SAE Technical Paper*, no. SAE900170, 1990. (Cited on pages 51 & 52).

[172] M. Brunt and C. Pond, "Evaluation of techniques for absolute cylinder pressure correction," *SAE Technical Paper*, no. SAE970036, 1997. (Cited on page 52).

[173] A. Randolph, "Cylinder-Pressure-Based Combustion Analysis in Race Engines," *SAE Technical Paper*, no. SAE942487, 1994. (Cited on page 52).

[174] H. S. Rai, M. F. Brunt, and C. P. Loader, "Quantification and Reduction of IMEP Errors Resulting from Pressure Transducer Thermal Shock in an S.I. Engine," *SAE International*, no. SAE1999-01-1329, 1999. (Cited on page 52).

[175] AVL List GmbH, "Data Sheet GU22C Pressure Sensor." 2011. (Cited on page 52).

[176] R. Stone, *Introduction to internal combustion engines*. Society of Automotive Engineers Inc, 3 ed., 1999. (Cited on pages 52 & 53).

[177] M. Brunt and A. Emtage, "Evaluation of IMEP routines and analysis errors," *SAE Technical Paper*, no. SAE960609, 1996. (Cited on page 53).

[178] C. A. Amann, "Cylinder-Pressure measurement and Its Use in Engine Research," *SAE International*, no. SAE852067, 1985. (Cited on page 53).

[179] M. Brunt, H. Rai, and A. Emtage, "The calculation of heat release energy from engine cylinder pressure data," *SAE International*, no. SAE981052, 1998. (Cited on page 53).

[180] G. M. Rassweiler and L. Withrow, "Motion Pictures of Engine Flames Correlated with Pressure Cards," *SAE International*, no. SAE380139, 1938. (Cited on page 53).

[181] M. Brunt and A. Emtage, "Evaluation of burn rate routines and analysis errors," *SAE Technical Paper*, no. SAE970037, 1997. (Cited on page 53).

[182] G. T. Kalghatgi, *Fuel/Engine Interactions*. SAE International, 2013. (Cited on pages 58 & 59).

[183] A. Amer, H. Babiker, J. Chang, G. Kalghatgi, P. Adomeit, A. Brassat, and M. Günther, "Fuel Effects on Knock in a Highly Boosted Direct Injection Spark Ignition Engine," *SAE International*, no. SAE2012-01-1634, pp. 1048–1065, 2012. (Cited on pages 58, 60 & 64).

[184] D. Turner, H. Xu, R. F. Cracknell, V. Natarajan, and X. Chen, "Combustion performance of bio-ethanol at various blend ratios in a gasoline direct injection engine," *Fuel*, vol. 90, pp. 1999–2006, May 2011. (Cited on pages 92 & 100).

[185] J. E. Anderson, U. Kramer, S. a. Mueller, and T. J. Wallington, "Octane Numbers of Ethanol and MethanolGasoline Blends Estimated from Molar Concentrations," *Energy & Fuels*, vol. 24, pp. 6576–6585, Dec. 2010. (Cited on page 96).

[186] J. E. Anderson, T. G. Leone, M. H. Shelby, T. J. Wallington, J. J. Bizub, M. Foster, M. G. Lynskey, and D. Polovina, "Octane Numbers of Ethanol-Gasoline Blends: Measurements and Novel Estimation Method from Molar Composition," *SAE International*, no. SAE2012-01-1274, 2012. (Cited on page 96).

[187] KBC Advanced Technolgies, "Petrofine Physical Properties Manual," 1999. (Cited on page 96).

[188] M. Grill, A. Schmid, M. Chiodi, H. Berner, and M. Bargende, "Calculating the properties of user-defined working fluids for real working-process simulations," *SAE Technical Paper*, no. SAE2007-01-0936, pp. 776–790, 2007. (Cited on page 99).

[189] M. Bargende, *Ein Gleichungsansatz zur Berechnung der instationaeren Wandwaermeverluste im Hochdruckteil von Ottomotoren.* PhD thesis, TU Darmstadt, 1991. (Cited on page 99).

[190] J. Serras-Pereira, P. G. Aleiferis, and D. Richardson, "An Analysis of the Combustion Behavior of Ethanol, Butanol, Iso -Octane, Gasoline, and Methane in a Direct-Injection Spark-Ignition Research Engine," *Combustion Science and Technology*, vol. 185, pp. 484–513, Feb. 2013. (Cited on page 100).

[191] P. Aleiferis, J. Serras-Pereira, and D. Richardson, "Characterisation of flame development with ethanol, butanol, iso-octane, gasoline and methane in a direct-injection spark-ignition engine," *Fuel*, vol. 109, pp. 256–278, July 2013. (Cited on page 100).

[192] E. P. Kasseris, *Knock Limits in Spark Ignited Direct Injected Engines Using Gasoline / Ethanol Blends by.* Phd, Massachusetts Institute of Technology, 2011. (Cited on pages 107 & 108).

[193] R. A. Strehlow, *Fundamentals of Combustion.* R. E. Krieger Publishing Company, 1979. (Cited on page 144).

[194] K. E. Far, F. Parsinejad, and H. Metghalchi, "Flame structure and laminar burning speeds of JP-8/air premixed mixtures at high temperatures and pressures," *Fuel*, vol. 89, pp. 1041–1049, May 2010. (Cited on page 145).

[195] K. Kar, T. Last, C. Haywood, and R. Raine, "Measurement of Vapor Pressures and Enthalpies of Vaporization of Gasoline and Ethanol Blends and Their Effects on Mixture Preparation in an SI Engine," *SAE International Journal of Fuels and Lubricants*, no. SAE2008-01-0317, 2008. (Cited on pages 157 & 159).

Appendix A

Laminar flame speed calculation methodology

A short summary of the simplified approach used in analyzing the spherical flame, as described by Yates et. al. [22], will be provided here.

For this method the flame thickness is considered to be negligibly thin with a step change in temperature from the burned to the unburned zone [71]. A more detailed approach is generally used in the case of optical combustion analysis methods, such as Schlieren technique, where the flame front is defined as having a finite thickness. In order to define the burned and unburned gas properties, the exact fuel composition needs to be known [22]. As these properties can only be estimated for commercial fuel products, the simplification for the pressure-based method was found to be both adequate and suitable. The calculation technique can be summarised as follows.

Assuming isentropic compression of the unburned gas for the one-step combustion analysis, the effective spherical flame radius, r_b can be derived in terms of the pressure, p as:

$$\frac{r_b}{r_o} = \left[1 - \left(\frac{p_i}{p}\right)^{\frac{1}{\gamma}} \frac{p_f - p}{p_f - p_i}\right]^{\frac{1}{3}} \tag{A.1}$$

r_o is the equivalent radius of the total gas-volume of the combustion chamber with due consideration for the access ports and spark plug electrodes. p_i and p_f are the initial and final bomb pressures respectively. Gamma, γ, is the ratio of the specific heats of the unburned mixture at constant pressure and constant volume. As the combustion radius approaches the chamber wall, heat loss results in the maximum pressure being slightly lower than the theoretical final pressure. The maximum pressure was determined

from chemical equilibrium calculations using single component fuels and a 5% offset was applied to account for the shortfall in the experimentally obtained pressure signal [22].

When considering the gas motion due to the flame expansion, the burning velocity,u_n, can be derived as follows [193]:

$$u_n = \frac{r_o}{3(p_f - p_i)} \left(\frac{p_i}{p}\right)^{\frac{1}{\gamma}} \left[1 - (\frac{p_i}{p})^{\frac{1}{\gamma}} \frac{p_f - p}{p_f - p_i}\right]^{-\frac{2}{3}} \frac{dp}{dt} \tag{A.2}$$

Determination of the value of γ

For an unknown fuel composition, the ratio of specific heats can be estimated using the following energy equation:

$$m_{Fuel} Q_c \eta_c = m_{Mix} cv_{Mix} (T_{Mix} - T_i) \tag{A.3}$$

m_{Fuel} is the mass of the fuel while m_{Mix} is that of the air-fuel mixture. Q_c is the lower enthalpy of stoichiometric combustion and η_c is the combustion efficiency. cv_{Mix} and T_{Mix} are the specific heat and temperature of the mixture respectively with T_i being the initial bomb temperature. The fuel mass can be expressed in terms of the air mass, m_{Air}, and the equivalence ratio, ϕ, together with the stoichiometric fuel/air ratio,F_{Stoich}. Using the ideal gas law, the temperature may be expressed in terms of the bomb volume, V and the specific mixture gas constant R_{Mix}:

$$\phi F_{Stoich} m_{Air} Q_c \eta_c = m_{Mix} cv_{Mix} \left(\frac{p_f v}{m_{Mix} R_{Mix}} - \frac{p_i v}{m_{Mix} R_{Mix}}\right) \tag{A.4}$$

Rearranged this becomes:

$$\frac{c_v}{R}|Mix = \frac{\phi F_{Stoich} m_{Air} Q_c \eta_c}{v(p_f - p_i)} \tag{A.5}$$

Using the ideal gas relationship the air mass can be expressed in terms of the initial conditions:

$$\frac{c_v}{R}|Mix = \frac{\phi F_{Stoich} Q_c \eta_c}{T_i R_{Air}} \left(\frac{p_i}{p_f - p_i}\right) \tag{A.6}$$

The average value of γ for the mixture can then be obtained from the definition:

$$\gamma = \frac{c_p}{c_v} = \frac{R + c_v}{c_v} = 1 + \frac{R}{c_v} \tag{A.7}$$

Flame stretch effect

Due to the fact that the preheating and reaction zones of the flame have a finite thickness in reality, this results in the burning process being affected by the curvature of the flame and the aerodynamic strain. For the present analysis it was adequate to only consider the total stretch influence. The distinction between the un-stretched laminar burning velocity, u_l, and the stretched one, u_n, is approximately proportional to the normalized rate of change of flame area, A.

$$u_l - u_n = L\frac{1}{A}\frac{dA}{dt} \tag{A.8}$$

The Markstein length, L, is defined as the constant of proportionality. In the case of a spherical flame, the normalized rate of change of area can be expressed in terms of the flame radius, which then results in:

$$u_n = u_l - \frac{2L}{r_b}\frac{dr_b}{dt} \tag{A.9}$$

This relationship between stretched and un-stretched laminar flame speed was used for the data analysis and will be explained in more detail later. Assuming isobaric conditions at each increment, the flame speed calculation was performed stepwise through the changing pressure temperature domain and the results were corrected to reference pressure and temperature conditions as illustrated in the following section.

Effect of pressure and temperature and air-fuel ratio

Since a pressure based analysis method was used it was crucial to include the effects of pressure and temperature on flame velocity in the analysis. Far et. al. suggested the following power law correlation [194]:

$$u_l = u_{l,o}(1 + a_1(1-\phi) + a_2(1-\phi)^2)\left(\frac{T_u}{T_{u,o}}\right)^{\alpha}\left(\frac{p}{p_o}\right)^{\beta} \tag{A.10}$$

Where $T_{u,0}$ and p_o allude to a reference condition at which u_l is calculated and a1 and a2 are empirical constants. This implicit parabolic form of the laminar flame velocity with regard to air-fuel equivalence ratio can be expressed as:

$$u_l = u_{l,Max,o}(1 + a(\phi_M - \phi)^2)\left(\frac{T_u}{T_{u,o}}\right)^{\alpha}\left(\frac{p}{p_o}\right)^{\beta} \tag{A.11}$$

Where ϕ_M is the equivalence ratio that corresponds to the maximum laminar flame velocity at the reference conditions, $u_{l,MAX,0}$. The value of ϕ_M typically is in the range

from 1.1 to 1.2 for gasoline. The temperature exponent α and the pressure exponent β are themselves functions of equivalence ratio and therefore provision was made for a linear dependence as follows [22]:

$$\alpha = \alpha_{Stoich} + \alpha_1(\phi - 1) \tag{A.12}$$

$$\beta = \beta_{Stoich} + \beta_1(\phi - 1) \tag{A.13}$$

Using the regression analysis, these coefficients were defined as described in the next section.

Data Analysis

The laminar flame speed was defined from pressure data recorded at a rate which provided about 90 data points from start of ignition to the peak pressure in the combustion bomb. Using the isentropic compression relationship the unburned gas temperature was calculated at each point:

$$T_u = T_{u,i}\left(\frac{P}{P_i}\right)^{\frac{\gamma-1}{\gamma}} \tag{A.14}$$

Using equation A.1, the flame radius was calculated at each point . By differentiating the pressure data with respect to time, the stretched laminar flame velocity at each point was calculated using equation A.2. The theoretical stretched laminar flame velocity was then determined at each experimental point using equations A.6 to A.11. To start the regression analysis, approximate values for the un-stretched laminar flame speed, the Markstein length, and all the parametric constants involved in the correction for pressure and temperature and air-fuel ratio were assumed.

The theoretical, stretched laminar flame velocity, $u_{n,TH}$, should ideally be equal to the experimentally calculated velocity, $u_{n,EXP}$ and the regression error analysis could then be used to improve the assumed values towards their final, optimal fit value. Isentropic compression of the unburned gas resulted in covariance of temperature and pressure for a given pressure trace. Combustion bomb data with different starting temperatures was therefore needed to calculate the α and β coefficients for the temperature and pressure.

Data for a variety of air-fuel ratios was furthermore required to define the influence on laminar flame speed and the pressure and temperature coefficients. Equation A.9 reveals that the Markstein length effect on the stretched laminar flame speed corresponds to the flame radius. Due to the non-linear inverse relationship between the pressure and flame

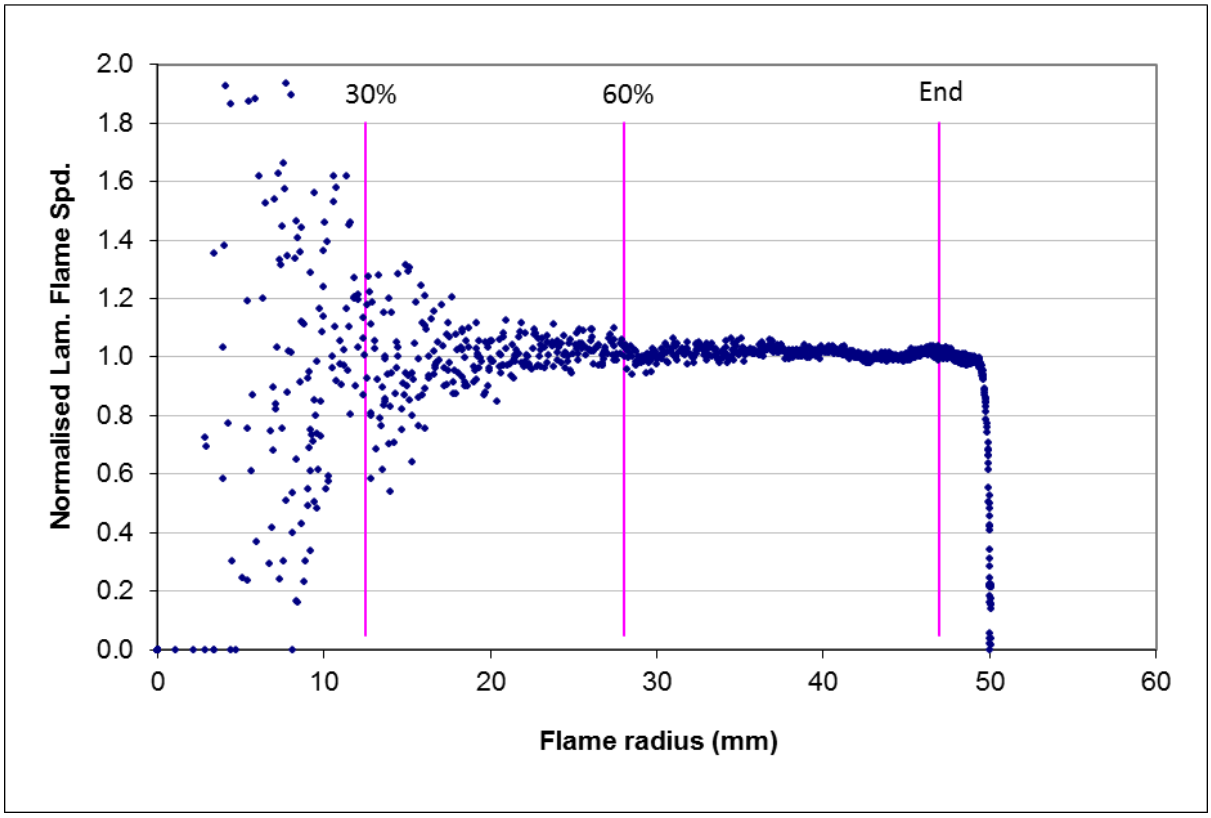

Figure A.1: *Ratio of uEXP/uTH of 95 RON crude pump fuel at ϕ=1 [21]*

stretch, the regression error was split into two sections according to the flame radius being below or above about 60% as shown in figure A.1 and figure A.2. Additionally a weighting factor was applied.

The solving process was further simplified by reducing the number of degrees of freedom, resulting in the Markstein length being parameterized to include fuel specific constants [22]. Furthermore it was found that a single, common set of temperature and pressure coefficients could be used for various fuels as long as they were pure hydrocarbon blends with similar carbon number lengths. The poor resolution of the pressure signal at small flame radii, shown by the large amount of scatter in the 30% to 60% range in figure A.1 and figure A.2, is a weakness of the pressure method. This makes accurate prediction of the Markstein length challenging and resulted in no useful information being deduced from the data. Marshall et. al. argued that their error due to stretch was low enough to warrant the exclusion of stretch correction as a result of the difficulties involved in accurately determining the Markstein length [65]. Poor signal to noise ratio at a flame radius below about 30%, resulted in this data to be discarded. Similarly when the flame front reached the combustion bomb wall, this resulted in considerable heat loss, and therefore in a sudden decrease in the calculated flame speed. As shown by the hairline in figure A.1, this resulted in the end of the meaningful and useable data. By making use of a relatively small bomb diameter, flame instability in the form of cellularity was

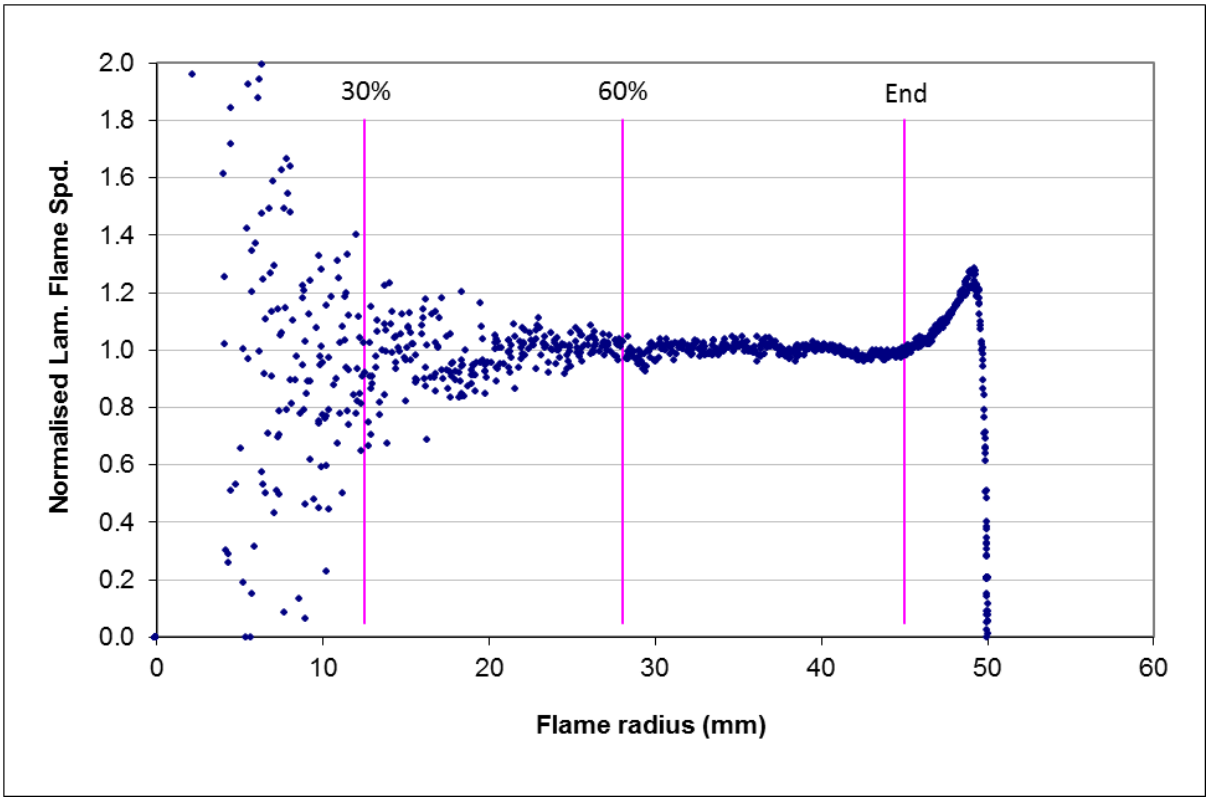

Figure A.2: *Ratio of uEXP/uTH of 95 RON crude pump fuel at ϕ=1.2 [21]*

minimized. The onset of flame instability for rich air fuel mixtures, manifested itself in a spontaneous increase in the experimental stretched laminar flame velocity. This increased velocity resulted in a deviation from the ratio value of one since it was not simulated in the theoretical flame speed value. A conservative approach was taken to manually inspect and remove the affected areas believed to be cellular as indicated by the hairline in figure A.2.

Appendix B

Analytical fuel analysis methods

Details surrounding the chemical analysis methods used at Sasol's analytical chemistry laboratory. The information was gathered from an internal memorandum at Sasol [48].

B.1 SFC

The equipment used for this investigation was a Selerity Series 4000 SFC system equipped with SFC pump, autosampler, SFC oven and a flame ionization detector operated at a temperature of 400 °C. To allow optimal separation of the groups (saturates, unsaturates, aromatics and oxygenates) on the SFC, a known variety of standards characteristic of HTFT light oil were used. Three analytical columns were used for the group type separation. A PVA-Silica column retained the oxygenates and a Petrosil column was utilised to separate the aromatics from the unsaturated components. The latter were retained by a PetroAG silver-loaded cation exchange column.

Furthermore the SFC oven is equipped with two six-port two-position switching valves that enables forward and reverse-flushing of the analytical columns. The silver-loaded cation exchange column was employed in a secondary column oven at a constant temperature of 140 °C which enabled more rapid clearance of the olefins and other unsaturated components through the column. The SFC mobile phase (carbon dioxide) was supplied at a constant pressure of 200 atm with an injection volume of 0.1 μl while the analysis temperature of 40 °C was maintained throughout.

It has been found that light carbonyls, esters and ethers are not retained effectively on the PVA-Silica column. Additionally the selectivity of the PVA-Silica column is geared towards alcohols resulting in the less polar carbonyls and esters to not be retained efficiently thereby proceeding to elude with the olefin fraction. However the separation

between olefins and aromatics is critical and alkylbenzenes with long non-polar alkyl chains may therefore overlap with alkylbenzenes and polar olefinic compounds.

B.2 NMR

A Bruker 500MHz spectrometer equipped with a 5mm QNP probe was used to collect ^{1}H NMR sprectra at an interval of 16 scans per sample. An exact amount of benzene and the sample were dissolved in deuterated chloroform.

The component classes in gasoline samples can be separated to a large degree by comprehensive chromatography, however it is often not possible to separate unsaturated classes such as olefins and napththenes completely. Due to the resulting overlap and the similarities in the mass spectrometry (MS) data of these classes, accurate identification and quantification is not possible. For complex samples it is frequently necessary to implement a combination of techniques to enable identification and NMR can aid to differentiate between the olefin classes of gasoline samples as shown in figure B.1. NMR can generally be used to distinguish between cis- and trans-isomers of single olefinic compounds. However for complex samples it is not possible to use coupling constants and therefore this differentiation is not possible. This lead to an investigation at Sasol's chemical laboratory to identify these classes in the NMR spectrum of gasoline samples.

The ^{1}H NMR sprectra of the samples containing olefins are characterized with a resonance between 6 and 4.5 ppm which can be ascribed to double bond protons with the remaining aliphatic protons resonating between 3 and 0.5 ppm while the aromatic protons resonate between 7.0 and 8.0 ppm.

Simulation results from ACD HNMR predictor established that α-olefins could be expected between 6 and 5.5 ppm and 5.3 and 4.9 ppm, vinylidenes between 5 and 4.5 ppm,

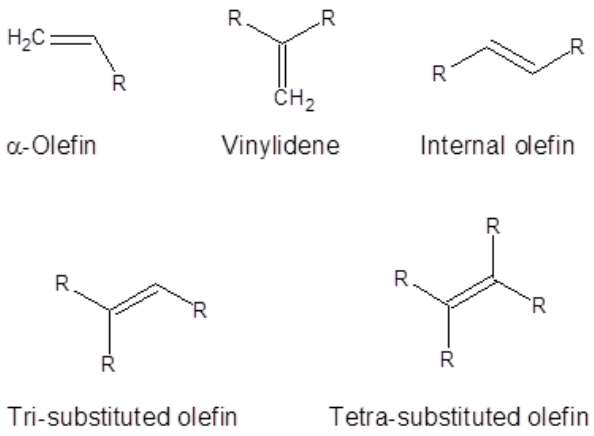

Figure B.1: *Olefin classes investigated*

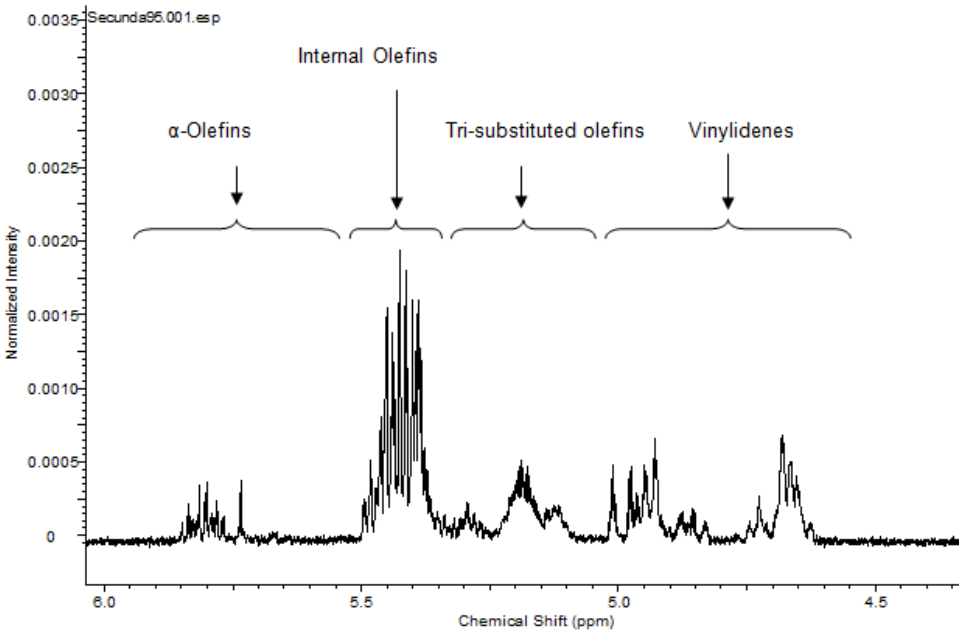

Figure B.2: *NMR spectra of synthetic gasoline corresponding to simulation results*

internal olefins between 5.7 and 4.9 ppm and tri-substituted olefins between 5.3 and 4.7 ppm. These zones could therefore be used for quantification of olefins in the 1H NMR spectra. It was noted during the simulations that branching in the carbon chain tends to widen the region in which a molecule from a certain class can be expected to resonate.

It was found that the olefinic region of the ^{1}H NMR sprectra included various groups of peaks that were similar for a range of samples. This section was therefore divided into groups that approximately correlate with the simulation results as shown in figure B.2. The identified peaks correspond to a single class of olefin as shown by the regions and their identifiers. Quaternary or fully- substituted olefins do not contain any olefinic protons and are therefore not detected.

By using benzene as an internal standard the concentration of the individual olefin classes can be calculated according to the relationship described in the following equation:

$$mass(O) = (\frac{I(O) * mole(benzene) * 6}{I(benzene) * n(O)}) * Mr(AO) \tag{B.1}$$

where:

mass(O) is the amount of the olefin in the sample
I(O) is the integral value of the relevant range
I(benzene) is the integral of the added benzene
mole(benzene) is the mole amount of benzene added
n(O) is the number of olefinic protons associated with the olefin class
Mr(AO) is the average molecular weight of the olefins in the sample

The correlation between the benzene and relevant olefin integral is equal to the amount of benzene protons relative to the olefin protons in the sample. If the molecular mass of the olefin is known their respective mass can be calculated. In petrol samples combinations of olefins with different chain lengths are found, which necessitated the determination of the average carbon number of the olefins from the available GCxGC data. Following this, the mass ratio of the various olefin classes could be determined by dividing the mass of the class with the mass of the sample added to the solution. Due to the fact that fully-substituted olefins could not be detected through ^{1}H NMR, it was determined by subtracting the sum of the calculated olefin classes from the total olefin content as ascertained by GC or SFC analysis.

The accuracy of the NMR method was evaluated by preparing a sample with known concentrations of seven compounds and then calculating the mass fractions of each component. The results shown in table B.1 indicated that the method was valid.

Olefin class	**Standard sample**	**Calculated amount**
α-olefins	25%	24%
Internal olefins	0%	0.4%
Tri-substituted olefins	37.5%	38.2%
Vinylidenes	12.5%	13%
Fully-substituted olefins	25%	24.4%

Table B.1: *Comparison of known and calculated olefin class content of a standard sample*

B.3 GCxGC

The primary chromatography run of two dimensional GC is employed to separate the sample using the first adsorbant material and carrier gas which results in an initial separation according to a desired characteristic. In order to separate according to another characteristic, these components are subsequently run separately through a second column with a different adsorbant and carrier gas.

The two columns are coupled by an interface or modulator which periodically samples a small fractions of eluent from the first column and passes it through the second column where the analysis is completed before the following sample is received. The sampling process ensures that the separation in the first dimension is maintained and that all components in the sample are exposed to both separation dimensions. The first dimension peak is generally sampled at least three times and the modulation period is synchronised with the separation time in the second column.

The large increase in peak capacity over conventional GC leading to an improvement in separation power, is the primary advantage of GCxGC. For a single GC column a few hundred peaks can theoretically be separated while for GCxGC the peak capacity is the product of two columns of different selectivities leading to tens of thousands. Due to the very fast separation occurring in the second dimension column, broadening of the peak signal is minimised which in essence improves the signal to noise ratio and in so doing the sensitivity by a factor of up to ten times compared to conventional 1D-GC.

Appendix C

Combined fuel analysis results

Test Fuel	**Density (kg/m^3)[a]**	**Molar mass (g/mol)**	**A/F[b]**	**HHV (MJ/kg)[c]**	**LHV (MJ/kg)[c]**	**ΔH_{vap} (kJ/kg)[d]**	**RON[e]**	**MON[e]**	**RVP (kPa)[f]**	**Boiling range (°C)[g]**
SGBC A	719.7	105.9	14.82	46.2	43.0	212.87	84.1	82.2	40	41.3 – 179.8
SGBC B	718.5	99.4	14.78	46.5	43.4	201.66	97.6	82.4	42	37.7 – 168.2
SGBC C	788.1	104.1	14.37	44.49	41.9	224.72	93.2	84.1	52	32.1 – 195.8
SGBC D	797.4	112.9	14.36	44.23	41.7	*NA*	76.8	70.5	25	54.6 – 203.6
SGBC E	801.5	95.01	13.94	43.4	41.1	270.92	98.4	86.1	29	54 – 208
SGBC F	649.2	70	14.78	46.6	43.5	361.72	92.5	78	115	29.4 – 49.8
TAME	769.5	102.1	12.18	39.3	36.4	249.40	112	98	19	80.7 – 91.9
Ethanol	794	46.1	9	29.7	27.0	677.02	109	90	20	78
Synthetic RON95 CAG	747.4	100.9	14.15	44.73	41.8	246.36	95.5	85.7	64	30.4 – 190.2
Crude RON95 CAG	753.6	98.5	14.47	45.14	42.3	243.87	95.1	85.2	59	31.1 – 194.2
Crude RON93 CAG	745.1	98.7	14.58	45.33	42.5	261.29	93.2	83.6	58	32.5 – 207.7

[a]ASTM D4052-11
[b]Stoichiometric Air/Fuel ratio
[c]ASTM D4809
[d]Calculated from vapor pressure data
[e]ASTM D2699-13b/ASTM D2700-14
[f]ASTM D323-08(2014)
[g]ASTM D86-12

Table C.1: *Fuel properties of commercial test fuels and synthetic gasoline blending components*

Test Fuel	**C/H ratio**	**Linear paraffins**	**Iso-paraffins**	**Cyclic-paraffins**	**α-olefins**	**Internal olefins**	**Branched olefins**	**Other olefins**	**Aromat-ics**	**Other**
SGBC A	0.494	12.5	61.4	5.1	0	0	0	0	19	0
SGBC B	0.5	0.3	0	6.2	0	4.8	28	60.4	0.3	0
SGBC C	0.586	21.2	19.6	0	0	0	0	0	60.5	0
SGBC D	0.588	19	11.6	9.2	0	0	0	0	57.7	0.2
SGBC E	0.703	11	3.3	0	2.1	1.2	2.8	9.3	70.7	0
SGBC F	0.5	21.2	8.1	0	21.7	43.6	5.5	0	0	0
TAME	0.428	*NA*	*NA*	*NA*	*NA*	*NA*	*NA*	*NA*	*NA*	*NA*
Ethanol	0.4	*NA*	*NA*	*NA*	*NA*	*NA*	*NA*	*NA*	*NA*	*NA*
Synthetic RON95 CAG	0.523	18.6	17.7	7.4	0	2.1	3	5.8	28.9	14.7
Crude RON95 CAG	0.561	26.8	13	5.1	0	0.1	0.3	11.6	43.17	0
Crude RON93 CAG	0.539	31.6	15.6	0	0	1.9	3.5	9.5	37.1	4.8

Table C.2: *Chemical fuel properties of commercial test fuels and synthetic gasoline blending components*

Test Fuel	**Density (kg/m^3)**[a]	**Molar mass (g/mol)**	**A/F**[b]	**HHV (MJ/kg)**[c]	**LHV (MJ/kg)**[c]	**ΔH_{vap} (kJ/kg)**[d]	**RON**[e]	**MON**[e]	**RVP (kPa)**[f]	**Boiling range (°C)**[g]
SBA20	732	101.8	14.28	45.0	42.0	241.7	94.1	84.7	59	32.8 – 180.9
SBB20	732.6	100.6	14.28	45.1	42.1	240.6	97.1	84.7	59	31.5 – 179.8
SBC20	742.3	101.6	14.20	44.7	41.8	244.9	95.2	84.6	60	31.7 – 184.3
SBD20	748.4	103.2	14.19	44.6	41.8	NA	93.1	83.2	57	32.9 – 187.5
SBE20	741.7	99.6	14.11	44.4	41.6	255.1	96.5	83.9	59	32.7 – 181.6
SBF20	717.7	93.45	14.27	45.1	42.1	267.4	95.6	83.6	76	28.4 – 180.5
T20	741.9	101.1	13.75	43.6	40.7	251.9	98.5	87.2	55	33.7 – 179
E20	744.8	46.1	13.06	41.6	38.7	355.4	100.1	87.2	65	35.5 – 182.4
SBA50	727.3	103.3	14.47	45.4	42.4	234.5	91.2	85	51	36.0 – 176.4
SBB50	729	100.2	14.47	45.6	42.6	232	97.7	84.8	50	36.5 – 174.8
SBC50	754.4	102.5	14.26	44.6	41.8	242.7	95.2	85.4	54	36.7 – 187.6
SBD50	767	106.8	14.25	44.5	41.8	118.3	89.4	80	44	39.8 – 193.6
SBE50	751.2	97.7	14.04	44	41.4	267.7	96.3	83.6	52	36.7 – 180.5
SBF50	691.7	83.6	14.45	45.6	42.6	301.1	94.4	82.2	92	27.4 – 170.7
T50	752.6	101.5	13.16	42.0	39.1	260.1	> 100	91.7	41	40.1 – 170.8
E50	766.4	62.5	11.48	37.0	34.1	513.6	> 100	> 100	54	39.6 – 162.6

[a]ASTM D4052-11

[b]Stoichiometric Air/Fuel ratio

[c]ASTM D4809

[d]Linear estimate from table C.1. Recognised to be inaccurate as discussed by [195].

[e]ASTM D2699-13b/ASTM D2700-14

[f]ASTM D323-08(2014)

[g]ASTM D86-12

Table C.3: *Fuel properties of 20% and 50% synthetic test fuel blends*

Test Fuel	C/H ratio	Linear paraffins	Iso-paraffins	Cyclic-paraffins	α-olefins	Internal olefins	Branched olefins	Other olefins	Aromat-ics	Other
SBA20	0.51	17.4	26.3	6.95	0	1.7	2.4	4.7	27	11.8
SBB20	0.51	15	14.2	7.2	0	2.6	7.9	16.5	23.3	11.8
SBC20	0.52	19.2	18.1	5.8	0	1.7	2.4	5	35.6	11.6
SBD20	0.53	18.7	16.4	7.8	0	1.7	2.4	4.6	35.0	11.6
SBE20	0.55	17	14.6	5.8	0.5	1.9	2.9	6.6	37.8	11.6
SBF20	0.51	19	16	6	3.9	9.6	3.5	4.7	23.7	12
T20	0.49	14.9	14.1	5.9	0	1.7	2.4	4.6	23	11.7
E20	0.49	14.7	14	5.8	0	1.7	2.4	5	22.8	11.6
SBA50	0.5	15.6	39.3	6.3	0	1	1.6	2.9	24	7.4
SBB50	0.5	9.6	9	6.8	0	3.4	15.3	32.8	14.8	7.4
SBC50	0.55	19.9	18.7	3.6	0	1	1.4	2.8	45.2	7.1
SBD50	0.55	18.8	14.5	8.3	0	1	1.4	2.8	43.9	7.2
SBE50	0.61	14.6	10.2	3.5	1	1.6	2.9	7.6	50.7	7.3
SBF50	0.5	19.8	13.2	3.9	10.2	21.6	4.2	3.1	15.4	7.8
T50	0.47	9.3	8.8	3.7	0	1	1.5	2.9	14.4	7.3
E50	0.45	9	8.6	3.6	0	1	1.4	2.8	14	7.1

Table C.4: *Chemical fuel properties of 20% and 50% synthetic test fuel blends*

Test Fuel	**Density (kg/m^3)**[a]	**Molar mass (g/mol)**	**A/F**[b]	**HHV (MJ/kg)**[c]	**LHV (MJ/kg)**[c]	**ΔH_{vap} (kJ/kg)**[d]	**RON**[e]	**MON**[e]	**RVP (kPa)**[f]	**Boiling range (°C)**[g]
SB-IMEP	672.2	90.1	14.05	44.3	41.4	282.2	97.9	84.7	55	36.4 – 180.9
SB-ISFCM	691.7	89.6	14.15	44.5	41.7	282.1	97.5	84.4	53	37.4 – 185.1
SB-ISFCV	755.4	97.0	14.32	44.5	41.9	263.0	95.8	84.8	51	36.1 – 194.1
SB-PP	742	49.3	10.11	33.1	30.1	687.7	> 100	> 100	73	32.6 – 102.1

[a]ASTM D4052-11
[b]Stoichiometric Air/Fuel ratio
[c]ASTM D4809
[d]Linear estimate from table C.1. Recognised to be inaccurate as discussed by [195].
[e]ASTM D2699-13b/ASTM D2700-14
[f]ASTM D323-08(2014)
[g]ASTM D86-12

Table C.5: *Fuel properties of optimised synthetic gasoline blends*

Test Fuel	C/H ratio	Linear paraffins	Iso-paraffins	Cyclic-paraffins	α-olefins	Internal olefins	Branched olefins	Other olefins	Aromat-ics	Other
SB-IMEP	0.55	8.9	3.5	1.6	5.6	11.5	9.4	18.6	23.2	0.1
SB-ISFCM	0.55	8.9	3.7	1.9	5.4	11.4	10.8	21.6	23.5	0.1
SB-ISFCV	0.6	19	14.9	0	2.8	5	1.2	2	56.1	0.1
SB-PP	0.42	4	1.6	0	4.2	8.3	1.1	0	0	0

Table C.6: *Chemical fuel properties of optimised synthetic gasoline blends*